OFF-CENTER-LINE SHOCK-INTERFERENCE HEATING PATTERNS ON BASIC SHAPES IN HYPERSONIC FLOWS

by J. Wayne Keyes

Langley Research Center
Hampton, Va. 23665

1. Report No. NASA TM X-2866	2. Government Accession No.	3. Recipient's Catalog No.
4. Title and Subtitle OFF-CENTER-LINE SHOCK-INTERFERENCE HEATING PATTERNS ON BASIC SHAPES IN HYPERSONIC FLOWS		5. Report Date December 1973
		6. Performing Organization Code
7. Author(s) J. Wayne Keyes		8. Performing Organization Report No. L-8942
9. Performing Organization Name and Address NASA Langley Research Center Hampton, Va. 23665		10. Work Unit No. 501-06-08-01
		11. Contract or Grant No.
12. Sponsoring Agency Name and Address National Aeronautics and Space Administration Washington, D.C. 20546		13. Type of Report and Period Covered Technical Memorandum
		14. Sponsoring Agency Code

15. Supplementary Notes

16. Abstract

   This paper presents the results of an experimental study of off-center-line shock-interference heating on basic shapes at hypersonic speeds. The study covered three types of shock-interference patterns over a range of nominal Mach numbers (6 to 20), specific heat ratios (1.40 and 1.67), free-stream Reynolds numbers (8×10^6 to 26×10^6 per meter), and impinging shock strengths. Heat-transfer rates higher than stagnation levels were measured over much of the off-center-line model surface. Peak heating up to 17 times the stagnation heating was measured.

17. Key Words (Suggested by Author(s)) Shock-interference heating Shear-layer attachment Shock—boundary-layer interaction Jet impingement Shock interactions	18. Distribution Statement Unclassified — Unlimited	
19. Security Classif. (of this report) Unclassified	20. Security Classif. (of this page) Unclassified	21. No. of Pages 94	22. Price* Domestic, $3.75 Foreign, $6.25

OFF-CENTER-LINE SHOCK-INTERFERENCE HEATING PATTERNS ON BASIC SHAPES IN HYPERSONIC FLOWS

By J. Wayne Keyes
Langley Research Center

SUMMARY

Experimental off-center-line shock-interference heating results on basic bodies are presented for a range of hypersonic Mach numbers, specific heat ratios, Reynolds numbers, and impinging shock strengths. Three interference flow patterns explicitly defined in previous studies were generated by the intersection between a plane impinging shock and the bow shock created by a hemisphere or a cylindrical fin.

Heat-transfer rates higher than stagnation values were measured over much of the off-center-line model surface. For example, heating levels equal to or much higher than stagnation existed over most of the lower half of the hemisphere. Heating amplifications up to 17 times that for stagnation were measured on the hemisphere because of jet impingement. The results of this study imply that shock interference on a high-speed flight vehicle can cause severe heating over large areas near the interaction region.

INTRODUCTION

Shock-interference heating can be a serious problem in the design of high-speed vehicles such as the space shuttle and hypersonic cruise aircraft. Heat-transfer values several times the stagnation-point values can occur on vehicle surfaces because of the interfering flow fields. (See refs. 1 to 3.) These interfering flow fields are influenced by free-stream flow conditions, real-gas effects, and angle-of-attack changes as the vehicle moves along its trajectory.

Edney (ref. 1) made a detailed study of the entire spectrum of interference flows and defined six types of shock-interference patterns. The local pressure and heating peaks were a result of either shock—boundary-layer interaction, free shear-layer attachment, or supersonic jet impingement. The results of an extensive analytical and experimental study of shock-interference heating at hypersonic speeds are reported in references 2 to 6. Reference 2 presented theoretical flow models and semiempirical methods of predicting the peak pressure and heat-transfer levels for the six types of shock-interference patterns; also included were center-line experimental pressure and heat-

transfer distributions on hemispheres, a 30° wedge, and a cylindrical leading-edge fin for different interference patterns.

This paper presents the effects of free-stream Mach number and Reynolds number, specific heat ratio (shock density ratio), and impinging shock strength on the interference heating amplification away from the plane of symmetry. Heat-transfer data were obtained over a range of nominal Mach numbers (6 to 20), specific heat ratios (1.40 and 1.67), and impinging shock strengths (5° to 25°). This investigation supplements the study reported in reference 2.

SYMBOLS

The measurements and values are given in SI units; calculations were made in U.S. Customary Units.

A   cylinder length (see fig. 2(a))

c   specific heat of model material

h   heat-transfer coefficient

k   thermal conductivity of model material

L   fin length

M   Mach number

N_{Re} Reynolds number

p   pressure

R_b radius of hemisphere

T   temperature

$X = x/L$

x   axial coordinate

x_i, y_i coordinates of shock intersection in plane of symmetry (see fig. 2)

2

γ ratio of specific heats

θ body angle for hemisphere (see figs. 2(a) and 5(a))

θ_i shock generator angle

θ_{SL} shear-layer angle relative to surface (see fig. 3(c))

λ sweep angle of fin

ρ density of model material

ρ_2/ρ_1 normal-shock density ratio

ϕ angle in a plane perpendicular to axis of hemisphere or cylindrical leading-edge fin (see figs. 2 and 5)

Subscripts:

aw   adiabatic wall

cyl   stagnation-line value

pk   peak value

ref   reference value

stag   stagnation value at outer edge of boundary layer

t   total value

w   wall value

∞ free-stream value

Abbreviations (see fig. 3):

BS   bow shock

IP   impingement point

IS   impinging shock

SL   shear layer

TS   ·   transmitted shock

APPARATUS AND TEST CONDITIONS

Test Facilities

The wind tunnels used in this study are summarized in table I:

TABLE I. - TEST FACILITIES

Facility	Test gas	γ	M_∞	Facility described in reference —
Langley 20-inch Mach 6 tunnel	Air	1.40	6	7
Langley 22-inch helium tunnel	Helium	1.67	20	8

Models

The experimental setup shown in figure 1 was designed to use interchangeable models. These interchangeable models (shown in fig. 2) consisted of a 2.54-cm- and a 5.08-cm-diameter hemisphere and a 2.54-cm-diameter cylindrical leading-edge fin. A 15.24-cm-wide by 25.40-cm-long sharp leading-edge plate which can be set at angles up to 30° was used as a shock generator. The main series of models were made of a silica-base epoxy material. Additional models of solid stainless steel (type 347) were used to measure peak heating in some tests.

The model thermophysical properties (density, specific heat, and thermal conductivity) were measured on samples of material for each model. The value of the product ρck used was approximately $1.798 \times 10^3 \ W\sqrt{sec}/m^2\text{-}K$ for the epoxy models and $7.260 \times 10^3 \ W\sqrt{sec}/m^2\text{-}K$ for the stainless-steel models. Further details are available in reference 2.

Test Parameters

A summary of the models, nominal flow conditions, and types of interference patterns investigated is presented in table II:

4

TABLE II. - SUMMARY OF TEST PARAMETERS

Test	Model	M_∞	γ	ρ_2/ρ_1	$p_{t,\infty}$, N/cm^2	$T_{t,\infty}$, K	$N_{Re,\infty}/m$	Type of interference (ref. 1)
6352	5.08-cm-diameter hemisphere	6	1.40	5.5	83 290	478	7.9×10^6 25.6	III and IV
6363	5.08-cm-diameter hemisphere	6	1.40	5.5	290	478	25.6	III and IV
6363	Fin	6	1.40	5.5	290	478	25.6	IVa and V
373	2.54-cm-diameter hemisphere	20.2	1.67	4.0	690	433	9.8	III and IV

The types of interference are discussed in a later section.

EXPERIMENTAL TECHNIQUE AND DATA ACCURACY

The methods of testing were similar for both facilities. The phase-change coating technique described in detail in references 9 and 10 was used to measure the heating. Because of the highly nonuniform heat-transfer distribution on the models, some models were tested with two or more temperature coatings. In some cases, peak heating was so intense that the coating temperature that would be needed was near T_{aw}. (This condition would indicate short melt times and the possibility of large errors.) To measure the peak heating in these cases, the stainless-steel model with its larger value of ρck was used; this model permitted the use of a coating with a lower melt temperature.

Phase-change heat-transfer data are subject to numerous errors. Errors in measuring the thermophysical properties of the model material, the melt temperature and time, the initial model wall temperature, and the initial time of exposure to the free stream can affect the accuracy of the heat-transfer data. Another important source of error is the determining of the adiabatic wall temperature distribution. In the present tests, T_{aw} was assumed to be equal to the free-stream total temperature. An analysis of these combined errors indicated that the heating amplification measured at Mach 6 in air may have a maximum error of about 29 percent (25 percent at Mach 20 in helium).

A semi-infinite slab solution of the general heat conduction equation was used to reduce the heating data. (See ref. 9.) In order for this assumption to be valid, the radius of curvature must be much greater than the depth of heat penetration. As stated in reference 10, the heat penetration depth for the semi-infinite slab is approximately independent of the aerodynamic heat-transfer coefficient and depends only on the thermal diffusivity of the wall material and the thermal diffusion time. The minimum distance

from peak heating for which the semi-infinite slab solution is valid can also be determined by using the melt time. (See ref. 10.) Although the phase-change method does not account for lateral conduction errors, these errors can be important. (See ref. 10 for additional details.)

Details of the interference flow regions were observed by using the schlieren technique. Surface flow patterns were obtained by using a mixture of titanium dioxide and silicone oil in the Mach 6 facility. Further details of the flow-visualization technique are given in reference 2.

TYPES OF SHOCK-INTERFERENCE PATTERNS

In estimating the effects of shock-interference heating, it is necessary to determine the type of interference pattern that will exist when two shocks of different strength intersect. The pattern that will occur depends on body geometry, Mach number, specific heat ratio, and strength of the impinging shock and its position relative to the body. (See ref. 1.) The six possible shock-interference-flow patterns as defined by Edney are shown in figure 3.

These interference patterns can be further grouped according to the flow mechanism that causes the heat-transfer change at the surface. Types I, II, and V are associated with a shock—boundary-layer interaction and type III is characterized by an attaching free shear layer. Type IV is characterized by an impinging or grazing supersonic jet (type IVa) and type VI by an expansion-fan—boundary-layer interaction. In the present study, only types III, IV, IVa, and V were investigated. Types III and IV occurred on the hemispheres and type IVa and V on the fin.

For a weak two-dimensional shock impinging on the bow shock of a hemisphere, the interference pattern in the plane of symmetry depends on the relative shock locations as shown in figure 4. The type of interference can be different away from the plane of symmetry where the bow-shock strength is weaker. A detailed description of these six types of shock-interference patterns and the transition from one type to another is given in references 1 and 2.

PRESENTATION OF RESULTS

The heat-transfer data are presented as nondimensional heat-transfer contours (h/h_{ref}) along with off-center-line peak heating distributions and the center-line heating distributions from reference 2. Selected schlieren photographs and oil-flow patterns are also shown. The data are presented according to the type of interference occurring on the center line, the free-stream Mach number and Reynolds number, the strength and

6

location of the impinging shock, and the model geometry. Table III provides an index to the figures presented in this paper.

TABLE III.- DATA FIGURES

(a) Hemisphere

Figure	Type	M_∞	$N_{Re,\infty}/m$	γ	ρ_2/ρ_1	θ_i nominal, deg	x_i/R_b	y_i/R_b	Model diameter, cm	Test-run numbers (ref. 2)
[a]6	III	5.94	7.9×10^6	1.40	5.5	15	0.214	-0.621	5.08	------------
7	III	↓	7.7	↓	↓	10	.228	-.417	↓	6352-16,17,30
8	III		7.9			15	.214	-.621		6352-12,13
9	III		7.6			20	.262	-.680		6352-21,22
10	III	↓	7.8			25	.262	-.786		6352-25,26
11	III	6.00	25.9			15	.233	-.548		6363-36,37
12	III	6.00	25.8	↓	↓	15	.209	-.650	↓	6363-39,40
13	III	20.2	9.9	1.67	4.0	5	----	-----	2.54	373-19,20
14	III	↓	9.7			5	----	-----		373-22,23,24
15	III		9.8			10	.310	-.370		373-11,12,26
16	III		9.7			10	.260	-.480		373-8,9
17	III		9.8			15	----	-----		373-5,6
18	III	↓	9.8	↓	↓	15	----	-----	↓	373-2,3
[a]19	IV	6.00	25.7	1.40	5.5	15	.252	-.427	5.08	------------
20	IV	5.94	7.6			5	.200	-.141		6363-48
21	IV		8.0			10	.218	-.340		6352-14,15
22	IV		7.5			15	.257	-.340		6352-27,28
23	IV		7.7			15	.248	-.513		6352-8,9,29
24	IV		7.6			20	.288	-.557		6352-18,19,20
25	IV	↓	7.8			25	.291	-.640		6352-23,24
26	IV	6.00	25.6			5	.204	-.199		6363-46
27	IV		25.0			10	.223	-.252		6352-31,32,33
28	IV		25.7			15	.252	-.427		6352-1,2,3
29	IV		25.6			20	.282	-.417		6363-41,42
30	IV	↓	25.4	↓	↓	25	.301	-.534	↓	6363-43,44

(b) Cylindrical fin

Figure	Type	M_∞	$N_{Re,\infty}/m$	γ	ρ_2/ρ_1	θ_i nominal, deg	x_i/L	y_i/L	λ nominal, deg	Test-run numbers (ref. 2)
[a]31	IVa	6.00	25.8×10^6	1.40	5.5	20	0.305	0.105	0	-------
32	IVa	5.94	8.1			10	.355	.080	0	6363-24
33	IVa		7.7			15	.435	.095	0	6363-22
34	IVa	↓	7.9			20	.310	.110	0	6363-18
35	IVa	6.00	26.2			10	.340	.075	0	6363-23
36	IVa		25.4			15	.425	.090	0	6363-20
37	IVa		25.8			20	.305	.105	0	6363-19
[a]38	V	↓	25.9			20	.300	.070	25	-------
39	V	5.94	7.2			10	.330	.060	25	6363-6
40	V		7.3			15	.360	.065	25	6363-3
41	V	↓	7.6			20	.310	.065	25	6363-14
42	V	6.00	25.7			10	.300	.050	25	6363-9
43	V		26.2			15	.340	.060	25	6363-10
44	V	↓	25.9	↓	↓	20	.300	.070	25	6363-13

[a]Schlieren and/or oil-flow photographs.

The off-center-line peak heating data on the hemisphere are plotted by using the coordinate system defined in figure 5(a); values of θ and ϕ were measured by using the intersections of the individual heating contours h/h_{stag} with the attachment line or jet impingement line. (See fig. 7(a), for example.) Since the body is axisymmetric, this system collapses the off-center-line data on to the center line in the vertical plane of symmetry. The values of θ and ϕ are listed on the heating-contour figures. Off-center-line peak heating data on the fin were plotted by using the coordinate ϕ as shown in figure 5(b). In this case ϕ is located in a plane perpendicular to the fin center line. The undisturbed heating levels on the hemisphere and cylindrical fin are included for comparison purposes.

Reference values h_{stag} for the hemispheres are obtained from an expression for laminar stagnation-point heating in reference 11. Laminar stagnation-line heating h_{cyl} calculated from a method in reference 12 is used for the cylindrical leading-edge fin.

DISCUSSION OF RESULTS

Type III Interference

An extensive investigation of type III interference (shear-layer attachment) on hemispheres was conducted at Mach 6 in air ($\gamma = 1.40$) and Mach 20 in helium ($\gamma = 1.67$). Typical schlieren and oil-flow photographs for a type III interference pattern on a hemisphere are shown in figure 6. The reshaped bow shock and the attaching free shear layer which emanates from the shock intersection can be seen in figure 6(a). The attaching shear layer with its accompanying high shear flow appears as a "feather" pattern on the surface with the flow moving away from the attachment line (fig. 6(b)).

Hemisphere (5.08-cm diameter). - Heat-transfer results for the 5.08-cm-diameter hemisphere at Mach 6, $\gamma = 1.40$ ($\rho_2/\rho_1 = 5.5$) are presented in figures 7 to 12 for a range of shock generator angles and two free-stream Reynolds numbers. The attaching shear layer has a strong influence on the heating along the lower surface of the hemisphere as shown in part (a) of figures 7 to 12. For example, the attachment line (dashed line on contour plots) extends from the vertical plane of symmetry around to the tangent point of the hemisphere and cylindrical afterbody. The extent of the high heating region near the nose decreases as the local unit Reynolds number increases for a given θ_i and θ_{pk}. (See, for example, figs. 8(a) and 12(a).) The size of this region is also influenced by the location of the impinging-shock—bow-shock intersection (x_i/R_b, y_i/R_b) relative to the sonic point ($\theta \approx 47^O$) for a given θ_i and Reynolds number. (See figs. 11(a) and 12(a).)

Comparisons of the undisturbed heating on the model with the vertical center-line heating and the off-center-line peak heating (along the attachment line) are presented in parts (b) and (c), respectively, of figures 7 to 12. Peak heating values from 7.5 to 14 times the stagnation values were measured on the vertical center line. It was shown in reference 2 that this peak heating is a function of shock generator angle θ_i, the shear-layer angle relative to the surface θ_{SL}, and the state of the shear layer at attachment (laminar, transitional, or turbulent). The shear layers at Mach 6 are either transitional or turbulent. (See ref. 2.) The entire heating on the center line is considerably higher than the local undisturbed level (for example, 10 to 15 times at $\theta = -80^O$). Off-center-line attachment heating distributions indicate that heating levels of comparable severity to center-line heating are also observed over large parts of the hemisphere surface. These results show that even though the maximum peak is located near the center line, severe heating can extend over much of the model surface.

Hemisphere (2.54-cm diameter). - Heating contours, center-line, and off-center-line peak heating distributions are presented in figures 13 to 18 at $\theta_i = 5^O$, 10°, and 15° for various shear-layer attachment locations on the 2.54-cm-diameter hemisphere at Mach 20, $\gamma = 1.67$ ($\rho_2/\rho_1 = 4.0$). In general, the heating data in helium followed the same trends as the Mach 6 air data. However, the peak heating ratios were lower in helium as a result of the lower normal-shock—density ratio and the laminar shear-layer attachment (refs. 5 and 6) as opposed to transitional or turbulent attachment for the Mach 6 data.

Type IV Interference

Of the six types of interference, type IV (supersonic jet impinging in a subsonic region) results in the most severe heating (refs. 1 and 2); therefore, considerable interference heating data were obtained. A typical schlieren photograph of the shock and jet patterns is shown in figure 19(a) at Mach 6 in air. The effect of jet impingement on the surface oil flow on a hemisphere is shown in figure 19(b). At $\theta_i = 15^O$, the surface flow pattern appears to be similar to the pattern for shear-layer attachment (fig. 6(b)). The model stagnation region is severely displaced since the jet stagnation pressure can be as high as 6 to 8 times the model stagnation value. (See ref. 2.)

Hemisphere (5.08-cm diameter). - Heating data at two Reynolds numbers for shock generator angles from 5° to 25° are presented in figures 20 to 30 for the 5.08-cm-diameter hemisphere at Mach 6, $\gamma = 1.40$ ($\rho_2/\rho_1 = 5.5$). The contours and center-line distribution at $\theta_i = 5^O$ in figures 20 and 26 are very similar to the shear-layer attachment patterns of type III; however, as θ_i increases, the heating patterns become very complex as shown in figures 21 to 25 and 27 to 30. The secondary areas of high heating appearing in these patterns are a result of flow distortions caused by shocks and expansions in the jet flow

moving along the surface. (See ref. 2.) Peak heating values 17 times the stagnation heating values were measured on the vertical center line. The variation of the maximum off-center-line peak heating along the jet impingement line (dashed line in part (c) of figs. 20 to 30) indicates that high heating extends far back on the model similar to type III off-center-line heating. The interference pattern may also change from one type to another with increasing distance from the vertical center line.

Cylindrical fin (2.54-cm-diameter leading edge). - A typical schlieren photograph of a type IVa grazing jet pattern is presented in figure 31 for a 2.54-cm-diameter leading-edge cylindrical fin at Mach 6, $\gamma = 1.40$ $(\rho_2/\rho_1 = 5.5)$. In this case the jet is turned upward and flows parallel to the model surface since the pressure in the lower subsonic region is higher than that in the upper region. The dark and light areas near the surface above the shock interaction are compressions and expansions in the jet flow. The flow in this region is unsteady as indicated by the wavy bow shock.

Heating contours, center-line, and off-center-line heating distributions for type IVa interference are shown in figures 32 to 37. The peaks and dips observed in the heating distributions are caused by the compressions and expansions in the grazing jet flow interacting with the fin boundary layer. The sharp increase in heating and the spike appearing near the lower end of the fin (figs. 33 and 36) are a result of the expansion waves from the trailing edge of the shock generator interacting with the lower segment of the bow shock. Heating levels as high as the stagnation-line values were measured on the cylindrical leading edge as far back as $\phi \approx 60^\circ$. (See part (c) of figs. 32 to 37.)

<p align="center">Type V Interference</p>

A schlieren photograph showing the complex flow pattern on the 2.54-cm-diameter leading-edge cylindrical fin at Mach 6, $\gamma = 1.40$ $(\rho_2/\rho_1 = 5.5)$ is shown in figure 38(a) at $\lambda = 25^\circ$ and $\theta_i = 20^\circ$. This photograph also shows that the jet flow is unsteady as for type IVa. The oil-flow pattern for the fin leading edge is shown in figure 38(b).

Heating contours, stagnation-line heating distributions, and off-stagnation-line peak values are presented in figures 39 to 44 for various θ_i values and two free-stream Reynolds numbers. In general, the heating contours and stagnation-line distributions exhibit similar shapes and trends, respectively, regardless of the impinging shock strength. The secondary peaks observed in the stagnation-line distribution are the result of the grazing jet and shear layer interacting with the boundary layer. (For example, compare the interactions shown in fig. 38(a) with the heating of fig. 39(c).) The peak-off-stagnation-line distributions show that heating as high as stagnation-line values can exist as far back as $\phi = 85^\circ$. (See fig. 30(c).) Small areas of high heating which appear to be caused by vortices from the lower corner were observed in some runs. (See figs. 43(a) and 44(a).)

10

CONCLUDING REMARKS

The results of an extensive experimental study of off-center-line shock interference heating on simple shapes are presented for three interference flow patterns. These patterns were formed by the intersection of a plane impinging shock and the bow shock created by a hemisphere or cylindrical fin. The study covered a range of hypersonic Mach numbers, specific heat ratios, Reynolds numbers, and impinging shock strengths.

Heating levels higher than stagnation values were found over a large percentage of the off-center-line body surface. For example, in most cases the lower half of the hemisphere was exposed to levels equal to or much greater than stagnation heating. Maximum amplifications up to 17 times the stagnation heating were measured on the hemisphere near the center line for an impinging jet. These results indicate that shock interference on high-speed flight vehicles can cause severe heating over significant areas in the vicinity of the interaction region.

Langley Research Center,
National Aeronautics and Space Administration,
Hampton, Va., September 19, 1973.

REFERENCES

1. Edney, Barry: Anomalous Heat Transfer and Pressure Distribution on Blunt Bodies at Hypersonic Speeds in the Presence of an Impinging Shock. FFA Rep. 115, Aeronaut. Res. Inst. of Sweden, 1968.

2. Keyes, J. Wayne; and Hains, Frank D.: Analytical and Experimental Studies of Shock Interference Heating in Hypersonic Flows. NASA TN D-7139, 1973.

3. Hains, F. D.; and Keyes, J. Wayne: Shock Interference Heating in Hypersonic Flows. AIAA J., vol. 10, no. 11, Nov. 1972, pp. 1441-1447.

4. Morris, Dana J.; and Keyes, J. Wayne: Computer Programs for Predicting Supersonic and Hypersonic Interference Flow Fields and Heating. NASA TM X-2725, 1973.

5. Keyes, J. Wayne; and Morris, Dana J.: Correlations of Peak Heating in Shock Interference Regions at Hypersonic Speeds. J. Spacecraft & Rockets, vol. 9, no. 8, Aug. 1972, pp. 621-623.

6. Birch, Stanley F.; and Keyes, J. Wayne: Transition in Compressible Free Shear Layers. J. Spacecraft & Rockets, vol. 9, no. 8, Aug. 1972, pp. 623-624.

7. Goldberg, Theodore J.; and Hefner, Jerry N. (With appendix by James C. Emery): Starting Phenomena for Hypersonic Inlets With Thick Turbulent Boundary Layer at Mach 6. NASA TN D-6280, 1971.

8. Arrington, James P.; Joiner, Roy C., Jr.; and Henderson, Arthur, Jr.: Longitudinal Characteristics of Several Configurations at Hypersonic Mach Numbers in Conical and Contoured Nozzles. NASA TN D-2489, 1964.

9. Jones, Robert A.; and Hunt, James L.: Use of Fusible Temperature Indicators for Obtaining Quantitative Aerodynamic Heat-Transfer Data. NASA TR R-230, 1966.

10. Hunt, James L.; and Jones, Robert A.: Effects of Several Ramp-Fairing, Umbilical and Pad Configurations on Aerodynamic Heating to Apollo Command Module at Mach 8. NASA TM X-1640, 1968.

11. Fay, J. A.; and Riddell, F. R.: Theory of Stagnation Point Heat Transfer in Dissociated Air. J. Aeronaut. Sci., vol. 25, no. 2, 1958, pp. 73-85, 121.

12. Beckwith, Ivan E.; and Gallagher, James J.: Local Heat Transfer and Recovery Temperature on a Yawed Cylinder at a Mach Number of 4.15 and High Reynolds Numbers. NASA TR R-104, 1961.

Interchangeable heat-transfer
model with fore-and-aft
adjustment

Flow ⟶

Variable incidence
shock generator

Model support
with vertical
adjustment
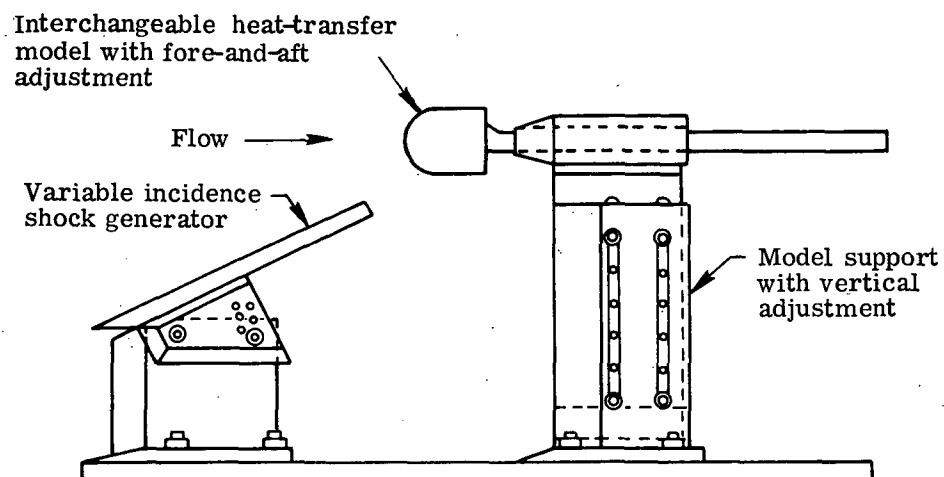
Figure 1.- Sketch of model test assembly.

(a) Hemispheres.

Model	R_b	A
2.54 cm dia.	1.27	1.91
5.08 cm dia.	2.54	3.81
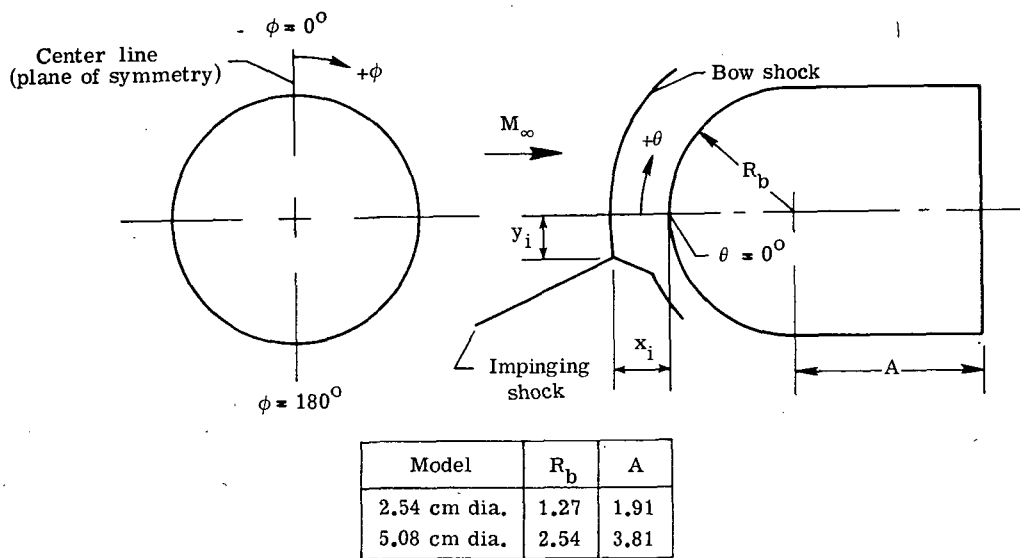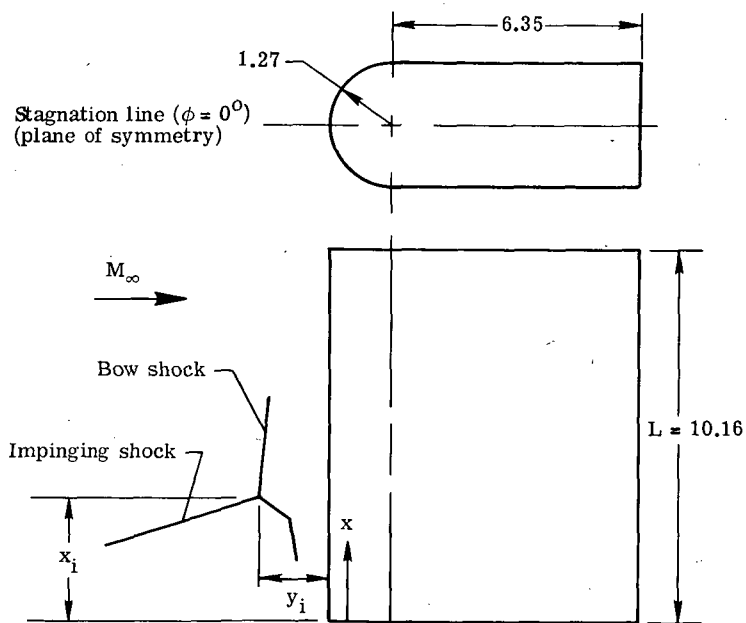
(b) Cylindrical fin.

Figure 2.- Sketch of models and center-line coordinate system. Dimensions are in cm.
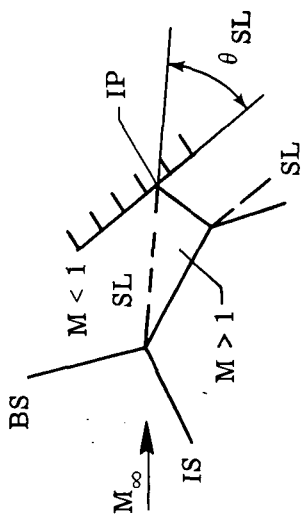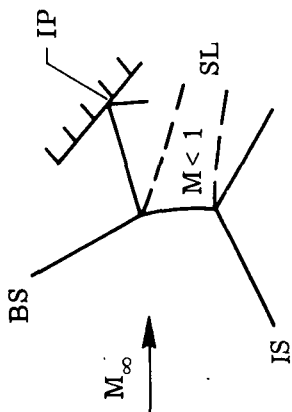
(a) Type I.

(b) Type II.
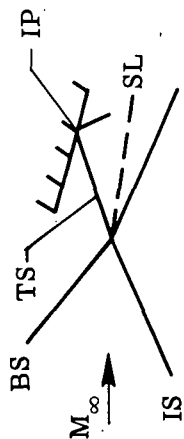
(c) Type III.
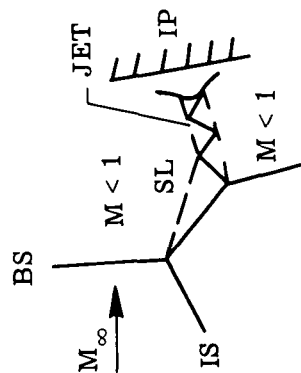
(d) Type IV.
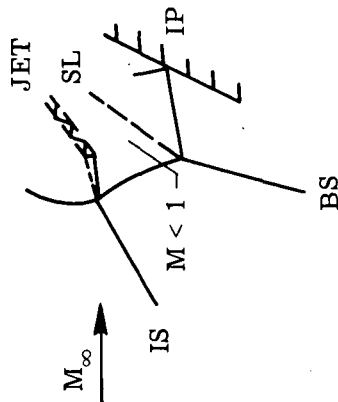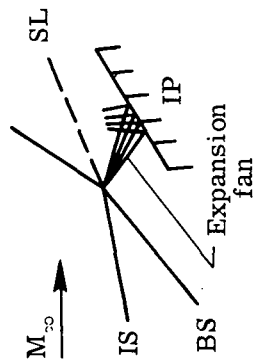
(e) Type V.

(f) Type VI.

Figure 3.– Six types of shock-interference patterns.

15
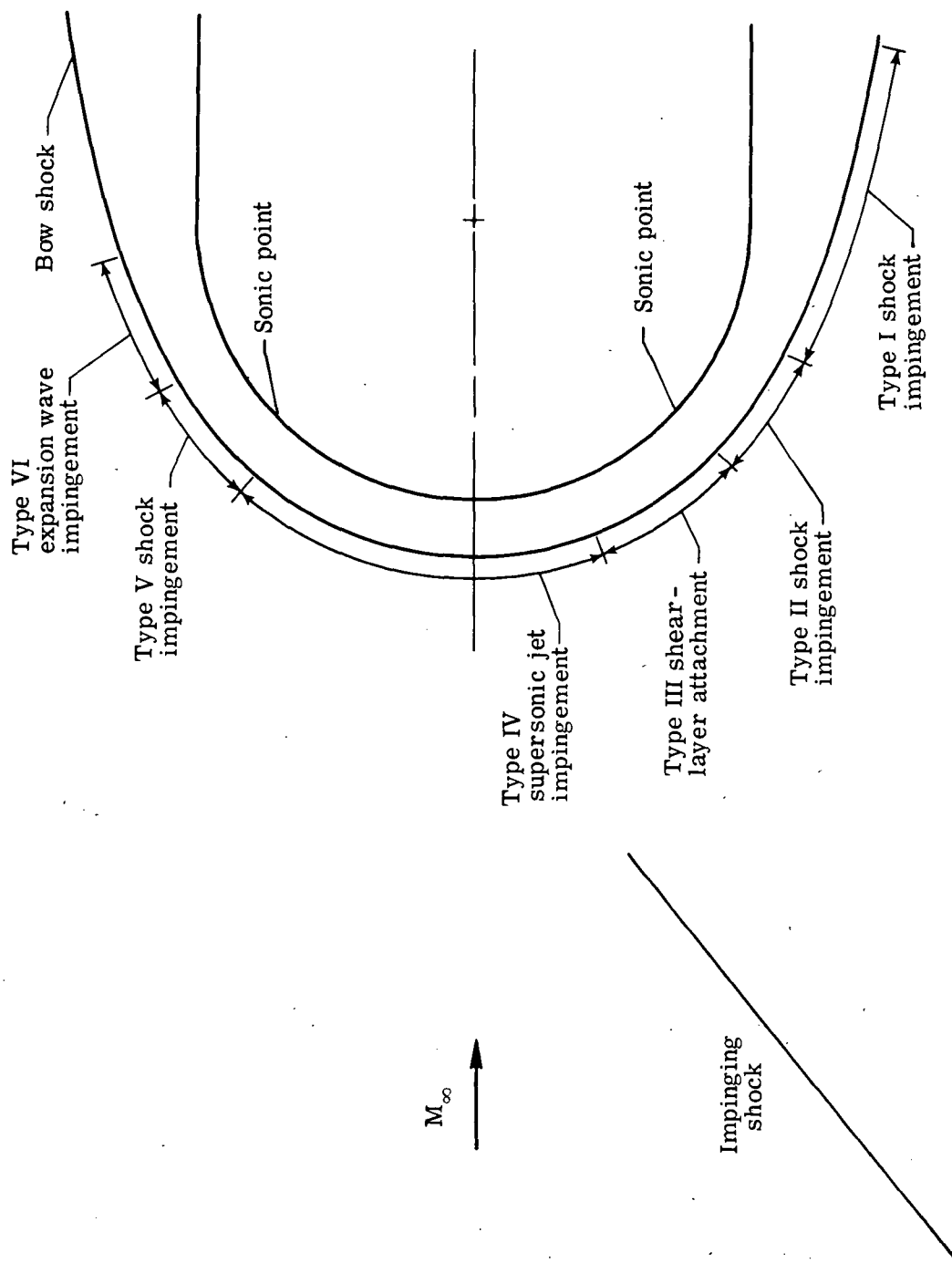
Figure 4.- Location of the types of interference on a hemisphere.
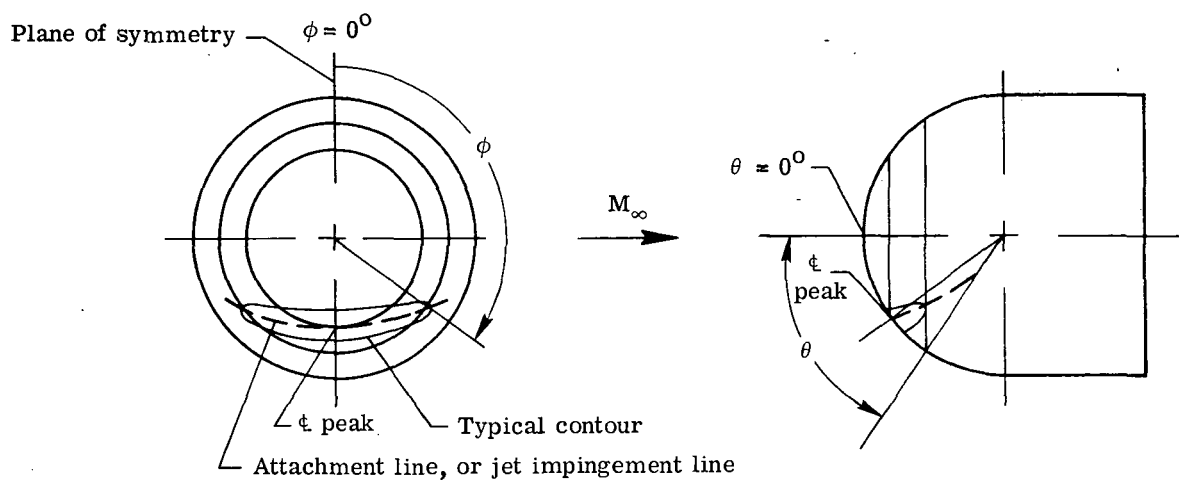
(a) Hemisphere.
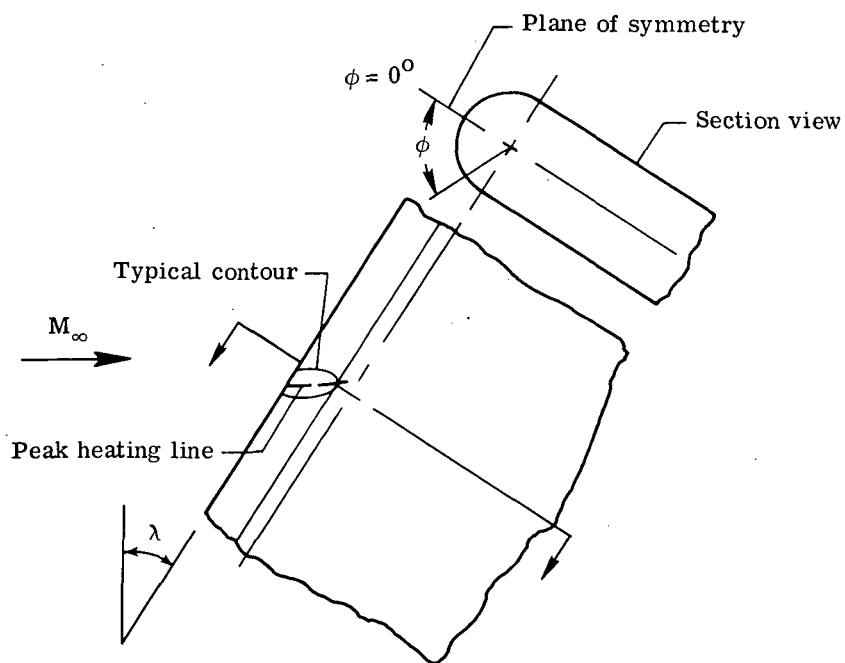
(b) Fin.

Figure 5.- Off-center-line coordinate system.

Figure labels:
- Hemisphere
- Bow shock (BS)
- Impinging shock (IS)
- Shear layer (SL)
- Peak heating
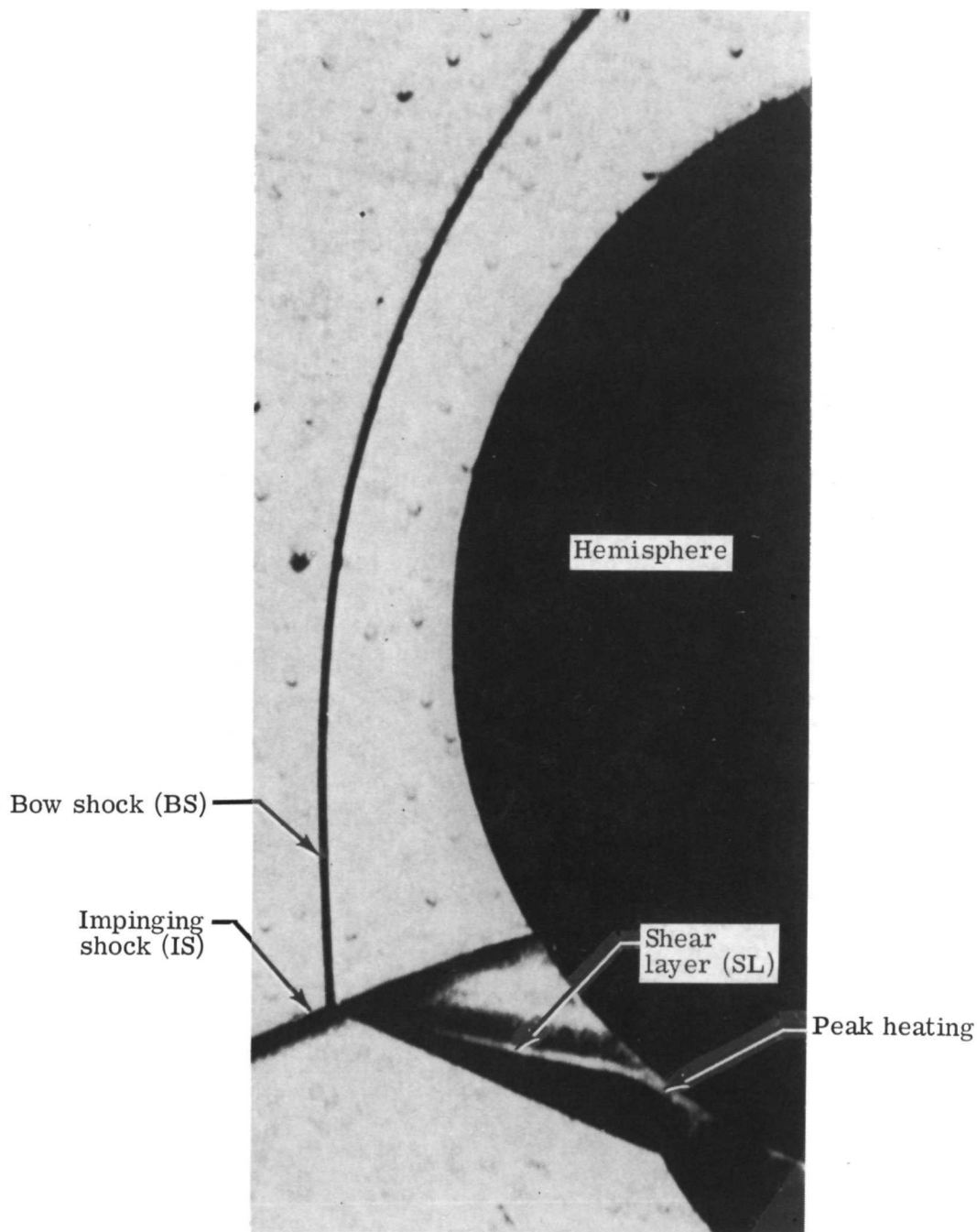
L-73-6871

(a) Schlieren photograph.

Figure 6.- Shock and oil-flow patterns on a 5.08-cm-diameter hemisphere at Mach 5.94 in air for a type III interference. $\theta_i = 14.8^O$; $N_{Re,\infty}/m = 7.9 \times 10^6$.

¢

Shear-layer attachment
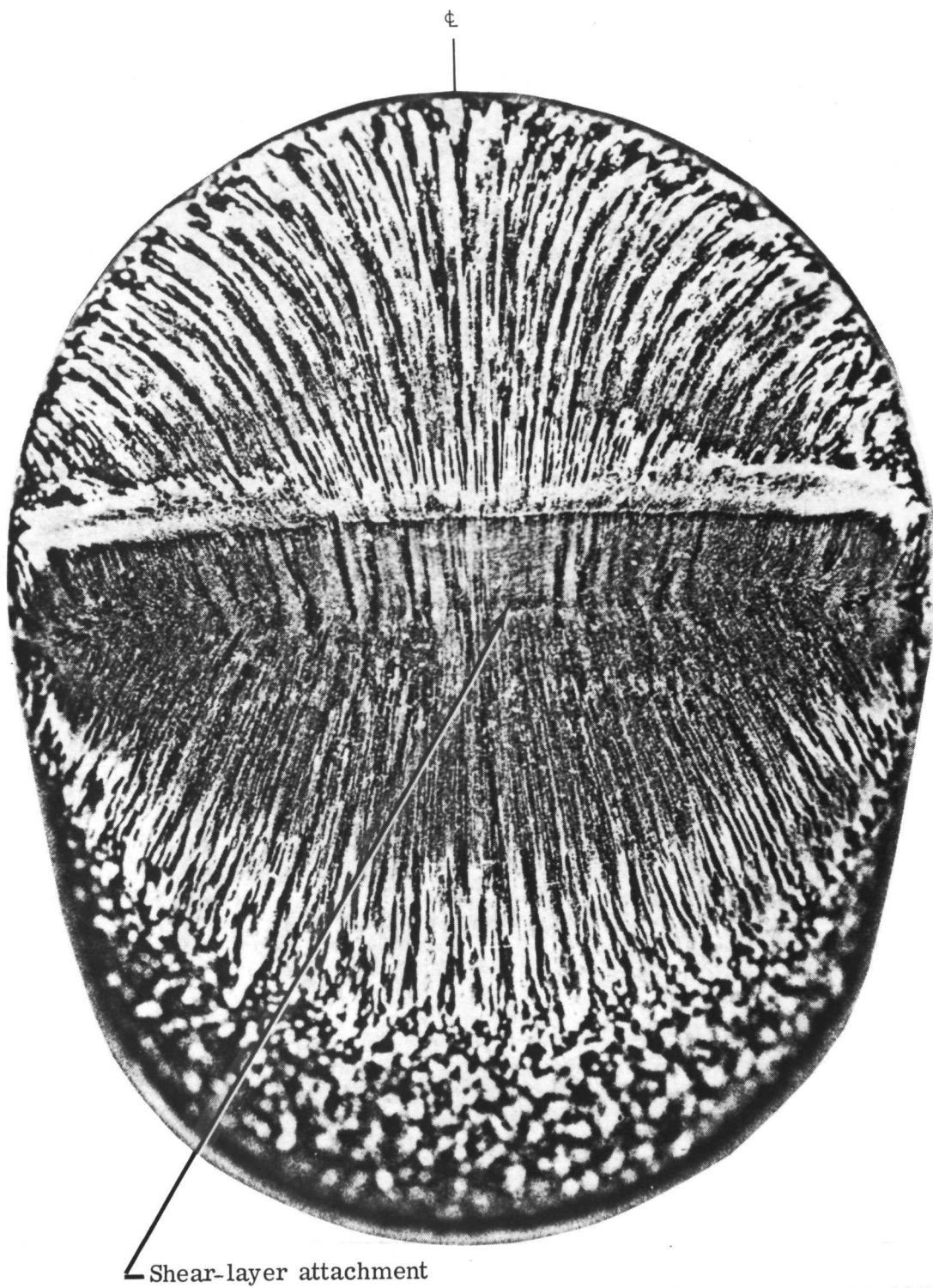
L-73-6872

(b) Oil-flow pattern.

Figure 6.- Concluded.

Test	Run	Model	Isotherm	h/h$_{stag}$	Off-center-line peak locations θ, deg	ϕ, deg
6352	16	Epoxy	1	11.42	37	160
	30		2	9.81	38	162
	16		3	9.55	39	158
	30		4	6.04	41	153
	16		5	5.51	49	139
	17		6	4.23	54	134
			7	3.36	58	132
			8	2.75	61	130
			9	2.45	63	129
			10	2.09	65	127
			11	1.98	67	126
			12	1.74	69	125
			13	1.61	71	124
			14	1.48	73	123
			15	1.37	79	120
			16	1.15	86	118
			17	1.03	89	116
			18	0.87	-	-
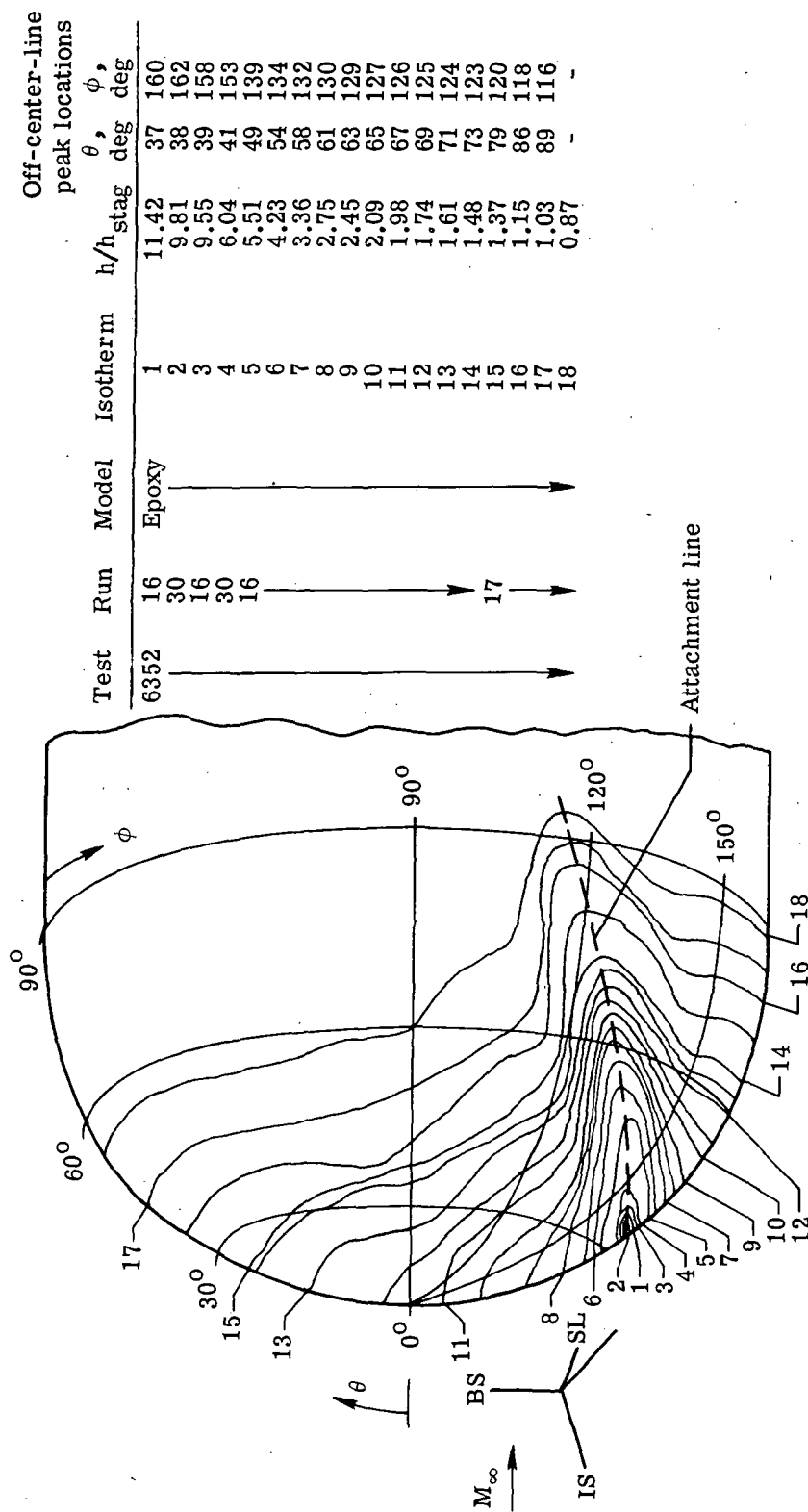
(a) Heating contours. $h_{stag} = 306.42$ W/m^2-K.

Figure 7.- Type III interference on a 5.08-cm-diameter hemisphere at Mach 5.94 in air.
$\theta_i = 9.9°$; $N_{Re,\infty}/m = 7.7 \times 10^6$.

Test-run		$p_{t,\infty}$, N/cm^2	$T_{t,\infty}$, K	T_w, K	h_{stag}, W/m^2-K	θ_i, deg
6352 - 30	○	81	474	436	306.42	9.9
6352 - 16	□	83	474	422	306.42	9.9
6352 - 17	◇	82	472	394	306.42	9.9

—— Fairing
- - - No interference
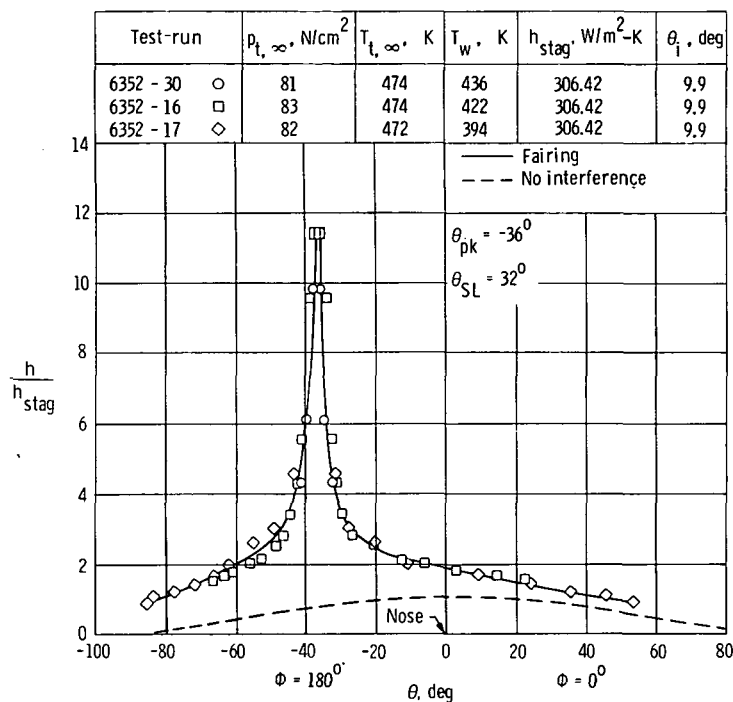
(b) Center-line heat-transfer distribution.

(c) Off-center-line peak heating.

Figure 7.- Concluded.

Test	Run	Model	Isotherm	h/h_{stag}	Off-center-line peak locations	
					θ, deg	ϕ, deg
6352	12	Epoxy	1	7.37	50	168
	13		2	6.30	51	166
			3	5.65	52	165
			4	4.23	53	163
			5	3.43	54	160
			6	3.27	71	142
			7	2.42	75	138
			8	1.98	81	136
			9	1.61	85	134
			10	1.39	88	132
			11	1.21	-	-
			12	1.11	-	-
			13	1.03	-	-

(a) Heating contours. h_{stag} = 306.42 W/m^2-K.

Figure 8.- Type III interference on a 5.08-cm-diameter hemisphere at Mach 5.94 in air. θ_i = 14.8°; $N_{Re,\infty}/m$ = 7.9 $\times$ 10^6.

Test-run		$P_{t, \infty}$, N/cm^2	$T_{t, \infty}$, K	T_w, K	h_{stag}, W/m^2-K	θ_i, deg
6352 - 12	O	84	476	436	306.42	14.8
6352 - 13	□	85	474	394	306.42	14.8

——— Fairing
– – – No interference

$\theta_{pk} = -50^0$

$\theta_{SL} = 27^0$
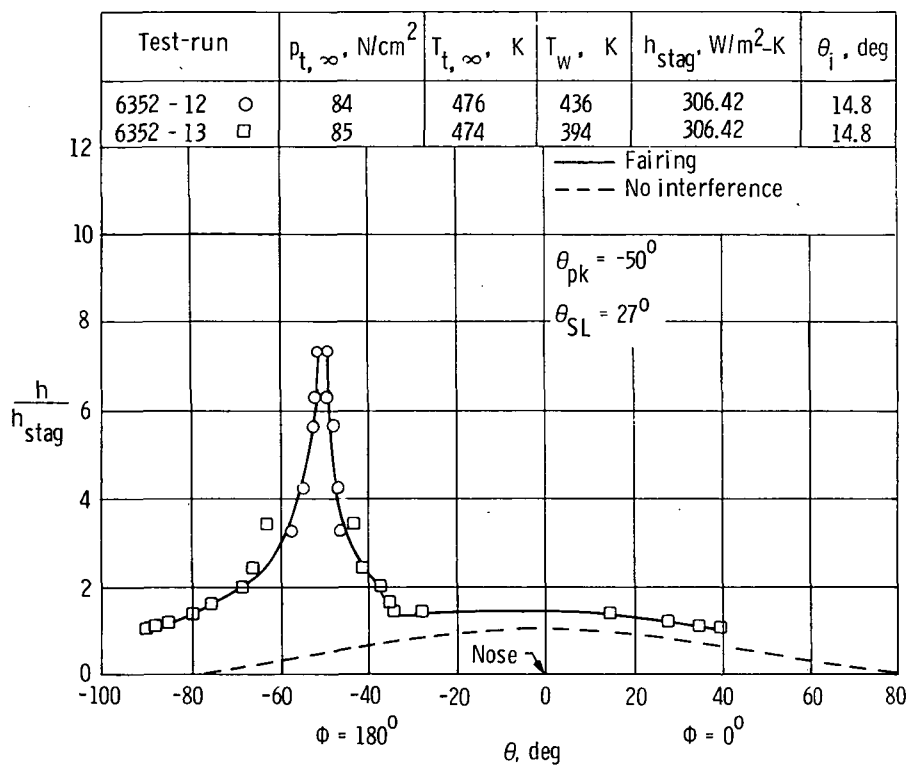
(b) Center-line heat-transfer distribution.

(c) Off-center-line peak heating.

Figure 8.- Concluded.

Test	Run	Model	Isotherm	h/h_{stag}	Off-center-line peak locations θ, deg	ϕ, deg
6352	21	Epoxy	1	11.91	47	165
	22		2	7.53	51	151
			3	5.33	57	144
			4	4.26	61	140
			5	3.24	66	137
			6	2.60	69	136
			7	2.29	72	133
			8	2.05	74	132
			9	1.83	77	130
			10	1.85	81	127
			11	1.56	85	124
			12	1.37	88	122
			13	1.23	-	-

(a) Heating contours. $h_{stag} = 306.42$ W/m^2-K.

Figure 9.- Type III interference on a 5.08-cm-diameter hemisphere at Mach 5.94 in air. $\theta_i = 19.7°$; $N_{Re,\infty}/m = 7.6 \times 10^6$.

Test-run		$p_{t,\infty}$, N/cm^2	$T_{t,\infty}$, K	T_w, K	h_{stag}, W/m^2-K	θ_i, deg
6352 - 21	○	81	477	422	306.42	19.7
6352 - 22	□	83	476	394	306.42	19.7

—— Fairing
--- No interference

$\theta_{pk} = -47^0$

$\theta_{SL} = 39^0$
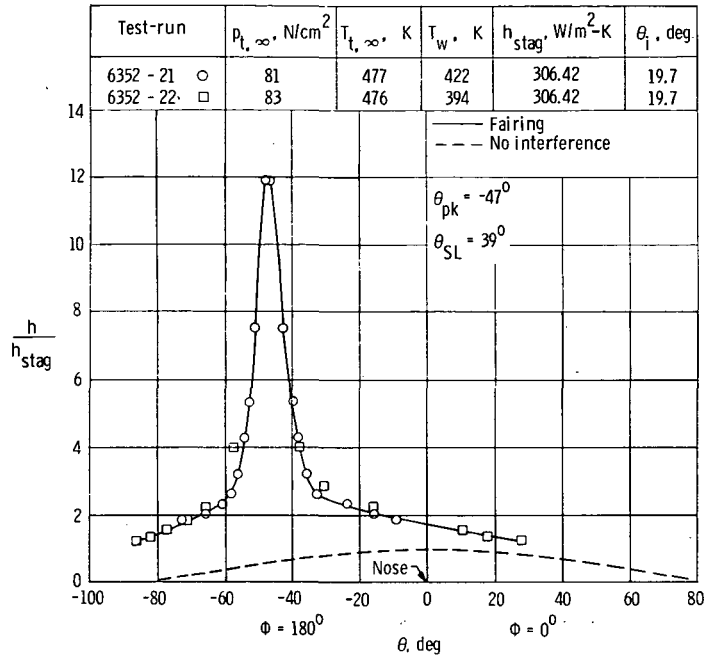
(b) Center-line heat-transfer distribution.

(c) Off-center-line peak heating.

Figure 9.- Concluded.

25

Test	Run	Model	Isotherm	h/h_{stag}	Off-center-line peak locations θ, deg	ϕ, deg
6352	25 26	Epoxy	1	9.63	51	170
			2	6.81	54	157
			3	4.81	61	147
			4	4.08	69	137
			5	2.88	74	131
			6	2.23	78	127
			7	1.87	81	124
			8	1.57	84	122
			9	1.29	88	119
			10	1.11	-	-

(a) Heating contours. $h_{stag} = 306.42$ W/m²-K.

Figure 10.- Type III interference on a 5.08-cm-diameter hemisphere at Mach 5.94 in air. $\theta_i = 24.6°$; $N_{Re,\infty}/m = 7.8 \times 10^6$.
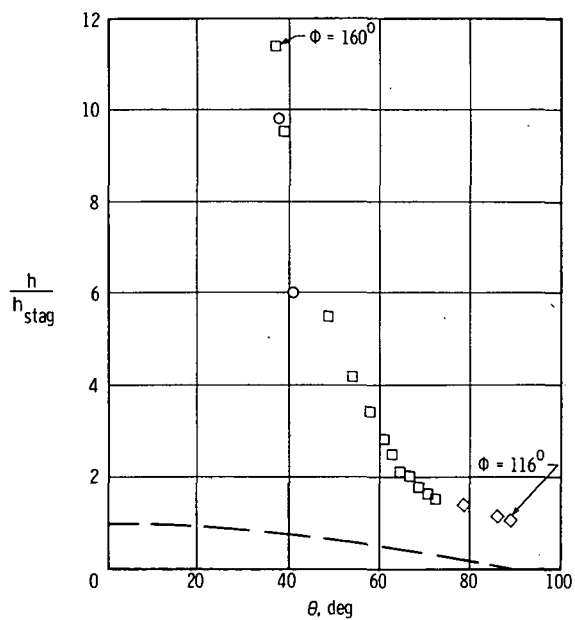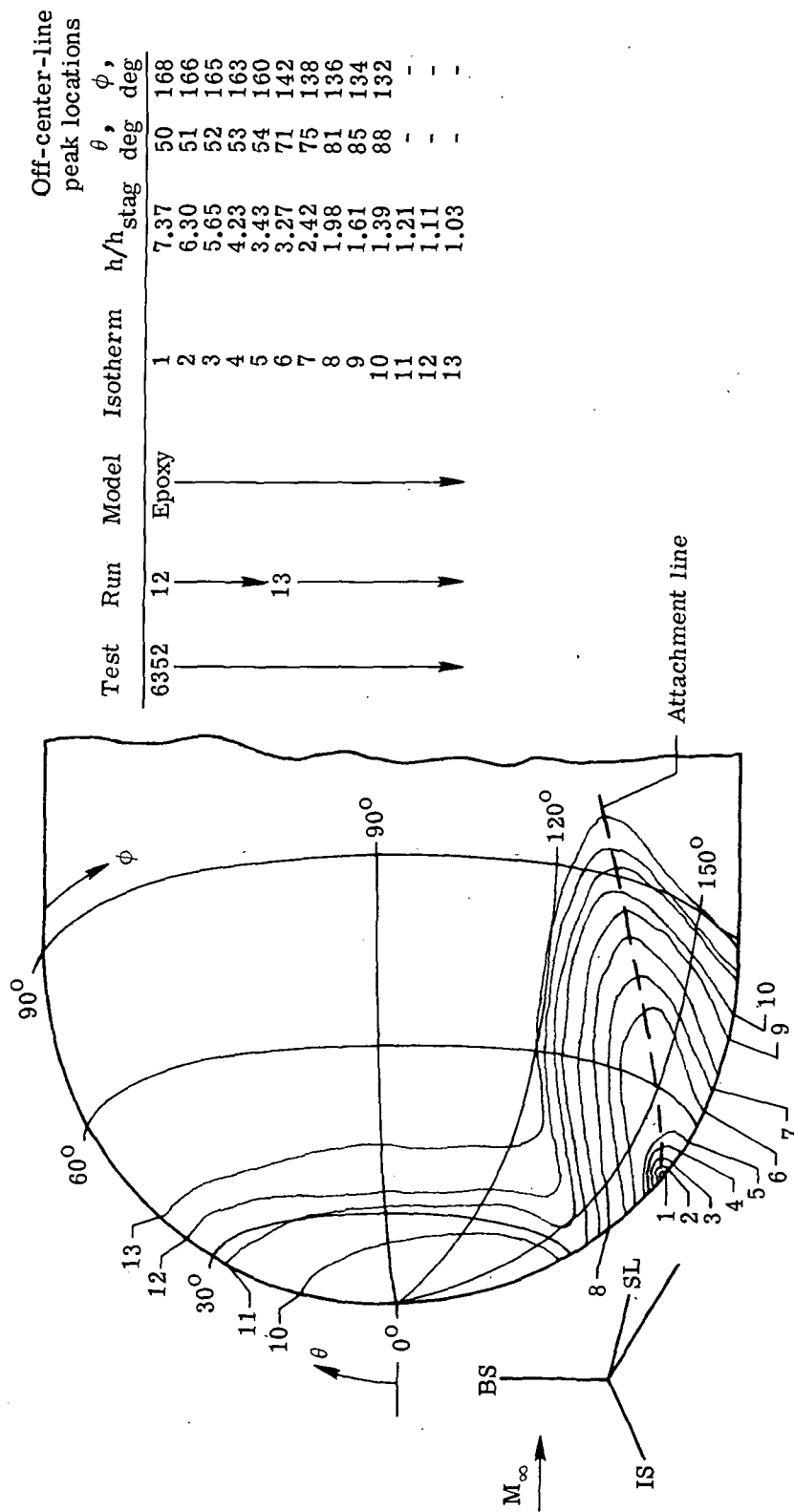
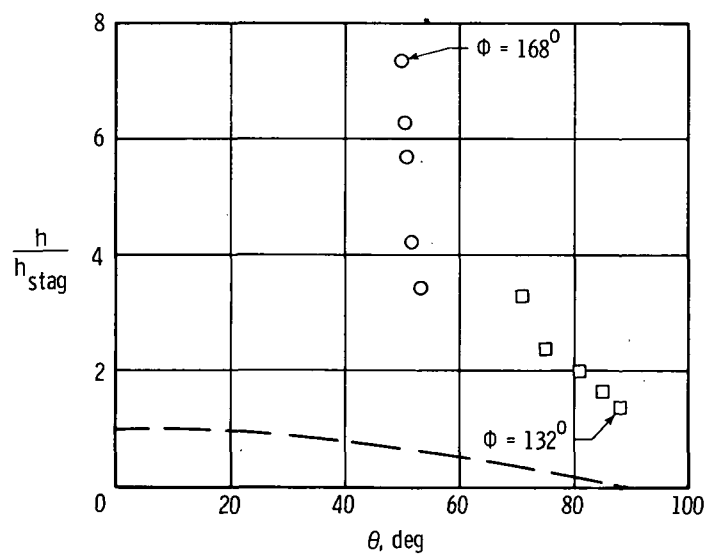| Test-run		$p_{t,\infty}$, N/cm^2	$T_{t,\infty}$, K	T_w, K	h_{stag}, W/m^2-K	θ_i, deg
6352 - 25	○	84	473	422	306.42	24.6
6352 - 26	□	83	476	394	306.42	24.6

——— Fairing
— — — No interference

$\theta_{pk} = -52^0$

$\theta_{SL} = 42^0$

$\frac{h}{h_{stag}}$

12

10

8

6

4

2

0

-100 -80 -60 -40 -20 0 20 40 60 80

Nose

$\Phi = 180^0$ $\Phi = 0^0$

θ, deg

(b) Center-line heat-transfer distribution.

$\frac{h}{h_{stag}}$

10

8

6

4

2

0

20 40 60 80 100

$\Phi = 170^0$

$\Phi = 119^0$

θ, deg
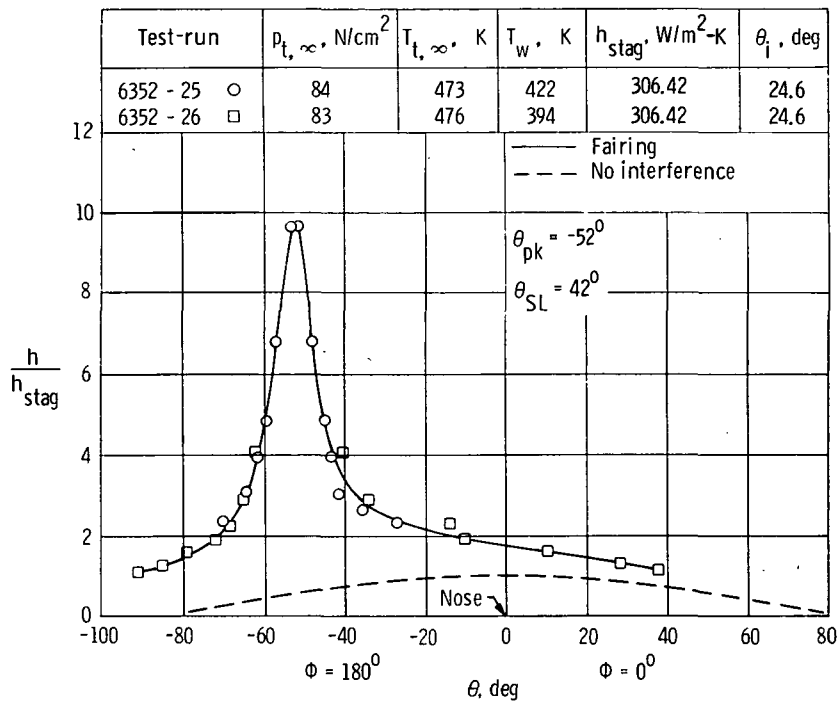
(c) Off-center-line peak heating.

Figure 10.- Concluded.

Test	Run	Model	Isotherm	h/h_{stag}	Off-center-line peak locations	
					θ, deg	ϕ, deg
6363	36	Steel	1	13.87	47	165
	37	Epoxy	2	11.33	48	161
			3	8.77	49	155
			4	4.80	53	145
			5	3.39	55	141
			6	2.77	56	139
			7	2.51	58	137
			8	2.15	61	135
			9	1.99	65	130
			10	1.86	67	129
			11	1.70	68	128
			12	1.52	69	127
			13	1.39	70	126
			14	1.18	72	125
			15	1.07	73	124

(a) Heating contours. $h_{stag} = 592.41 \ W/m^2\text{-}K$.

Figure 11.- Type III interference on a 5.08-cm-diameter hemisphere at Mach 6 in air. $\theta_i = 14.8^{\circ}$; $N_{Re,\infty}/m = 25.9 \times 10^6$.
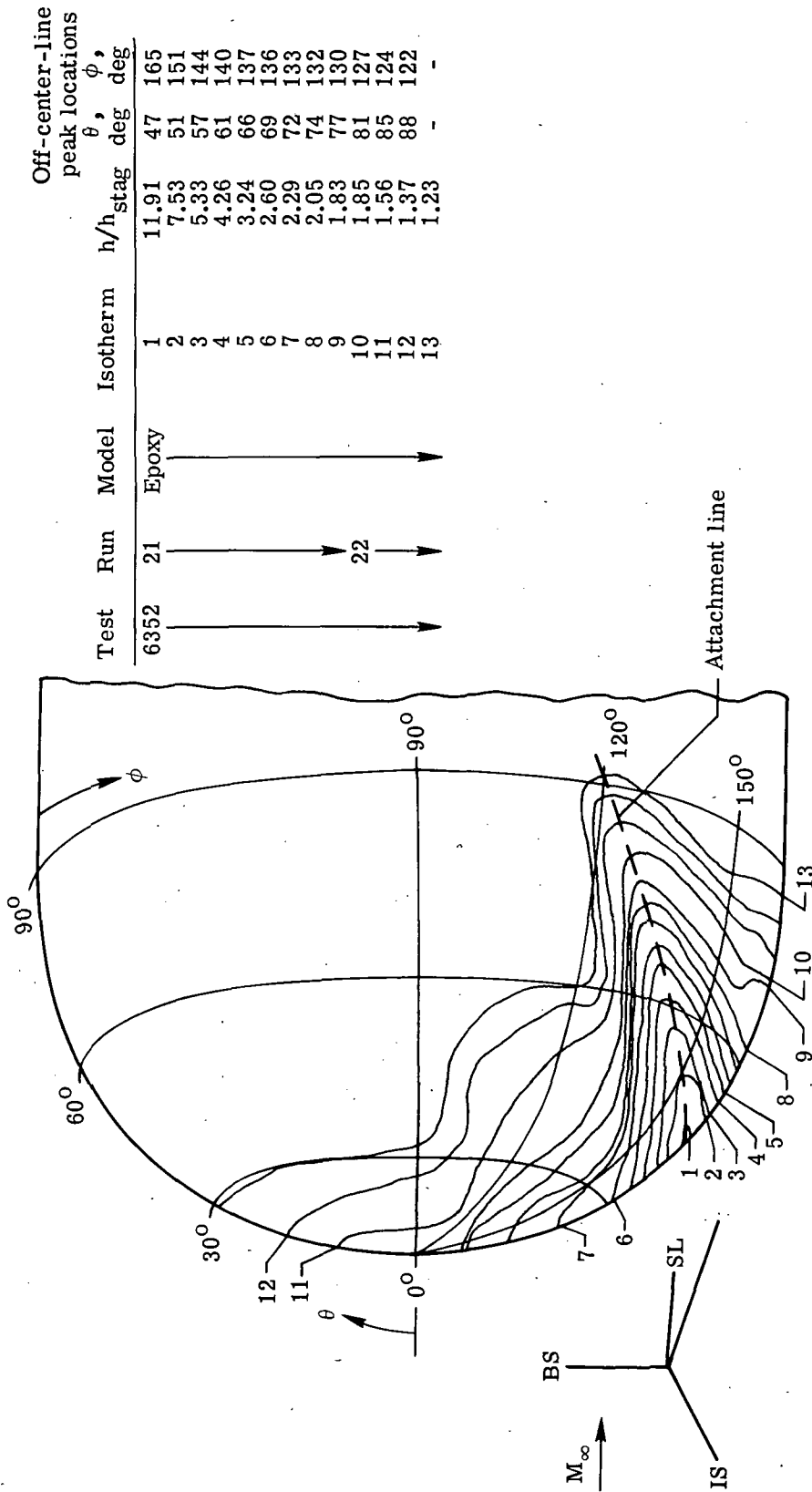
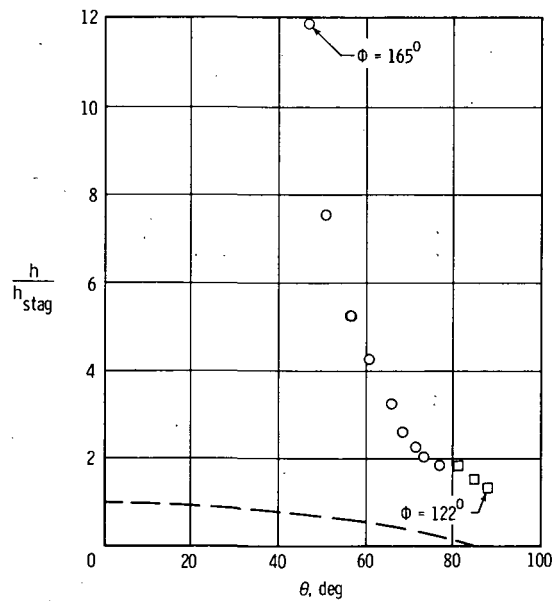| Test-run		$p_{t,\infty}$, N/cm^2	$T_{t,\infty}$, K	T_w, K	h_{stag}, W/m^2-K	θ_i, deg
6363 - 36	O	289	486	408	592.81	14.8
6363 - 37	□	292	488	436	592.81	14.8
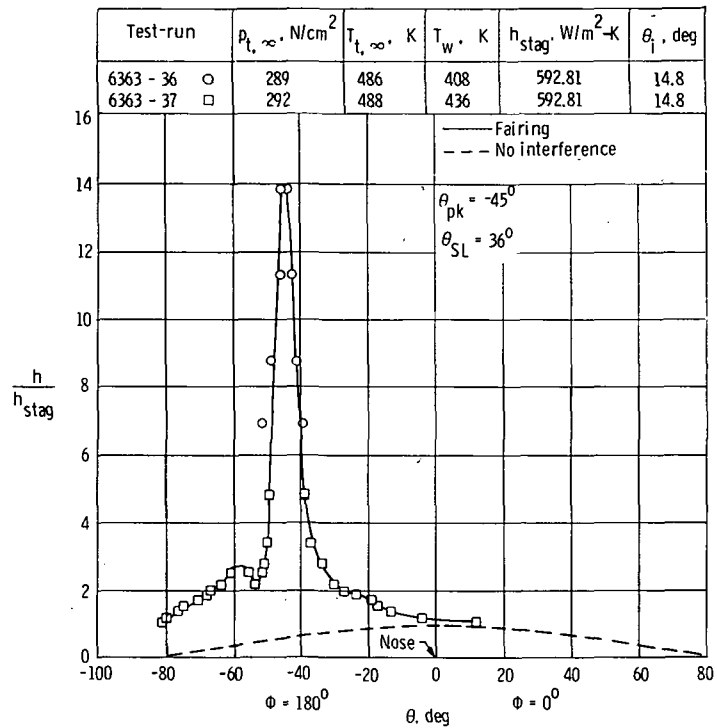
(b) Center-line heat-transfer distribution.
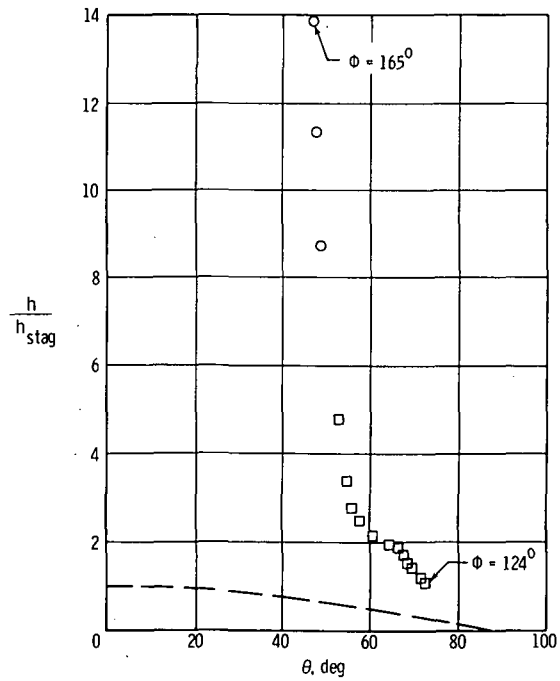
(c) Off-center-line peak heating.

Figure 11.- Concluded.

Test	Run	Model	Isotherm	h/h_{stag}	Off-center-line peak locations θ, deg	ϕ, deg
6363	40	Epoxy	1	7.80	51	163
	39		2	5.51	54	153
			3	3.90	57	145
			4	2.60	62	139
			5	1.74	68	135
			6	2.11	76	129
			7	1.58	79	127
			8	1.18	82	126
			9	0.96	-	-
			10	0.90	85	123
			11	0.80	87	122

(a) Heating contours. h_{stag} = 571.98 W/m^2-K.

Figure 12.- Type III interference on a 5.08-cm-diameter hemisphere at Mach 6 in air. $\theta_i = 14.8°$; $N_{Re,\infty}/m = 25.8 \times 10^6$.
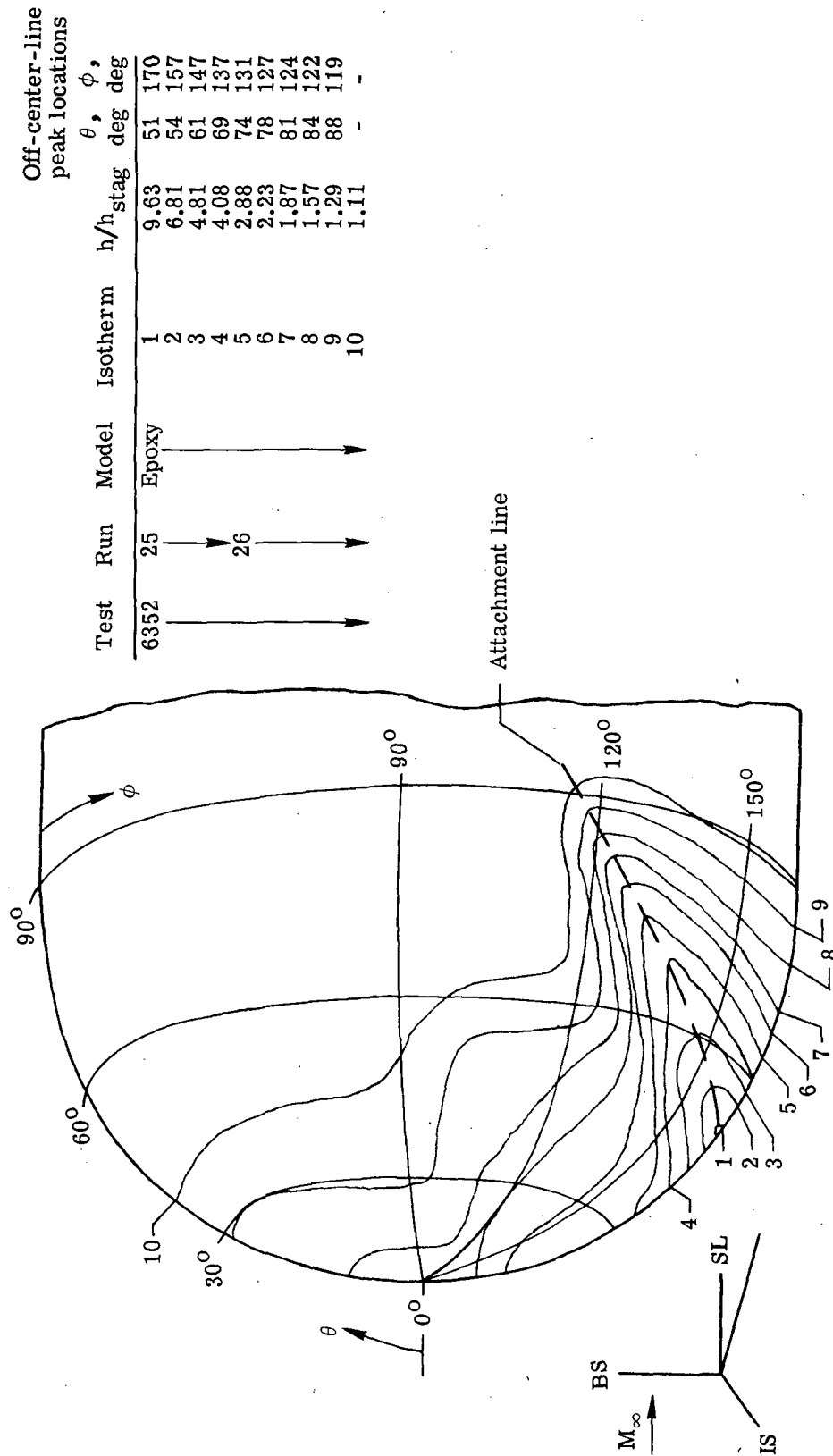
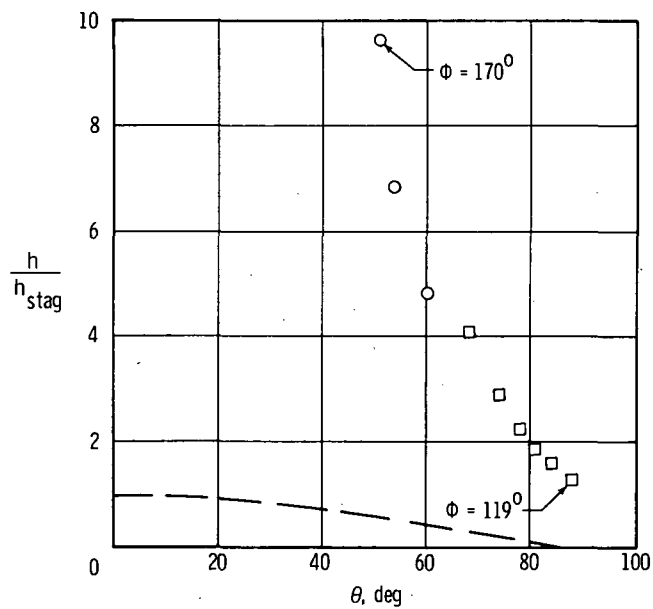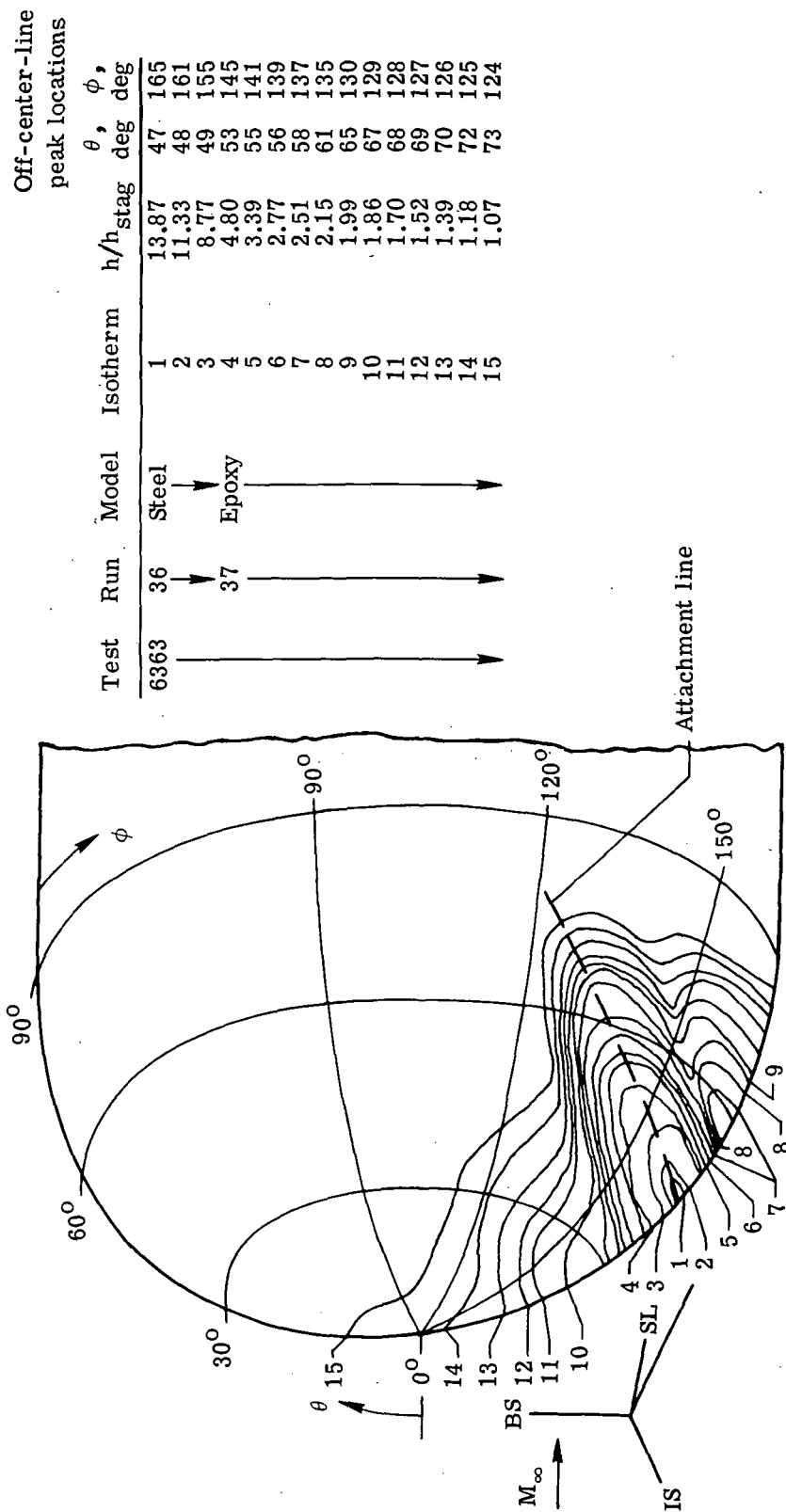| Test-run		$p_{t,\infty}$, N/cm^2	$T_{t,\infty}$, K	T_w, K	h_{stag}, W/m^2-K	θ_i, deg
6363 - 40	O	290	489	436	571.98	14.8
6363 - 39	□	290	486	408	571.98	14.8

———— Fairing
– – – No interference

$\theta_{pk} = -50^0$

$\theta_{SL} = 30^0$

$\dfrac{h}{h_{stag}}$

Nose

$\Phi = 180^0$ θ, deg $\Phi = 0^0$

(b) Center-line heat-transfer distribution.

$\dfrac{h}{h_{stag}}$

$\Phi = 163^0$

$\Phi = 122^0$

θ, deg
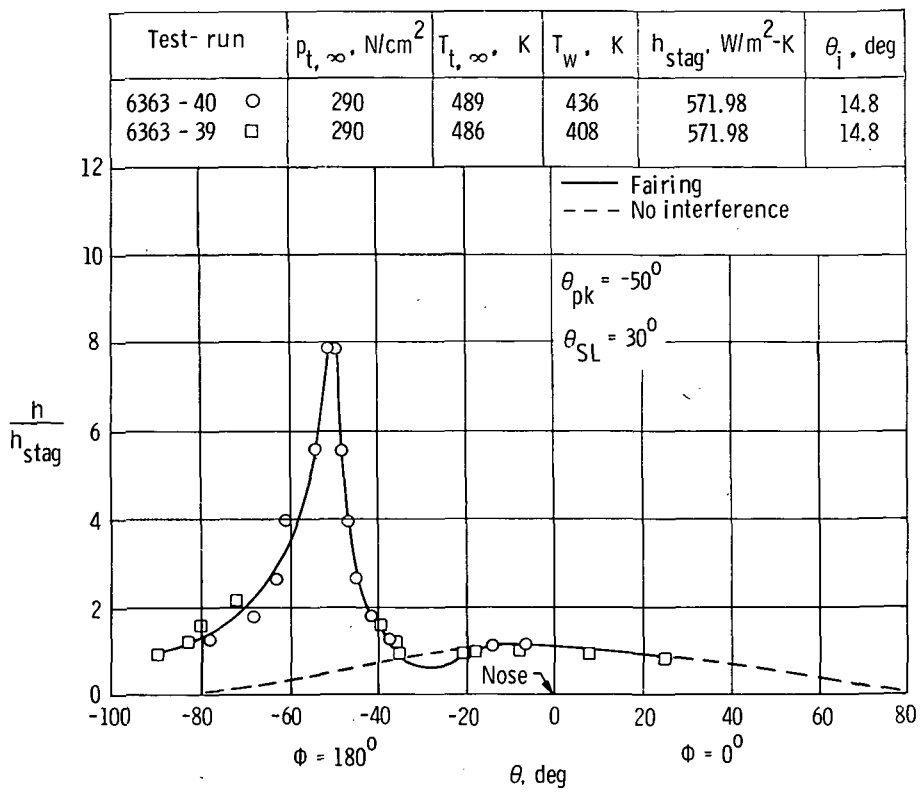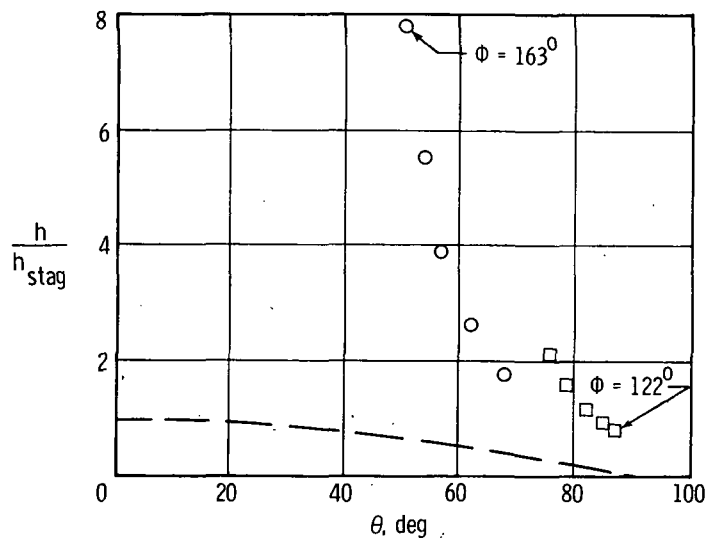
(c) Off-center-line peak heating.

Figure 12.- Concluded.

31

Test	Run	Model	Isotherm	h/h_{stag}	Off-center-line peak locations θ, deg	ϕ, deg
373	19	Steel	1	5.69	39	145
	20	Epoxy	2	3.14	41	142
			3	2.83	52	133
			4	1.60	54	132
			5	1.06	57	131
			6	0.82	60	128
			7	0.67	–	–
			8	0.54	–	–
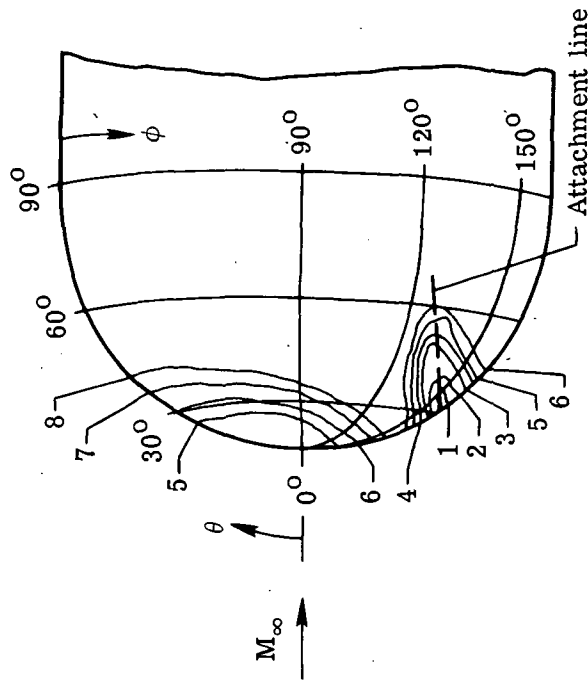
(a) Heating contours. $h_{stag} = 1205.25$ W/m^2-K.

Figure 13.- Type III interference on a 2.54-cm-diameter hemisphere at Mach 20.2 in helium.

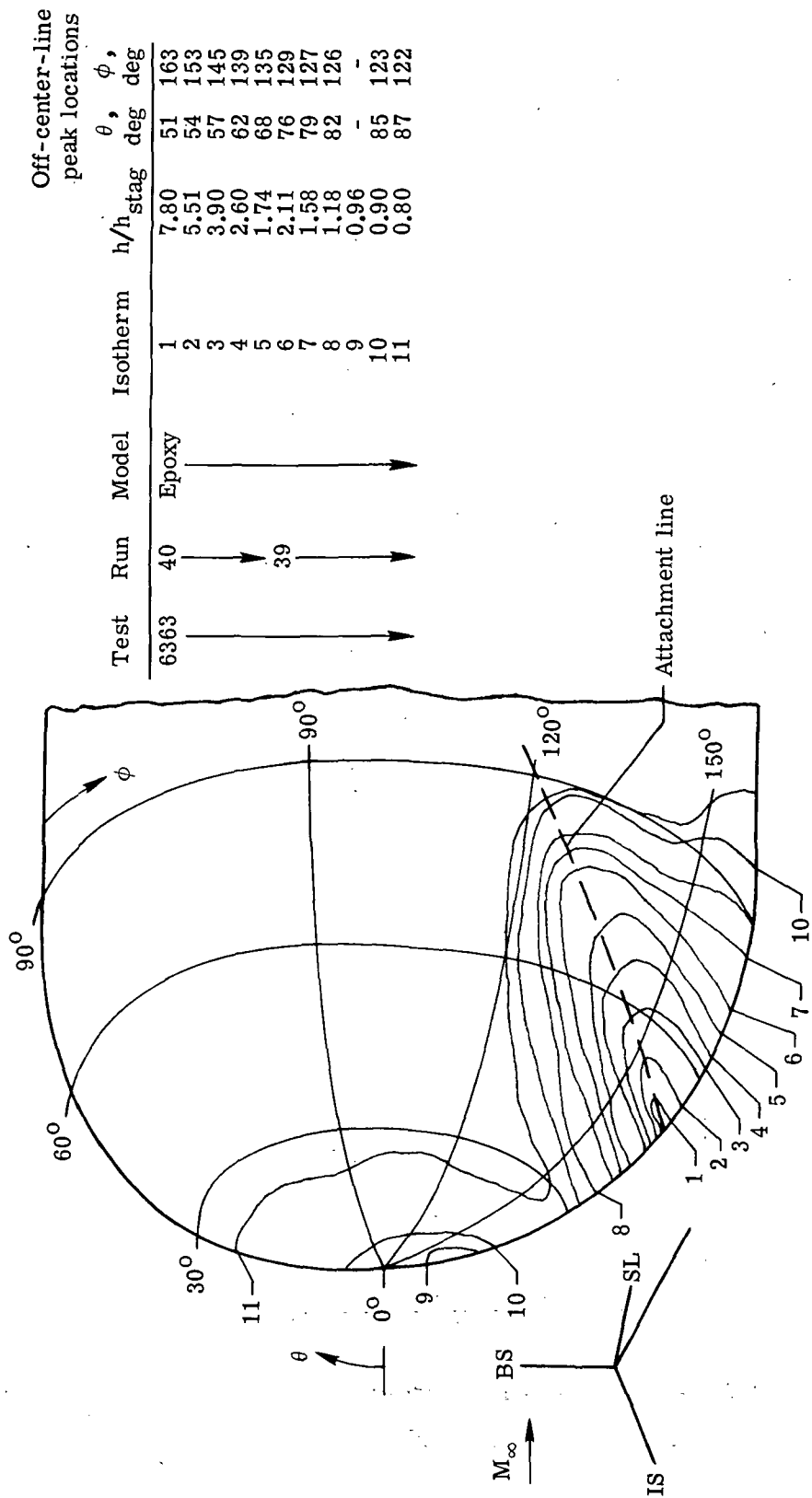$\theta_i = 5.1^\circ$; $N_{Re,\infty}/m = 9.9 \times 10^6$.

Test-run		$P_{t,\infty}$, N/cm^2	$T_{t,\infty}$, K	T_w, K	h_{stag}, W/m^2-K	θ_i, deg
373 - 19	○	704	428	381	1205.25	5.1
373 - 20	□	704	429	381	1205.25	5.1

——— Fairing
– – – No interference

$\theta_{pk} = -34^0$
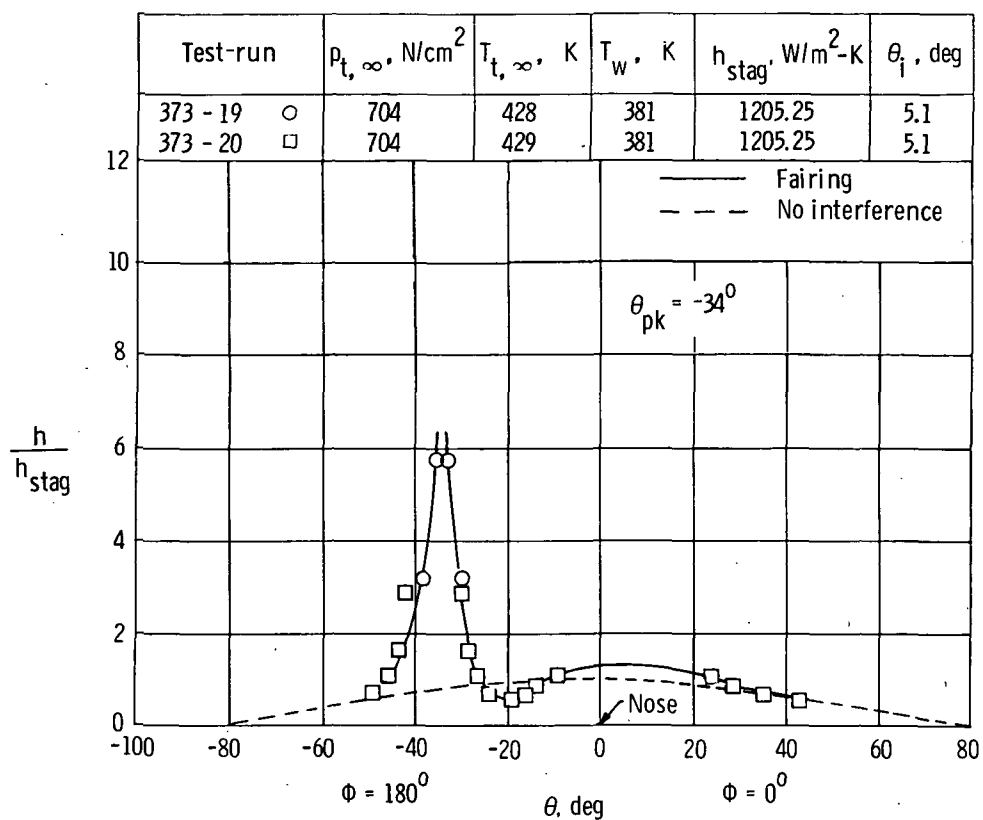
(b) Center-line heat-transfer distribution.
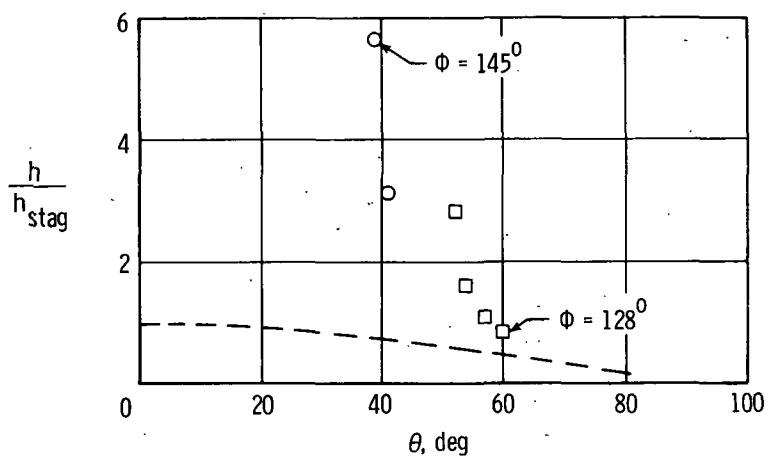
(c) Off-center-line peak heating.

Figure 13.- Concluded.

Test	Run	Model	Isotherm	h/h$_{stag}$	Off-center-line peak locations	
					θ, deg	ϕ, deg
373	22	Steel	1	2.53	46	164
	24	Epoxy	2	2.05	49	158
	23		3	1.25	55	152
			4	0.97	58	150
			5	0.82	64	145
			6	0.56	68	143
			7	0.45	69	142
			8	0.38	72	140
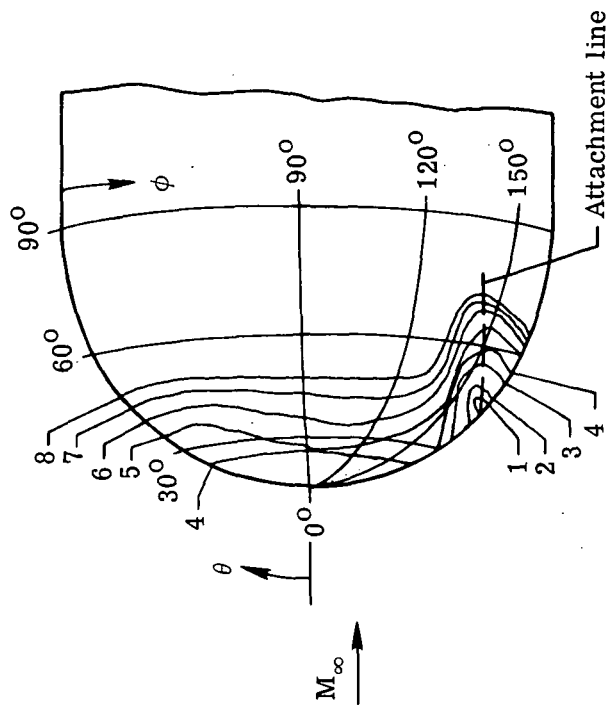
(a) Heating contours. $h_{stag} = 1205.25$ W/m^2-K.

Figure 14.- Type III interference on a 2.54-cm-diameter hemisphere at Mach 20.2 in helium.

$\theta_i = 5.1°$; $N_{Re,\infty}/m = 9.7 \times 10^6$.

Test-run		$p_{t,\infty}$, N/cm^2	$T_{t,\infty}$, K	T_w, K	h_{stag}, W/m^2-K	θ_i, deg
373 – 22	○	705	438	367	1205.25	5.1
373 – 23	□	707	434	367	1205.25	5.1
373 – 24	◇	703	429	381	1205.25	5.1

——— Fairing
— — — No interference
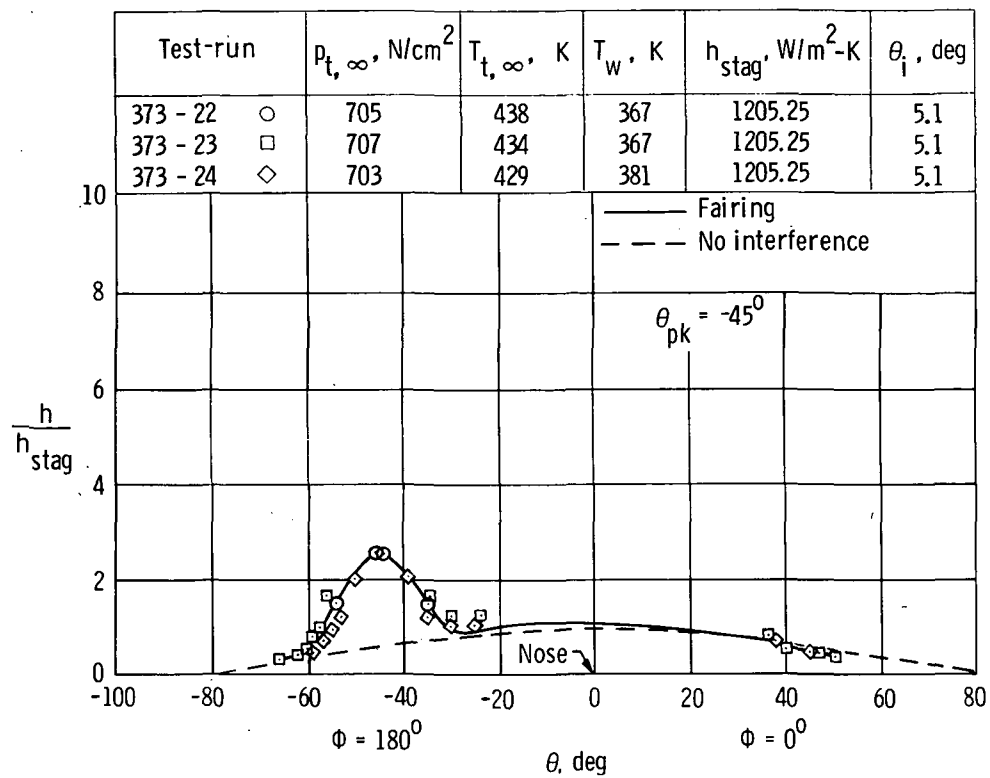
(b) Center-line heat-transfer distribution.
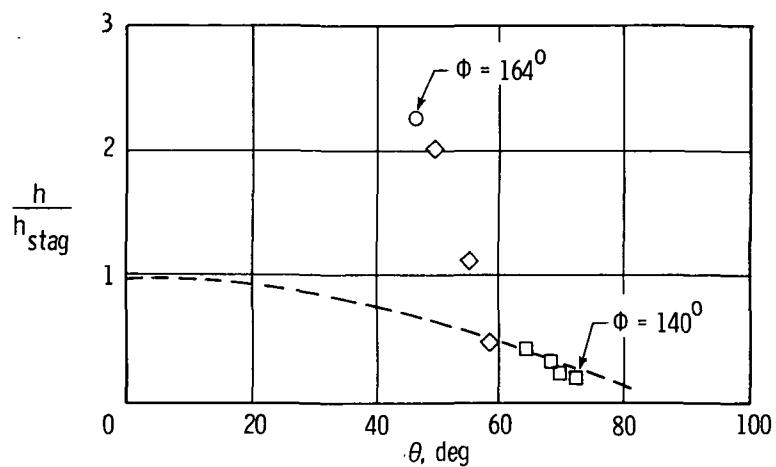
(c) Off-center-line peak heating.

Figure 14.- Concluded.

Test	Run	Model	Isotherm	h/h_{stag}	Off-center-line peak locations θ, deg	ϕ, deg
373	26	Steel	1	8.12	37	139
	11	Epoxy	2	5.04	40	132
	12		3	3.04	42	130
			4	1.36	47	123
			5	0.59	54	118
			6	0.37	62	114
			7	0.31	72	109
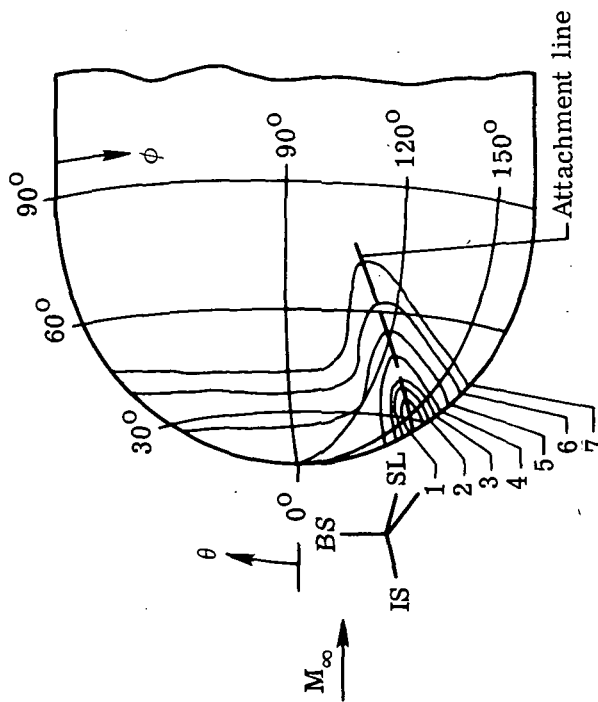
(a) Heating contours. h_{stag} = 1205.25 W/m^2-K.

$\theta_i = 10^\circ$; $N_{Re,\infty}/m = 9.8 \times 10^6$.

Figure 15.- Type III interference on a 2.54-cm-diameter hemisphere at Mach 20.2 in helium.

Test-run		$p_{t,\infty}$, N/cm^2	$T_{t,\infty}$, K	T_w, K	h_{stag}, W/m^2-K	θ_i, deg
373 – 26	○	707	436	381	1205.25	10.1
373 – 11	□	705	431	381	1205.25	- 10.1
373 – 12	◇	705	435	367	1205.25	10.1

Fairing ———
No interference — — —

$\theta_{pk} = -28^0$

$\theta_{SL} = 42^0$

Nose

$\Phi = 180^0$ θ, deg $\Phi = 0^0$

(b) Center-line heat-transfer distribution.

$\Phi = 139^0$

$\Phi = 109^0$

θ, deg

(c) Off-center-line peak heating.

Figure 15.- Concluded.

Off-center-line peak locations

Test	Run	Model	Isotherm	h/h_{stag}	θ, deg	ϕ, deg
373	8	Steel	1	5.82	38	149
	9	Epoxy	2	3.03	42	140
			3	2.08	45	134
			4	1.40	48	130
			5	1.68	52	127
			6	0.87	54	125
			7	0.68	59	121
			8	0.55	65	118
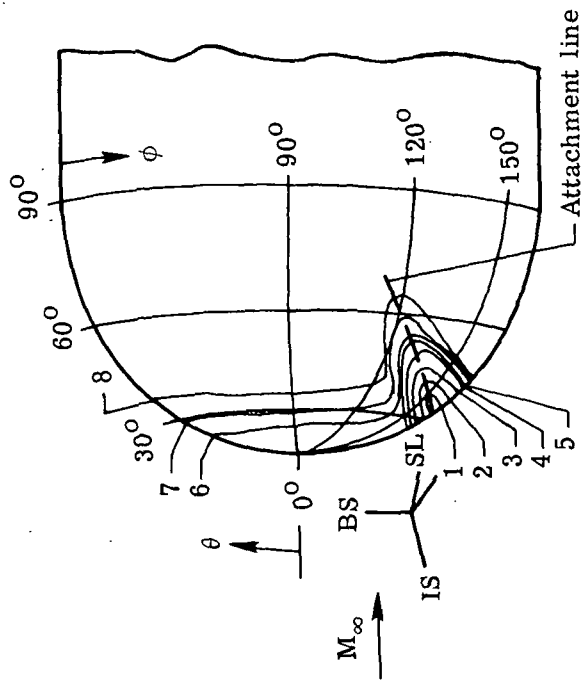
(a) Heating contours. $h_{stag} = 1205.25$ W/m^2-K.

Figure 16. - Type III interference on a 2.54-cm-diameter hemisphere at Mach 20.2 in helium.
$\theta_i = 10^{\circ}$; $N_{Re,\infty}/m = 9.7 \times 10^6$.

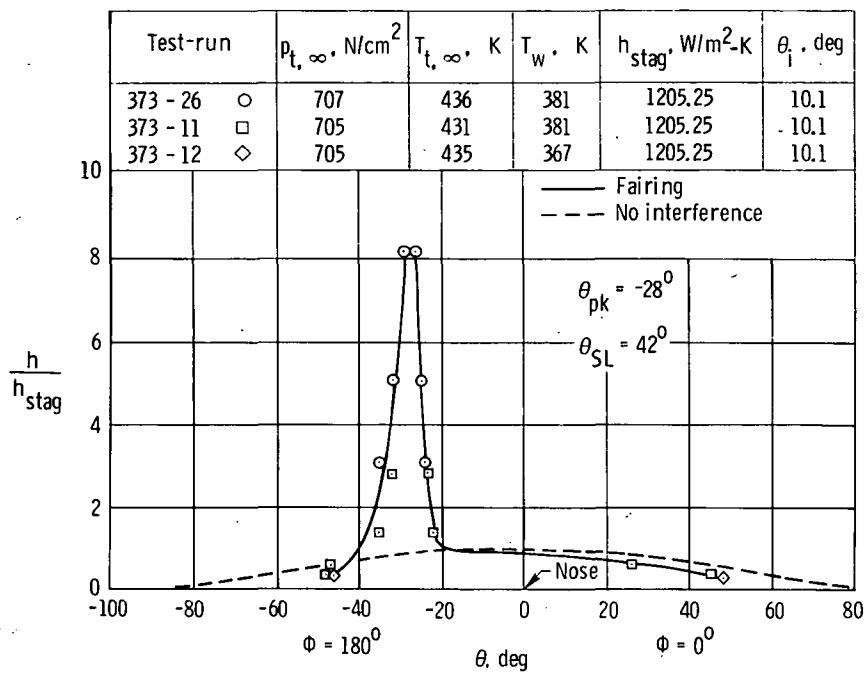| Test-run		$p_{t,\infty}$, N/cm^2	$T_{t,\infty}$, K	T_w, K	h_{stag}, W/m^2-K	θ_i, deg
373-8	○	706	434	367	1205.25	10.1
373-9	□	707	434	381	1205.25	10.1

——— Fairing
– – – No interference

$\theta_{pk} = -34^0$

$\theta_{SL} = 42^0$

Nose

$\dfrac{h}{h_{stag}}$

θ, deg

$\Phi = 180^0$ $\Phi = 0^0$

(b) Center-line heat-transfer distribution.

$\dfrac{h}{h_{stag}}$

$\Phi = 149^0$

$\Phi = 118^0$

θ, deg
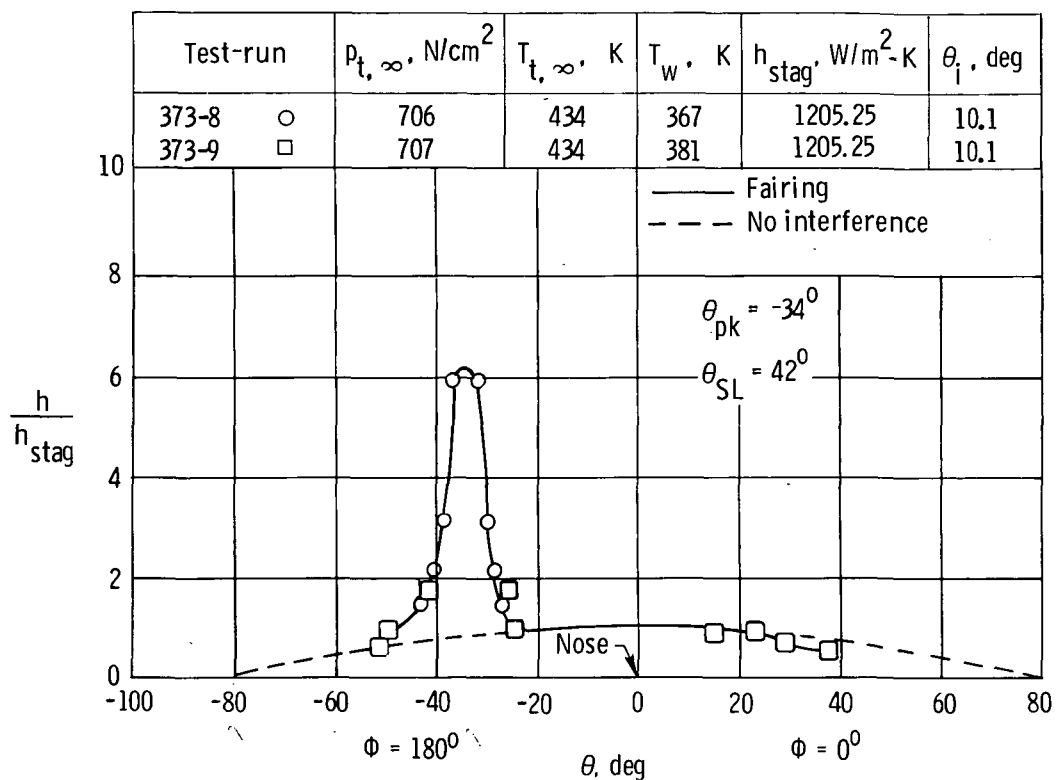
(c) Off-center-line peak heating.

Figure 16.- Concluded.

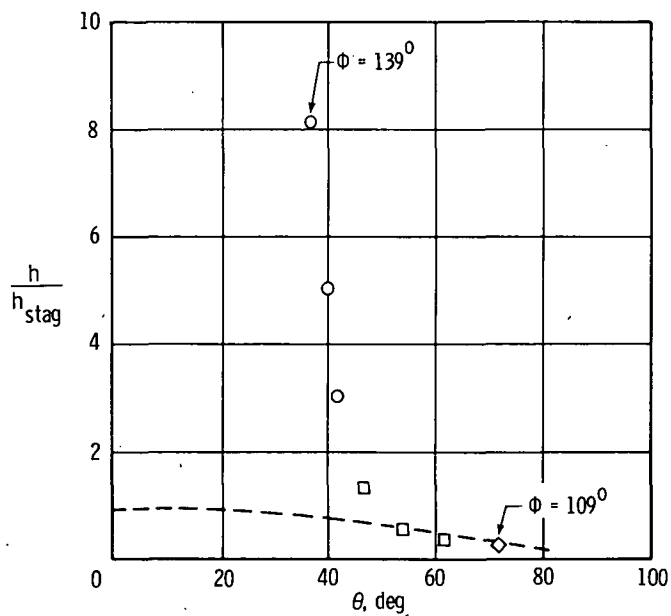| Test	Run	Model	Isotherm	h/h_{stag}	Off-center-line peak locations	
					θ, deg	ϕ, deg
373	5 → 6	Steel → Epoxy →	1	6.84	34	150
			2	4.59	39	136
			3	2.58	47	127
			4	1.47	51	125
			5	0.88	56	121
			6	0.59	63	117
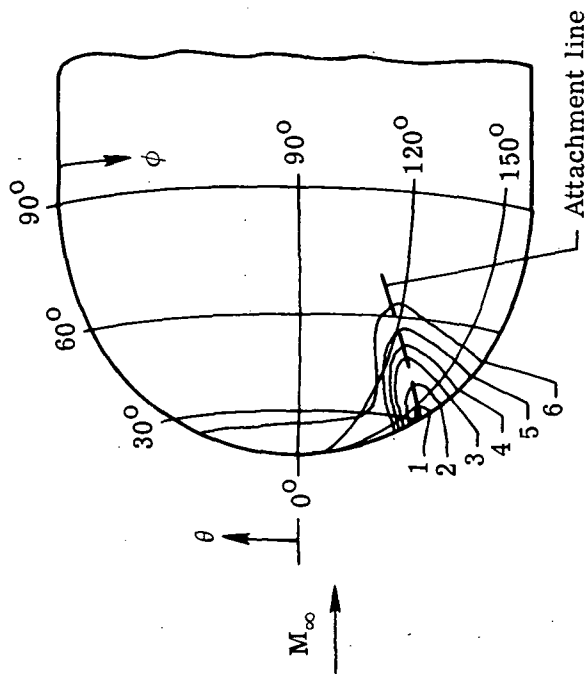
(a) Heating contours. h_{stag} = 1205.25 W/m²-K.

Figure 17.- Type III interference on a 2.54-cm-diameter hemisphere at Mach 20.2 in helium. $\theta_i = 15°$; $N_{Re,\infty}/m = 9.8 \times 10^6$.

Test-run		$p_{t,\infty}$, N/cm^2	$T_{t,\infty}$, K	T_w, K	h_{stag}, W/m^2-K	θ_i, deg
373-5	○	705	434	394	1205.25	15.1
373-6	□	708	432	381	1205.25	15.1

——— Fairing
– – – No interference

$\theta_{pk} = -32^0$

$\theta_{SL} = 40^0$
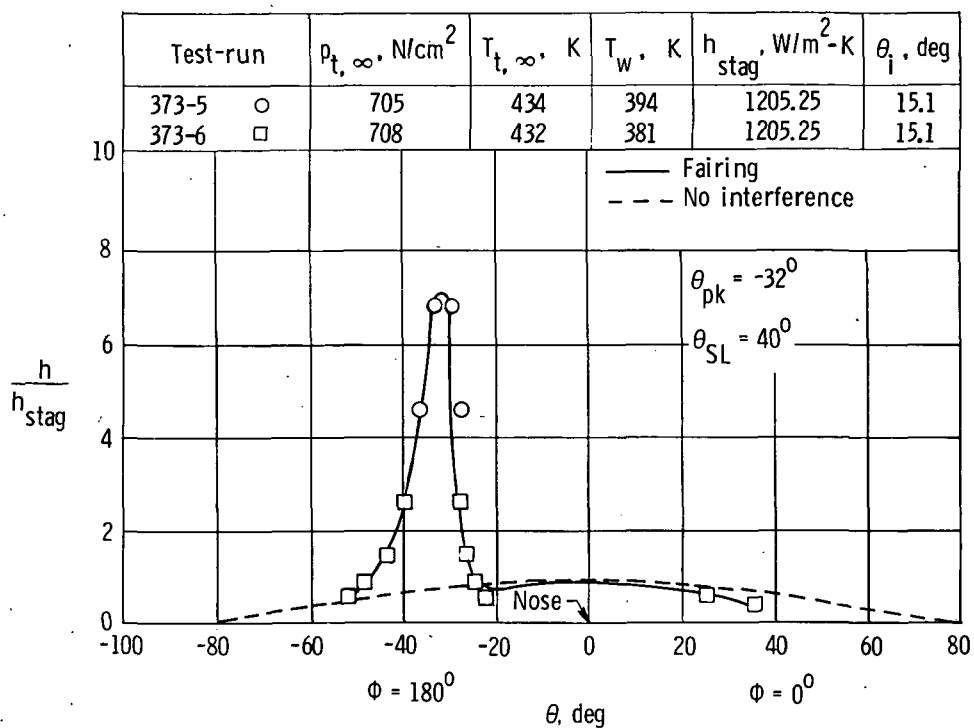
(b) Center-line heat-transfer distribution.

(c) Off-center-line peak heating.

Figure 17.- Concluded.

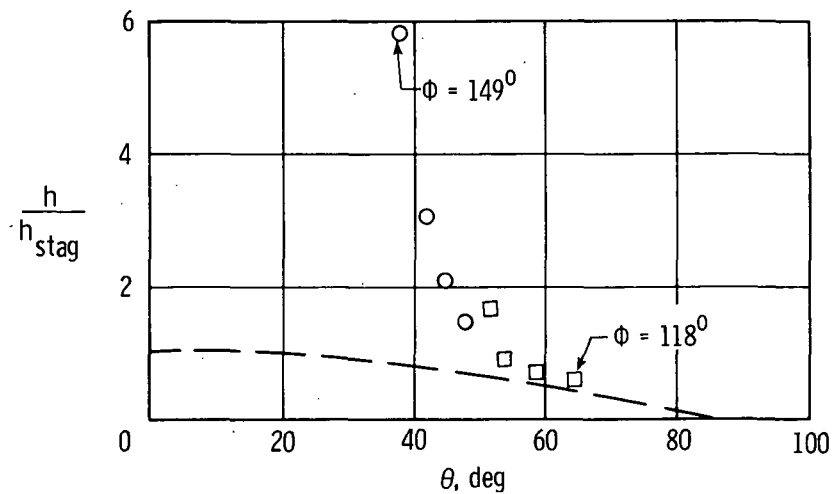| Test	Run	Model	Isotherm	h/h_{stag}	θ, deg	ϕ, deg
373	2	Steel	1	7.48	51	159
	3	Epoxy	2	4.93	57	149
			3	2.11	63	140
			4	1.73	66	137
			5	1.37	72	134
			6	0.99	80	130
			7	0.76	85	127
			8	0.64	–	–
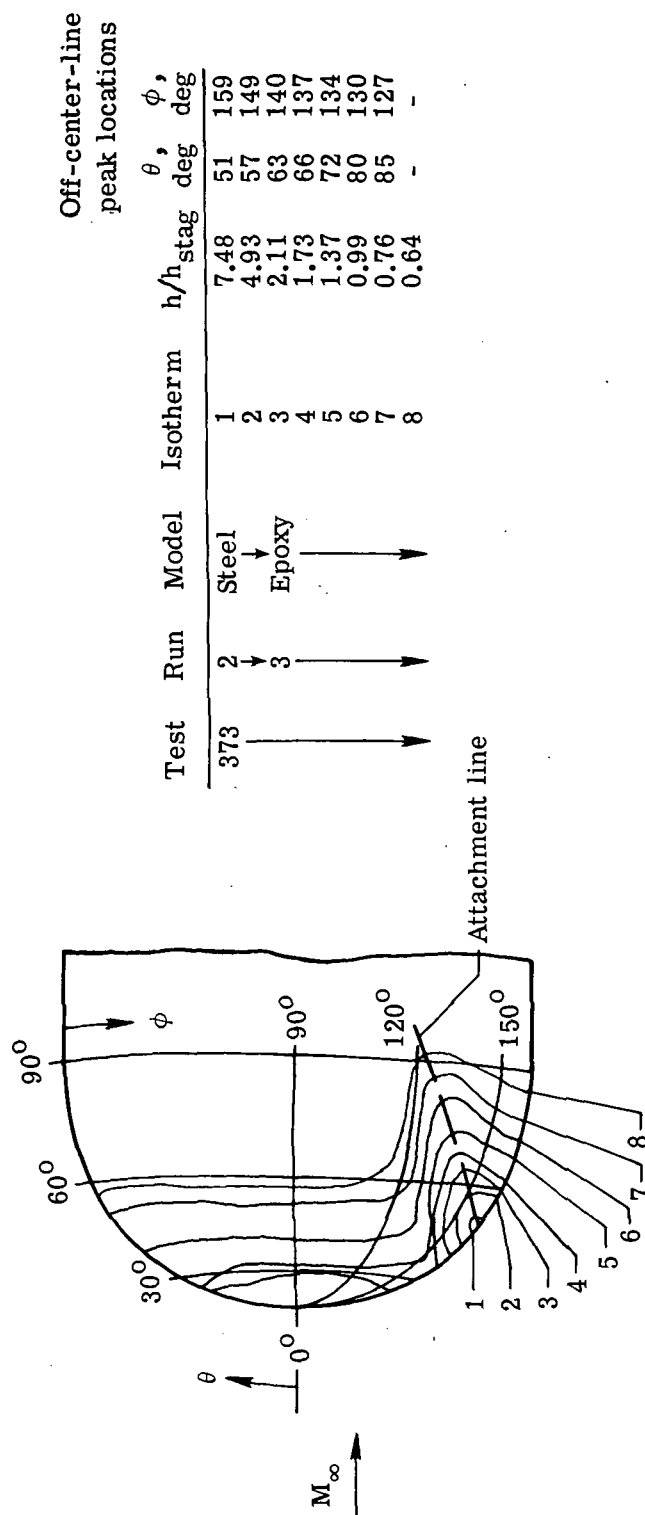
(a) Heating contours. $h_{stag} = 1205.25$ W/m^2-K.

Figure 18.- Type III interference on a 2.54-cm-diameter hemisphere at Mach 20.2 in air. $\theta_i = 15^\circ$; $N_{Re,\infty}/m = 9.8 \times 10^6$.

Test-run		$P_{t,\infty}$, N/cm^2	$T_{t,\infty}$, K	T_w, K	h_{stag}, W/m^2-K	θ_i, deg
373-2	O	705	432	394	1205.25	15.1
373-3	□	703	432	394	1205.25	15.1

——— Fairing
— — — No interference

$\theta_{pk} = -50^0$

$\theta_{SL} = 40^0$

Nose

$\Phi = 180^0$ $\Phi = 0^0$

θ, deg

(b) Center-line heat-transfer distribution.

$\Phi = 159^0$

$\Phi = 127^0$

θ, deg
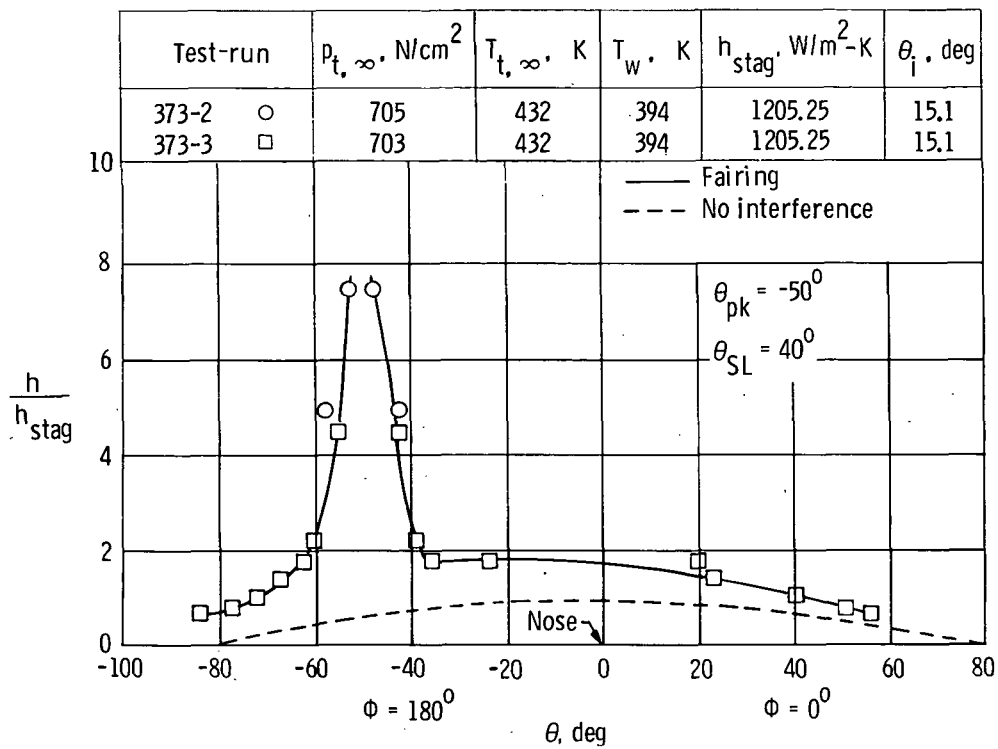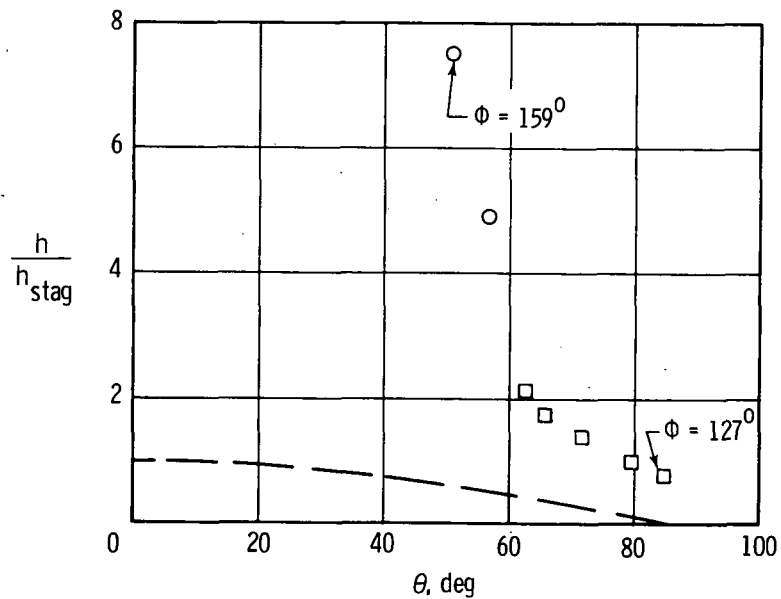
(c) Off-center-line peak heating.

Figure 18.- Concluded.
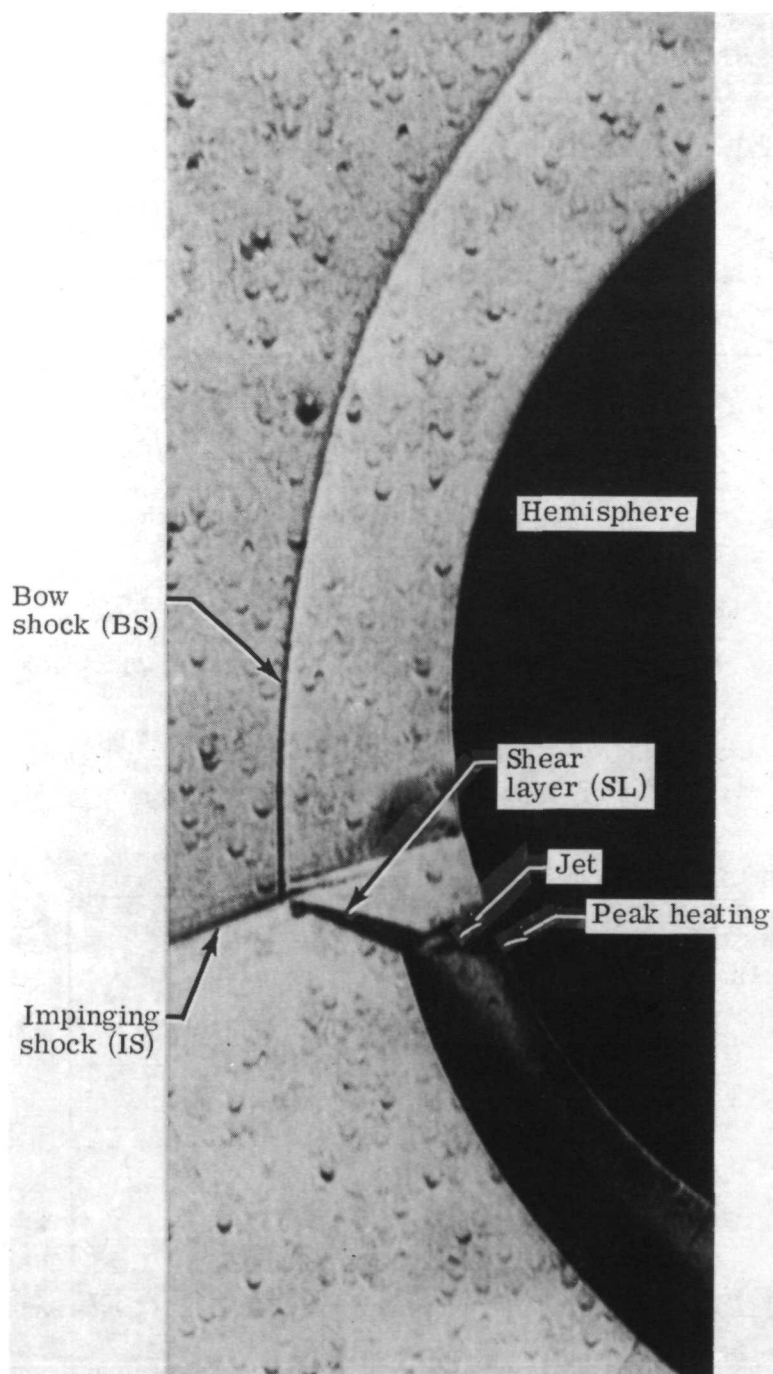
43

(a) Schlieren photograph.

Figure 19.- Shock and oil-flow patterns on a 5.08-cm-diameter hemisphere at Mach 6 in air. $\theta_i = 14.8^O$; $N_{Re,\infty}/m = 25.7 \times 10^6$.

$\mathbb{C}$

Jet impingement

(b) Oil-flow pattern.

L-73-6874

Figure 19.- Concluded.

Test	Run	Model	Isotherm	h/h_{stag}	Off-center-line peak locations θ, deg	ϕ, deg
6363	48	Epoxy	1	7.80	15	120
			2	4.77	18	113
			3	3.61	26	105
			4	2.76	36	100
			5	2.34	39	99
			6	2.20	44	98
			7	1.82	49	97
			8	1.64	52	96
			9	1.44	54	96
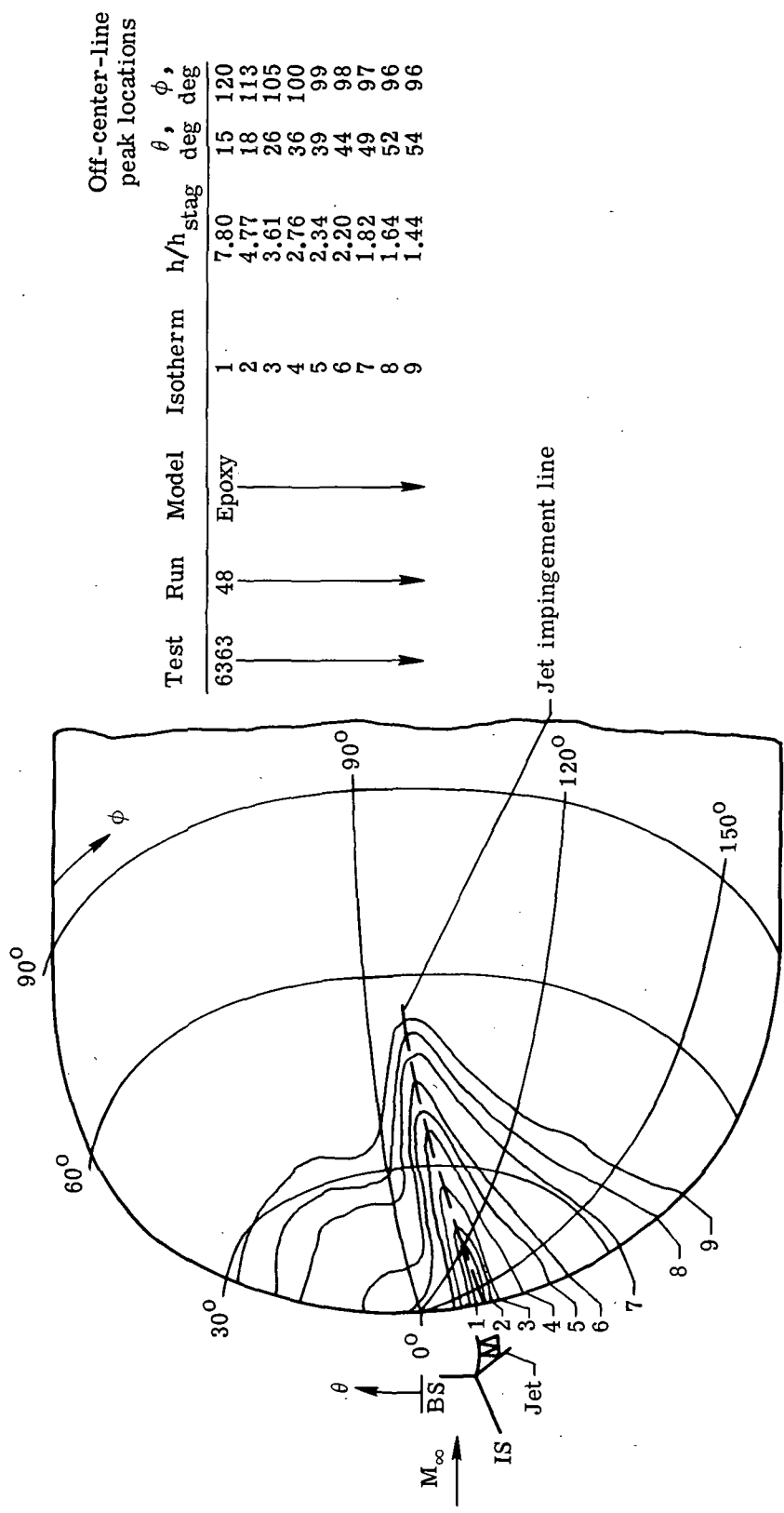
(a) Heating contours. h_{stag} = 306.42 W/m^2-K.
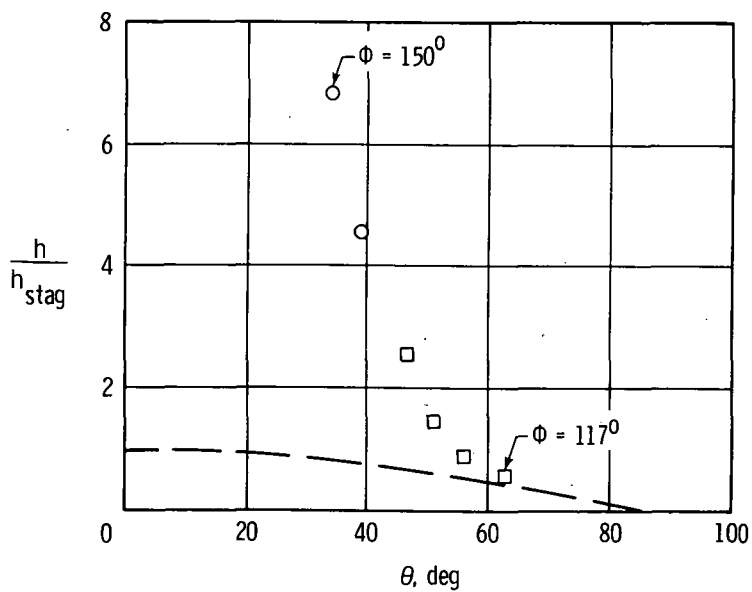
Figure 20. - Type IV interference on a 5.08-cm-diameter hemisphere at Mach 5.94 in air.

$\theta_i = 5°$; $N_{Re,\infty}/m = 7.6 \times 10^6$.

Test-run		$p_{t,\infty}$, N/cm^2	$T_{t,\infty}$, K	T_w, K	h_{stag}, W/m^2-K	θ_i, deg
6363 - 48	○	82	476	422	306.42	5.0

——— Fairing
— — — No interference

$\theta_{pk} = -10^0$

Nose

$\dfrac{h}{h_{stag}}$

θ, deg

$\Phi = 180^0$ $\Phi = 0^0$

(b) Center-line heat-transfer distribution.

$\dfrac{h}{h_{stag}}$

$\Phi = 120^0$

$\Phi = 96^0$

θ, deg
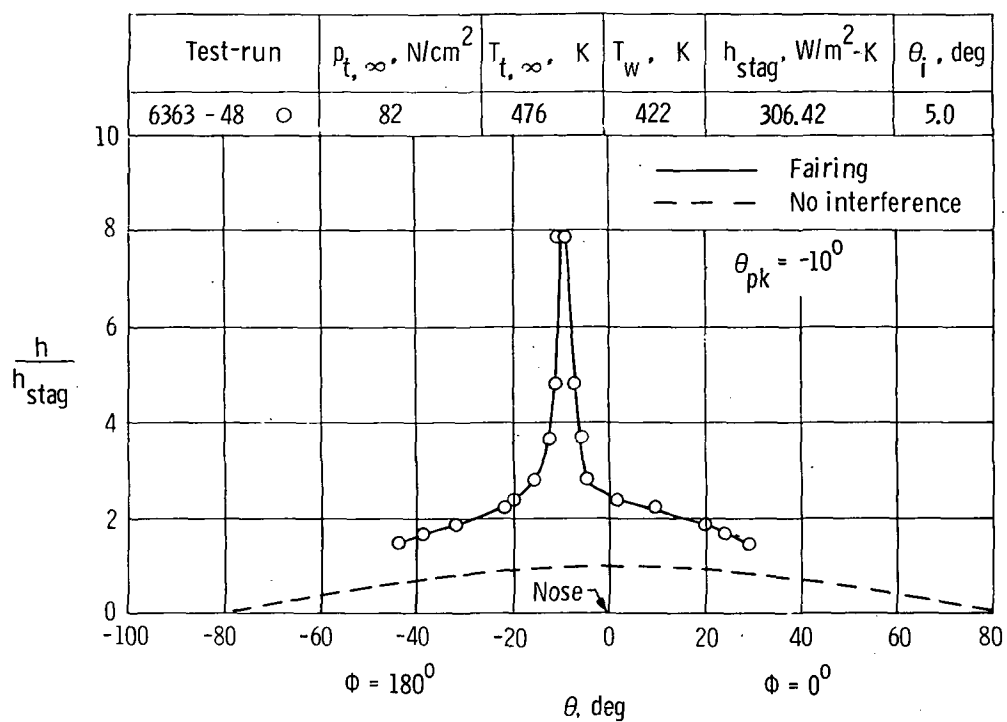
(c) Off-center-line peak heating.

Figure 20.- Concluded.

Off-center-line peak locations

Test	Run	Model	Isotherm	h/h_{stag}	θ, deg	ϕ, deg
6352	14	Epoxy	1	12.20	29	170
	15		2	9.18	32	160
			3	7.11	34	154
			4	5.06	39	140
			5	4.57	52	125
			6	3.88	-	-
			7	3.58	57	122
			8	3.20	59	120
			9	2.53	62	119
			10	2.05	65	117
			11	1.78	69	115
			12	1.52	72	114
			13	1.30	76	112
			14	1.13	79	111
			15	1.01	81	110
			16	0.88	85	108

(a) Heating contours. $h_{stag} = 306.42$ W/m^2-K.

Figure 21.- Type IV interference on a 5.08-cm-diameter hemisphere at Mach 5.94 in air. $\theta_i = 9.8°$; $N_{Re,\infty}/m = 8.0 \times 10^6$.

Test-run		$p_{t,\infty}$, N/cm^2	$T_{t,\infty}$, K	T_w, K	h_{stag}, W/m^2-K	θ_i, deg
6352 - 14	○	83	468	436	306.42	9.9
6352 - 15	□	86	472	394	306.42	9.9
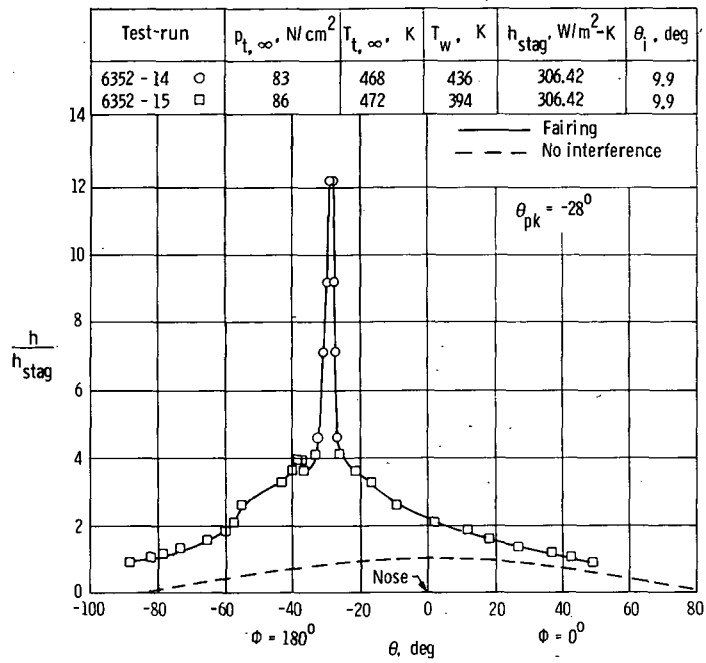
(b) Center-line heat-transfer distribution.

(c) Off-center-line peak heating.

Figure 21.- Concluded.

49

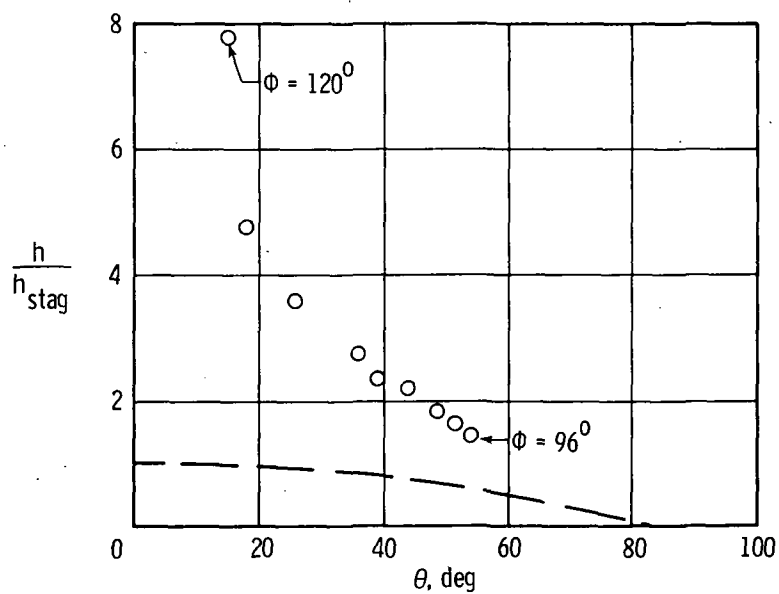| Test	Run	Model	Isotherm	h/h_{stag}	Off-center-line peak locations	
					θ, deg	ϕ, deg
6352	27	Epoxy	1	16.91	22	157
	28		2	13.09	25	140
			3	8.28	35	123
			4	5.86	42	115
			5	4.60	45	112
			6	3.24	57	106
			7	2.64	60	105
			8	2.05	62	104
			9	1.61	68	103
			10	1.38	71	102

(a) Heating contours. $h_{stag} = 306.42$ W/m^2-K.

Figure 22. - Type IV interference on a 5.08-cm-diameter hemisphere at Mach 5.94 in air.
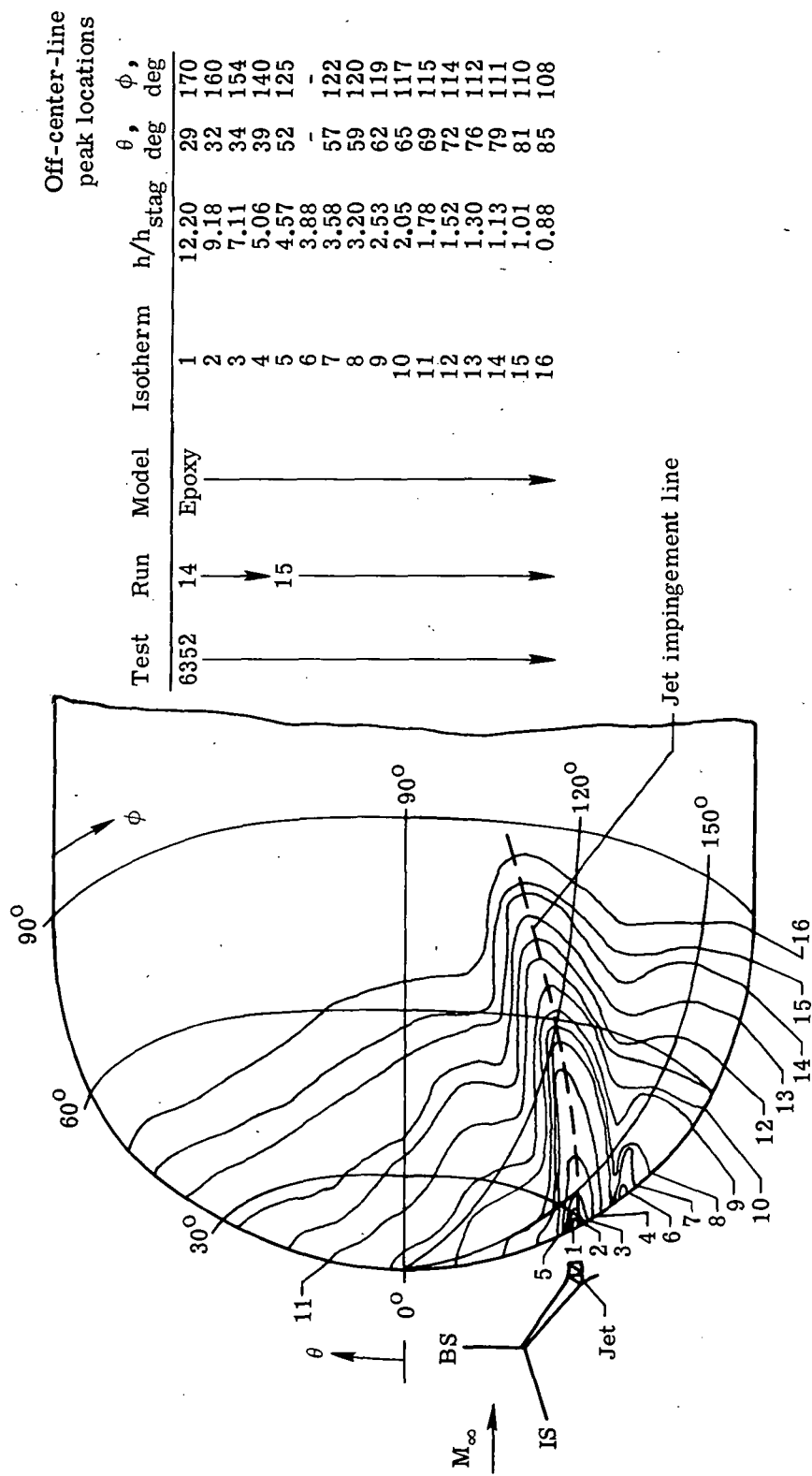
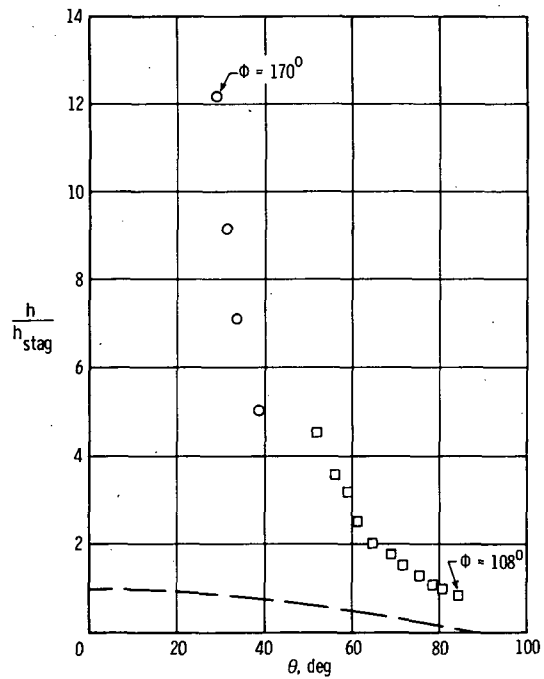$\theta_i = 14.8°$; $N_{Re,\infty}/m = 7.5 \times 10^6$.

Test-run		$p_{t,\infty}$, N/cm^2	$T_{t,\infty}$, K	T_w, K	h_{stag}, W/m^2-K	θ_i, deg
6352 - 27	O	84	493	450	306.42	14.8
6352 - 28	□	83	478	394	306.42	14.8

Fairing
— — — No interference

$\theta_{pk} = -21^0$

(b) Center-line heat-transfer distribution.

$\Phi = 157^0$

$\Phi = 102^0$
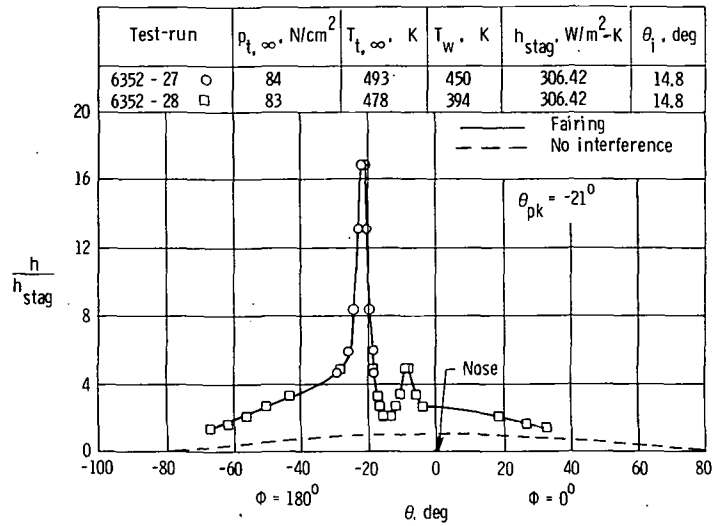
(c) Off-center-line peak heating.

Figure 22.- Concluded.

Off-center-line
peak locations

Test	Run	Model	Isotherm	h/h_{stag}	θ, deg	ϕ, deg
6352	29	Epoxy	1	14.62	41	166
	8		2	11.05	43	160
	9		3	10.76	44	158
			4	7.42	48	150
			5	5.31	49	147
			6	5.10	52	143
			7	3.76	57	137
			8	3.61	65	132
			9	2.52	72	126
			10	2.06	79	122
			11	1.79	82	121
			12	1.60	83	120
			13	1.47	87	119
			14	1.31	88	118
			15	1.20	-	-
			16	1.13	-	-
			17	1.03	-	-

(a) Heating contours. $h_{stag} = 306.42 \ W/m^2\text{-}K$.

Figure 23.- Type IV interference on a 5.08-cm-diameter hemisphere at Mach 5.94 in air. $\theta_i = 14.8^\circ$; $N_{Re,\infty}/m = 7.7 \times 10^6$.
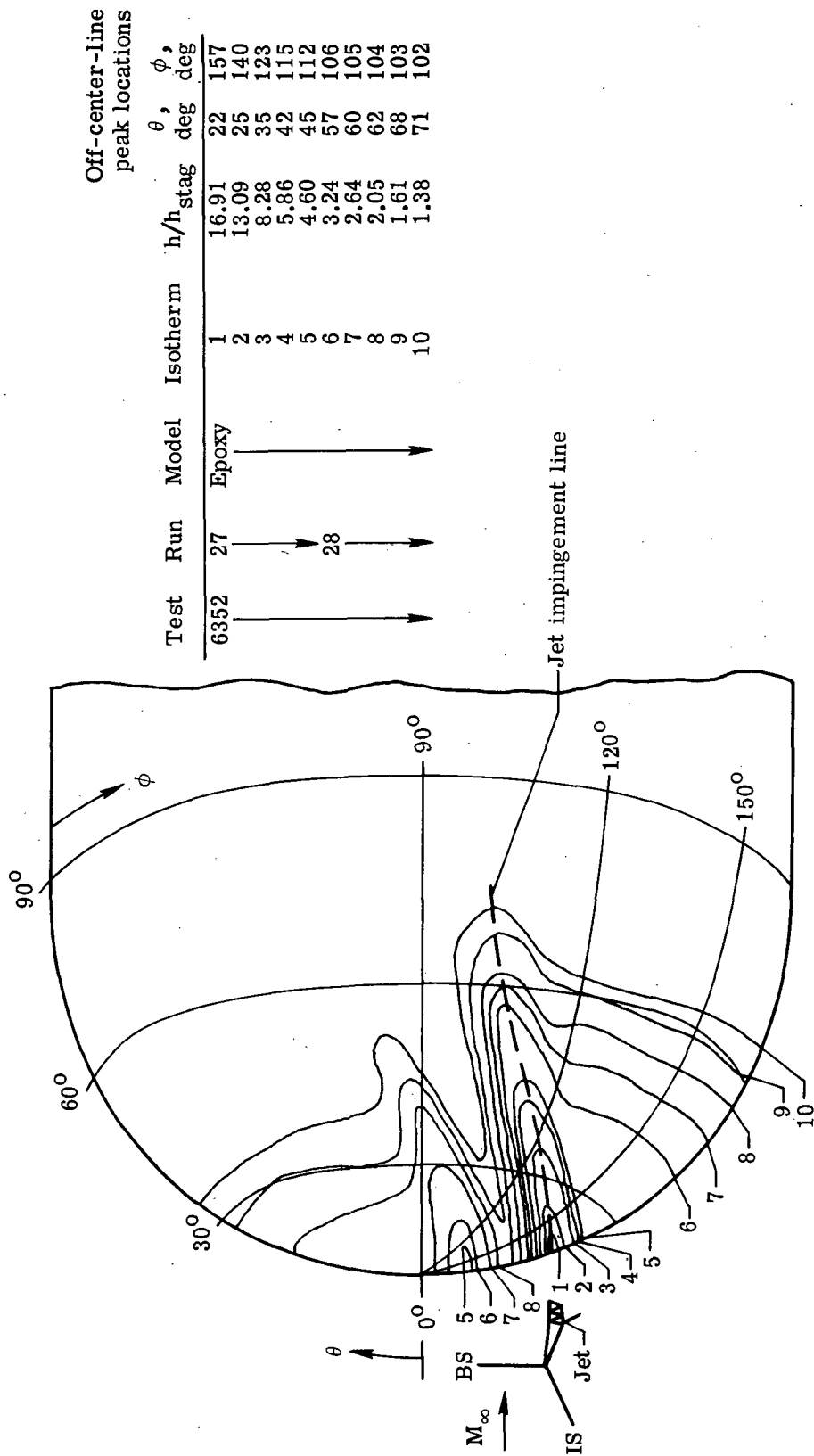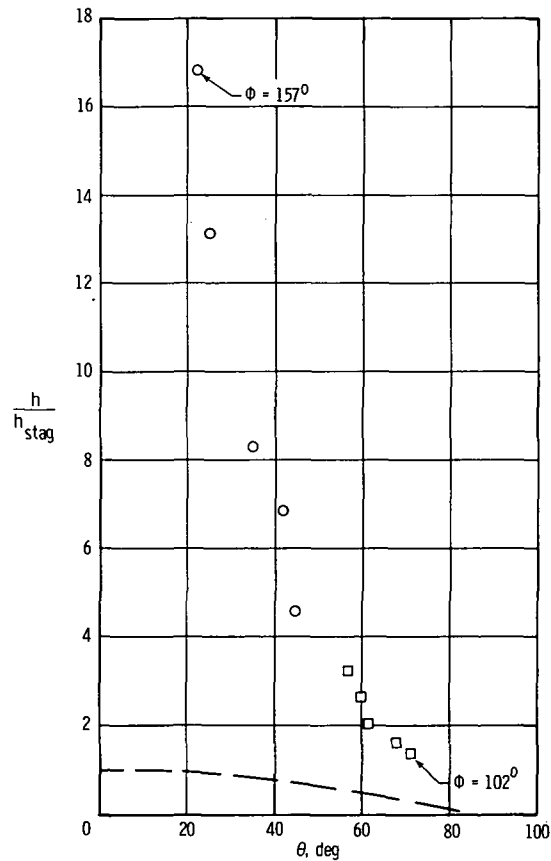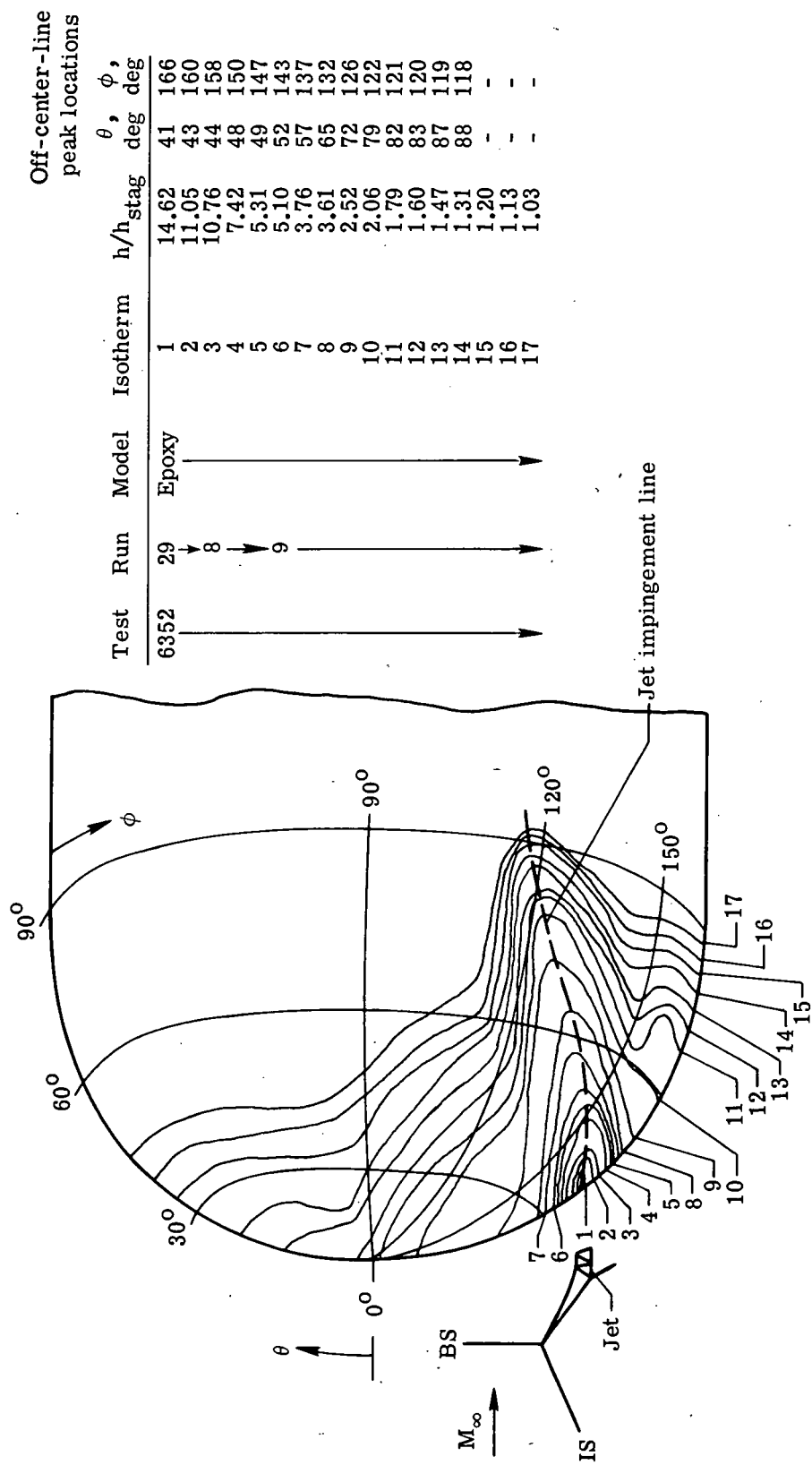
Test-run		$P_{t,\infty}$, N/cm^2	$T_{t,\infty}$, K	T_w, K	h_{stag}, W/m^2-K	θ_i, deg
6352 - 8	○	85	484	436	306.42	14.8
6352 - 29	□	85	493	450	306.42	14.8
6352 - 9	◇	86	473	394	306.42	14.8

Fairing ——————
No interference — — —
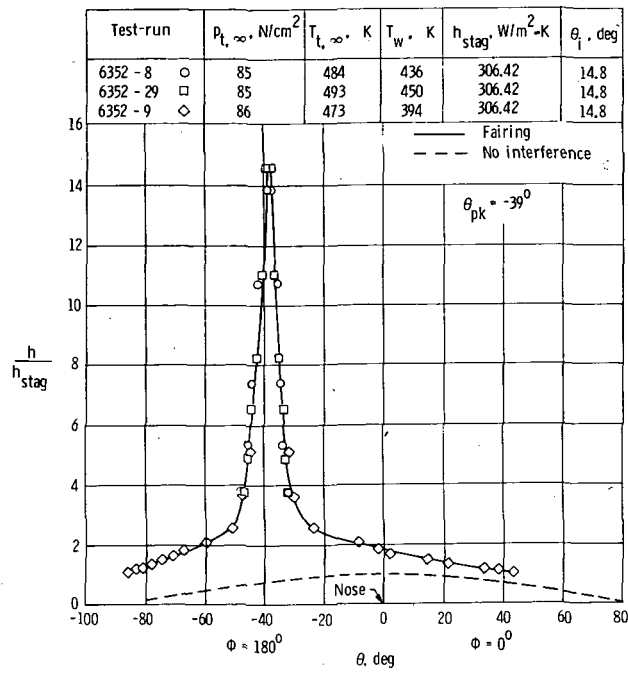
(b) Center-line heat-transfer distribution.
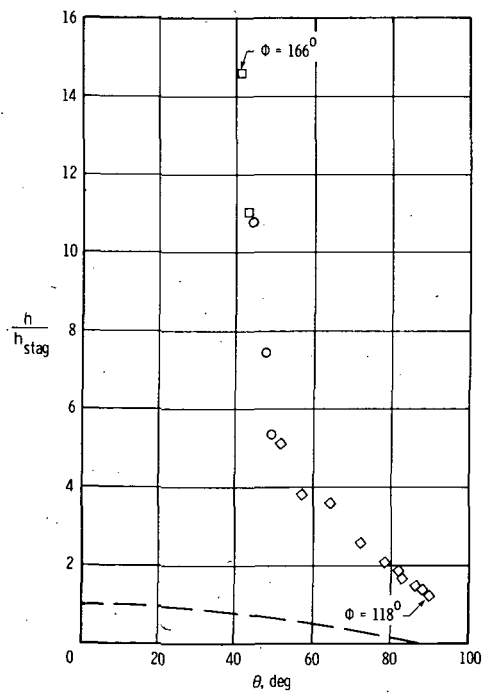
(c) Off-center-line peak heating.

Figure 23.- Concluded.

Off-center-line
peak locations

Test	Run	Model	Isotherm	h/h_{stag}	θ, deg	ϕ, deg
6352	20	Epoxy	1	14.93	36	165
	18		2	10.01	37	159
	19		3	8.96	40	150
	18		4	8.18	42	146
	19		5	6.34	48	134
			6	5.01	54	128
			7	4.48	-	-
			8	3.88	-	-
			9	3.36	-	-
			10	3.13	-	-
			11	2.82	-	-
			12	2.38	59	124
			13	2.31	62	122
			14	2.05	65	119
			15	1.82	67	118
			16	1.63	71	116
			17	1.41	74	114
			18	1.27	79	112
			19	1.08	82	110
			20	0.99	84	109
			21	0.89	87	107

Jet impingement line

90°

90°

120°

60°

150°

30°

ϕ

0°

θ

BS

M_∞

IS

Jet
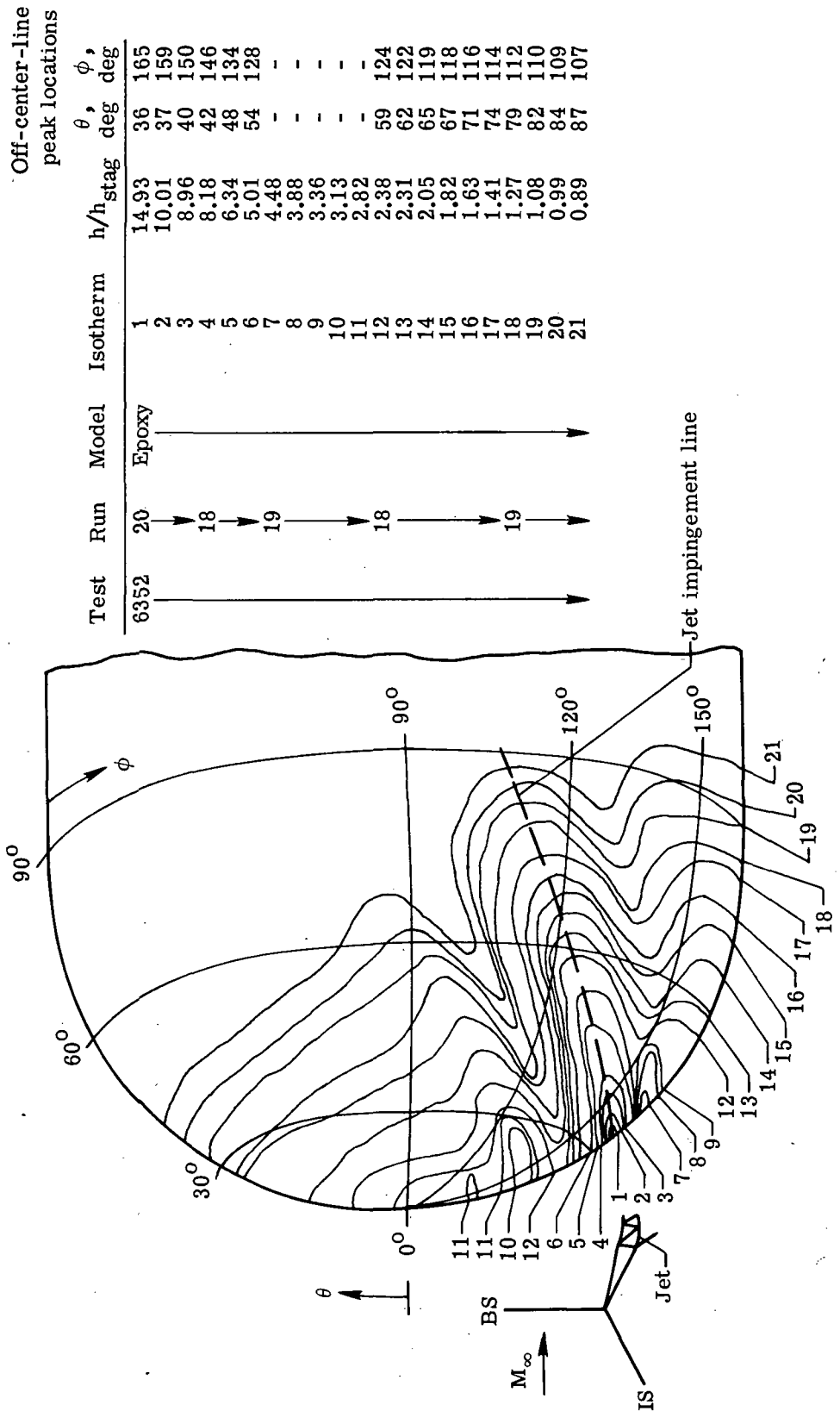
(a) Heating contours. $h_{stag} = 306.42$ W/m^2-K.

$\theta_i = 19.7^o$; $N_{Re,\infty}/m = 7.6 \times 10^6$.

Figure 24.- Type IV interference on a 5.08-cm-diameter hemisphere at Mach 5.94 in air.

Test-run		$p_{t,\infty}$, N/cm^2	$T_{t,\infty}$, K	T_w, K	h_{stag}, W/m^2·K	θ_i, deg
6352 - 20	○	79	473	436	306.42	19.7
6352 - 18	□	81	477	422	306.42	19.7
6352 - 19	◇	84	473	394	306.42	19.7
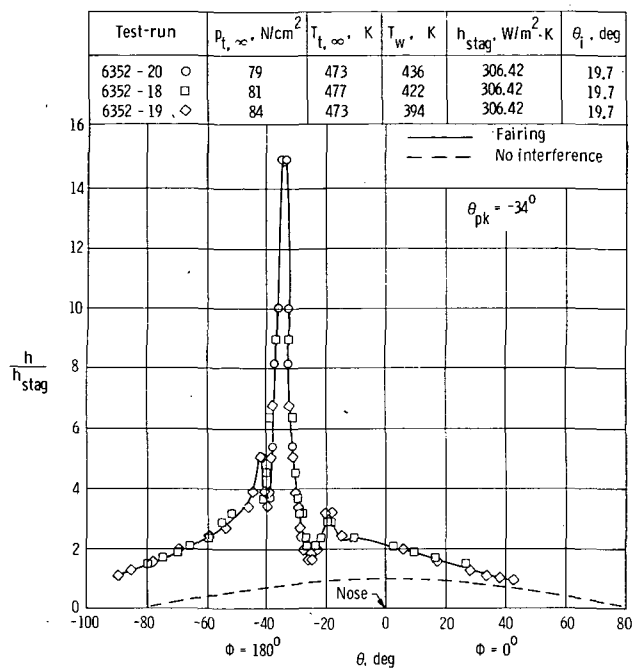
(b) Center-line heat-transfer distribution.
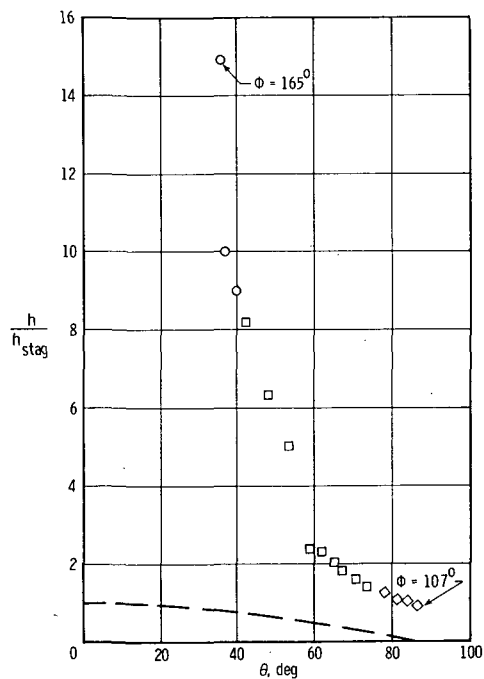
(c) Off-center-line peak heating.

Figure 24.- Concluded.

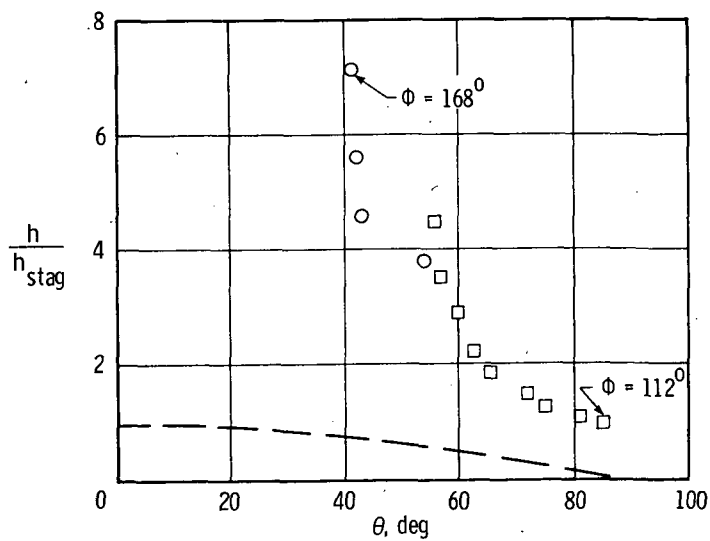| | Off-center-line peak locations | | |
Isotherm	h/h_{stag}	θ, deg	ϕ, deg
1	7.15	41	168
2	5.59	42	162
3	4.58	43	156
4	3.79	54	152
5	4.52	56	133
6	3.50	57	132
7	3.32	-	-
8	2.86	60	128
9	2.19	63	126
10	1.86	66	124
11	1.49	72	119
12	1.27	75	117
13	1.10	81	114
14	0.97	85	112

Test	Run	Model
6352	23	Epoxy
	24	
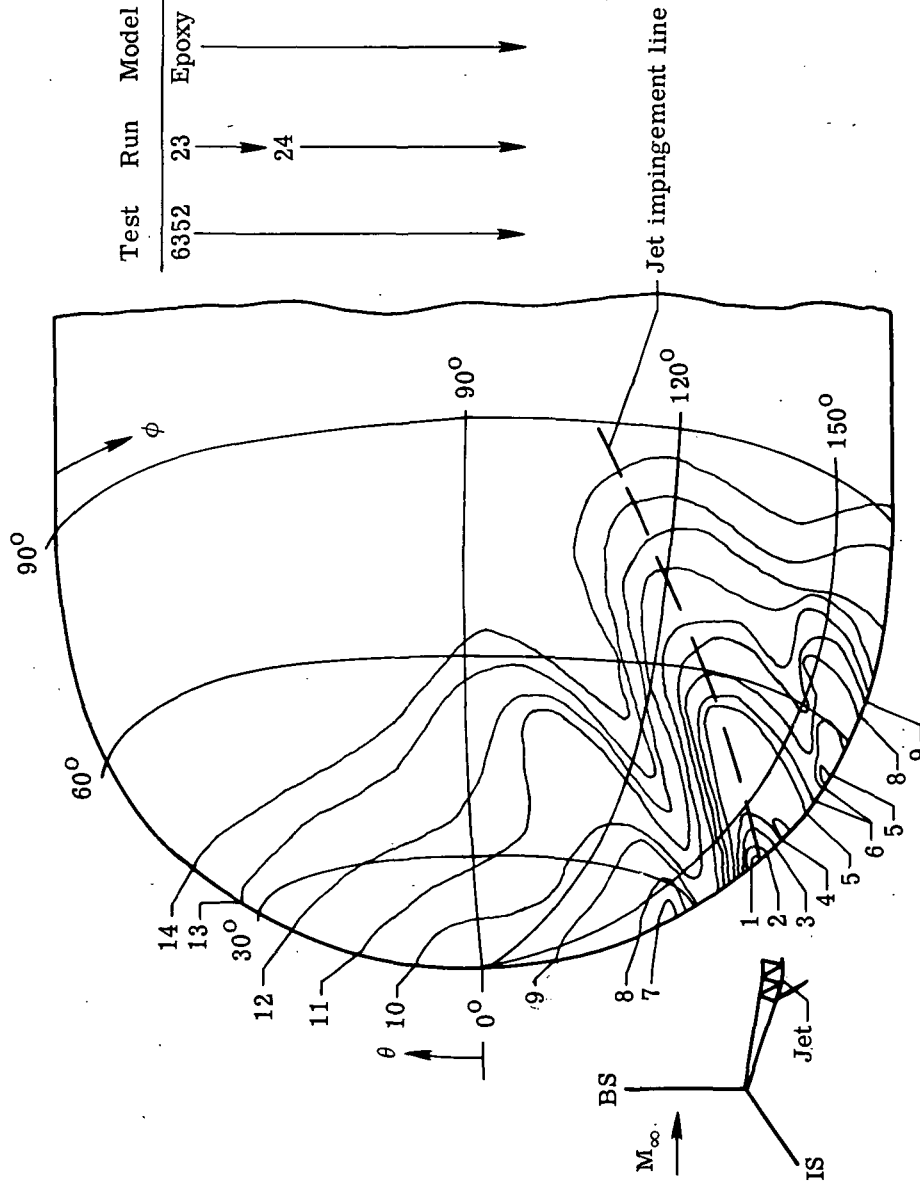
(a) Heating contours. $h_{stag} = 306.42$ W/m^2-K.

Figure 25.- Type IV interference on a 5.08-cm-diameter hemisphere at Mach 5.94 in air. $\theta_i = 24.6°$; $N_{Re,\infty}/m = 7.8 \times 10^6$.

Test-run		$p_{t,\infty}$, N/cm^2	$T_{t,\infty}$, K	T_w, K	h_{stag}, W/m^2-K	θ_i, deg
6352 - 23	○	83	474	436	306.42	24.6
6352 - 24	□	84	476	394	306.42	24.6

Fairing

No interference

$\theta_{pk} = -41^o$

Nose

$\Phi = 180^o$

θ, deg

$\Phi = 0^o$

(b) Center-line heat-transfer distribution.

$\Phi = 168^o$

$\Phi = 112^o$

θ, deg
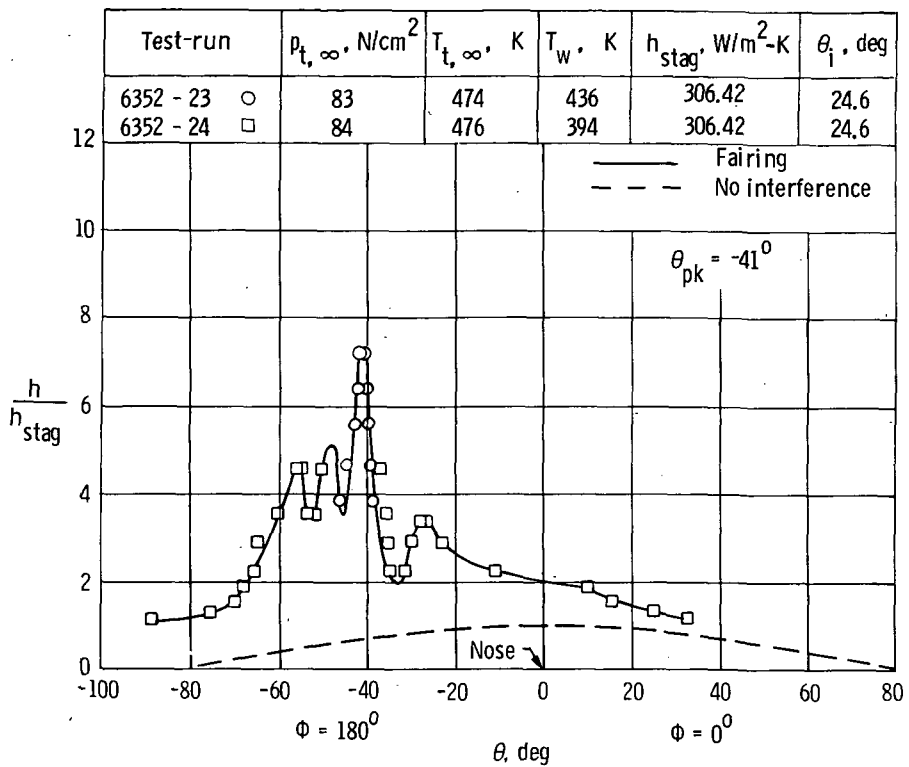
(c) Off-center-line peak heating.

Figure 25.- Concluded.

57

Test	Run	Model	Isotherm	h/h_{stag}	Off-center-line peak locations	
					θ, deg	ϕ, deg
6363	46	Epoxy	1	8.01	24	138
			2	4.00	35	119
			3	2.83	43	115
			4	2.06	45	114
			5	1.79	47	113
			6	1.50	50	111
			7	1.27	54	110
			8	1.07	55	109

(a) Heating contours. $h_{stag} = 571.98$ W/m^2-K.

Figure 26.- Type IV interference on a 5.08-cm-diameter hemisphere at Mach 6 in air. $\theta_i = 5^\circ$; $N_{Re,\infty}/m = 25.6 \times 10^6$.

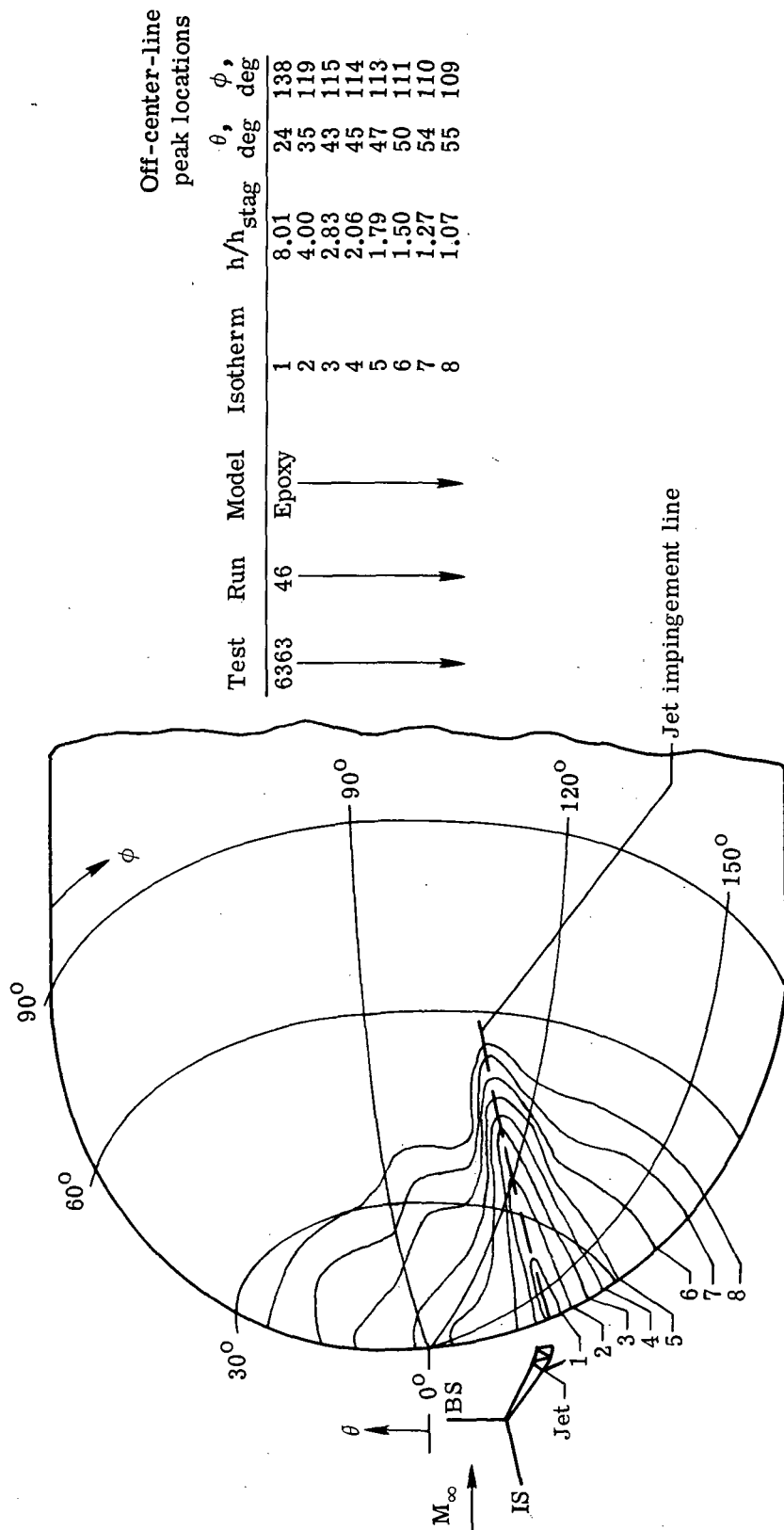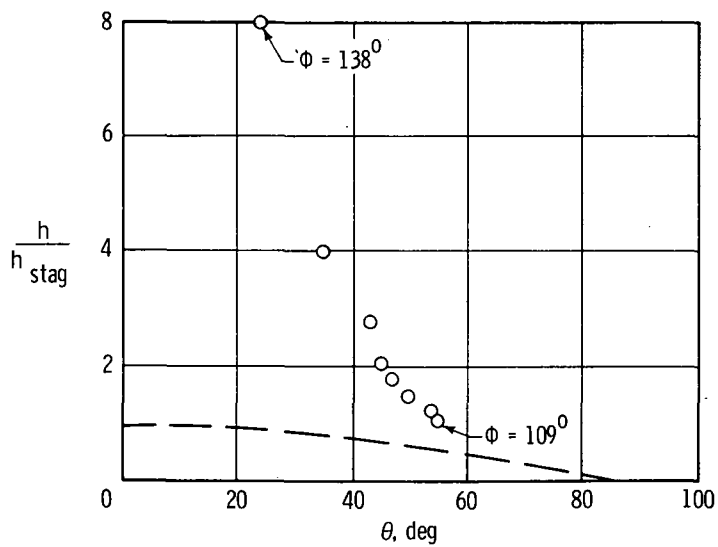| Test-run	$p_{t,\infty}$, N/cm^2	$T_{t,\infty}$, K	T_w, K	h_{stag}, W/m^2·K	θ_i, deg
6363 – 46　○	288	488	436	571.98	5.0

——— Fairing
– – – No interference

$\theta_{pk} = -20^0$

$\Phi = 180^0$　　　　$\Phi = 0^0$

θ, deg

(b) Center-line heat-transfer distribution.

$\Phi = 138^0$

$\Phi = 109^0$

θ, deg
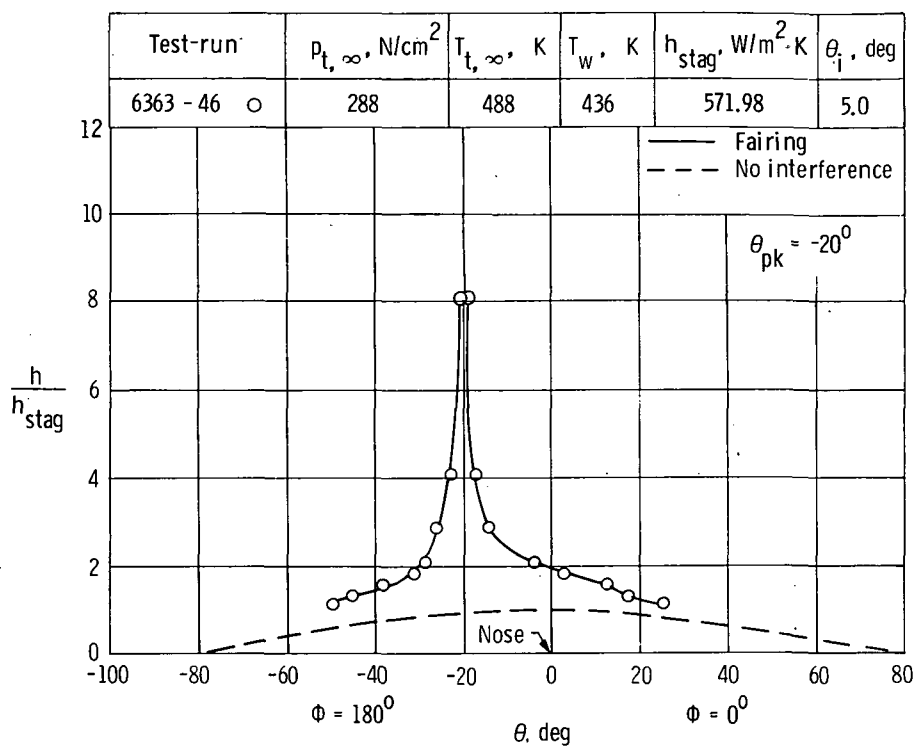
(c) Off-center-line peak heating.

Figure 26.- Concluded.

59

Test	Run	Model	Isotherm	h/h_{stag}	θ, deg	ϕ, deg
6352	31	Steel				
	32					
	33	Epoxy				
	32					

Off-center-line peak locations

Isotherm	h/h_{stag}	θ, deg	ϕ, deg
1	11.03	21	155
2	8.54	28	135
3	4.68	35	126
4	3.63	38	123
5	2.26	61	109
6	2.00	64	107
7	1.30	69	105
8	0.79	70	100

Jet impingement line

(a) Heating contours. $h_{stag} = 551.56$ W/m²-K.

Figure 27.- Type IV interference on a 5.08-cm-diameter hemisphere at Mach 6 in air. $\theta_i = 9.8°$; $N_{Re,\infty}/m = 25.0 \times 10^6$.
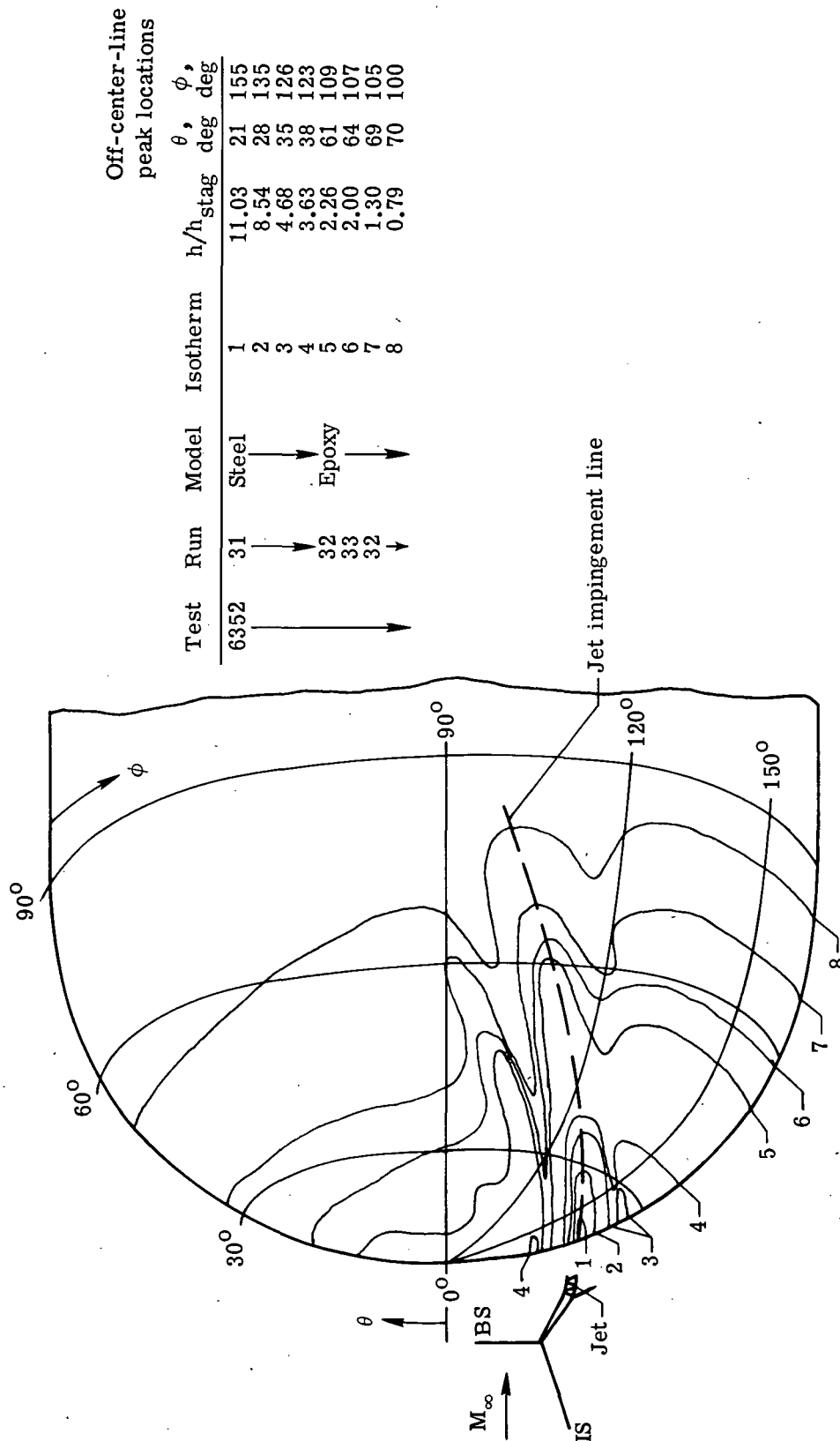
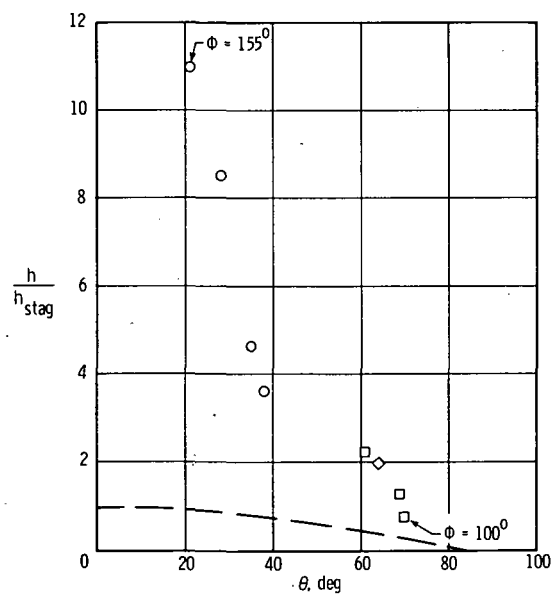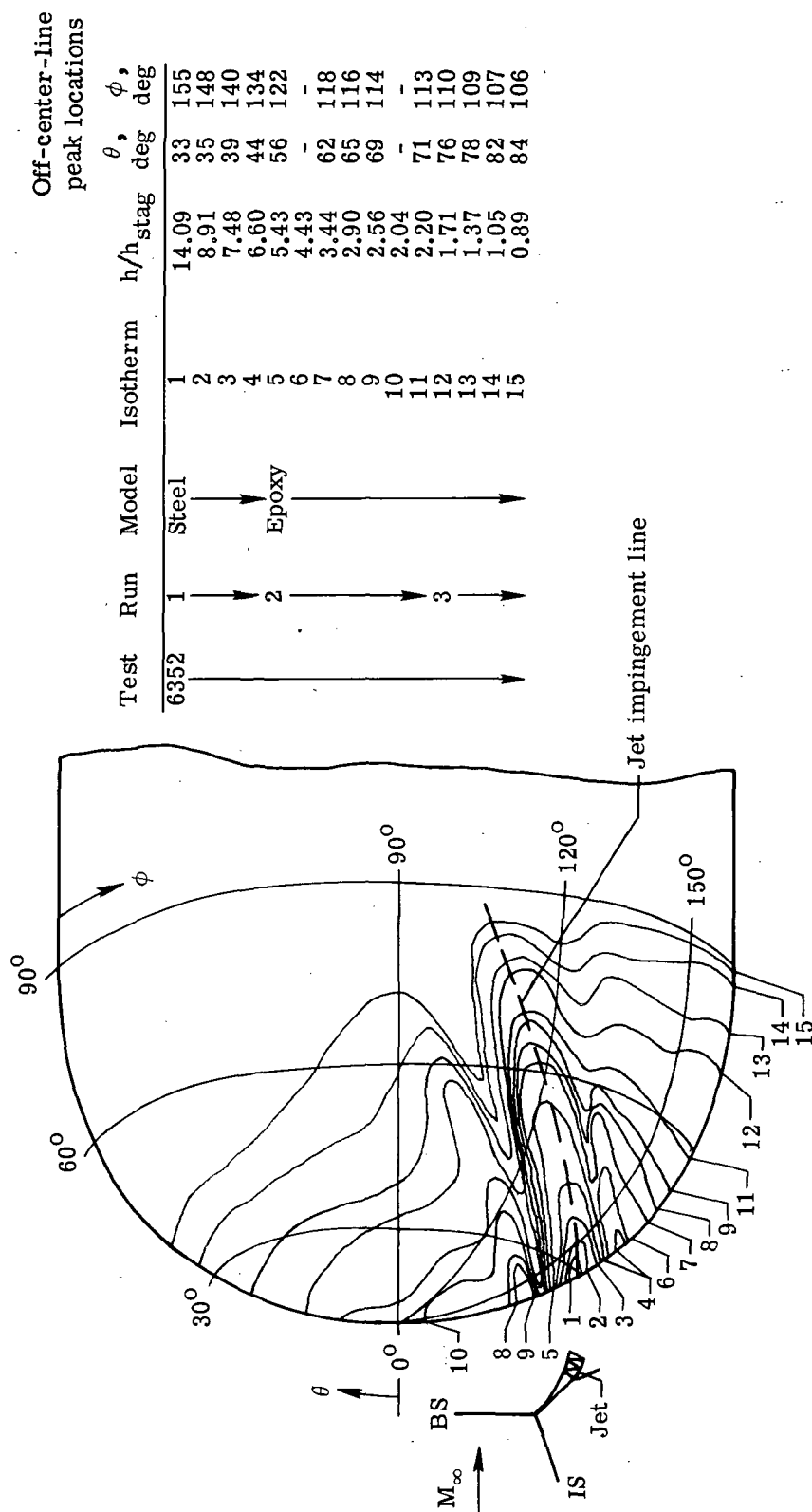| Test-run		$p_{t,\infty}$, N/cm^2	$T_{t,\infty}$, K	T_w, K	h_{stag}, W/m^2-K	θ_i, deg
6352 - 31	○	290	492	408	551.56	9.9
6352 - 32	□	277	486	394	551.56	9.9
6352 - 33	◇	291	487	422	551.56	9.9

Fairing ———
No interference — — —
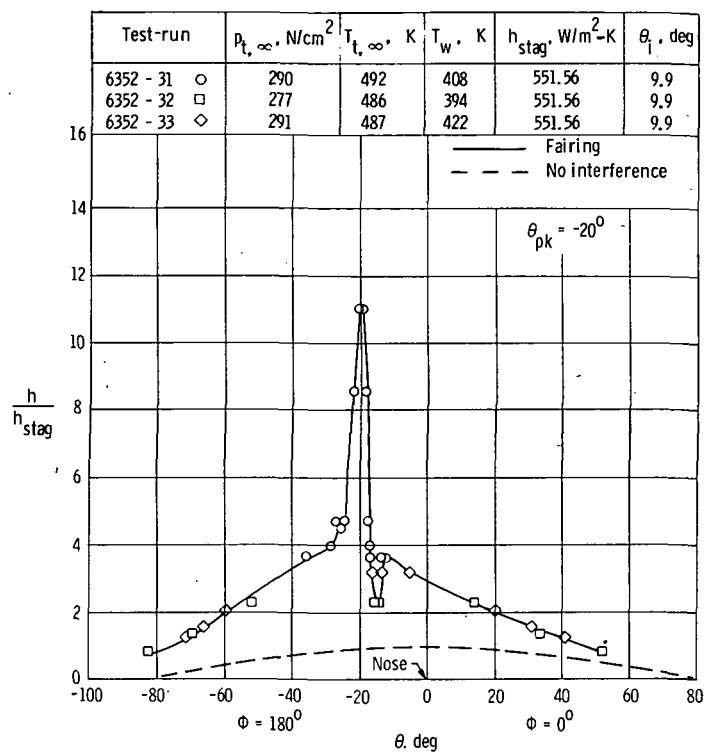
(b) Center-line heat-transfer distribution.

(c) Off-center-line peak heating.

Figure 27.- Concluded.

Off-center-line peak locations

Test	Run	Model	Isotherm	h/h_{stag}	θ, deg	ϕ, deg
6352	1	Steel	1	14.09	33	155
	2	Epoxy	2	8.91	35	148
	3		3	7.48	39	140
			4	6.60	44	134
			5	5.43	56	122
			6	4.43	-	-
			7	3.44	62	118
			8	2.90	65	116
			9	2.56	69	114
			10	2.04	-	-
			11	2.20	71	113
			12	1.71	76	110
			13	1.37	78	109
			14	1.05	82	107
			15	0.89	84	106

(a) Heating contours. $h_{stag} = 551.56 \text{ W/m}^2\text{-K}$.

$\theta_i = 14.8°$; $N_{Re,\infty}/m = 25.7 \times 10^7$.

Figure 28.- Type IV interference on a 5.08-cm-diameter hemisphere at Mach 6 in air.

Test-run		$p_{t,\infty}$, N/cm^2	$T_{t,\infty}$, K	T_w, K	h_{stag}, W/m^2-K	θ_i, deg
6352 – 1	○	277	478	422	551.56	14.8
6352 – 2	□	290	471	422	551.56	14.8
6352 – 3	◇	283	489	394	551.56	14.8

——————— Fairing
— — — No interference
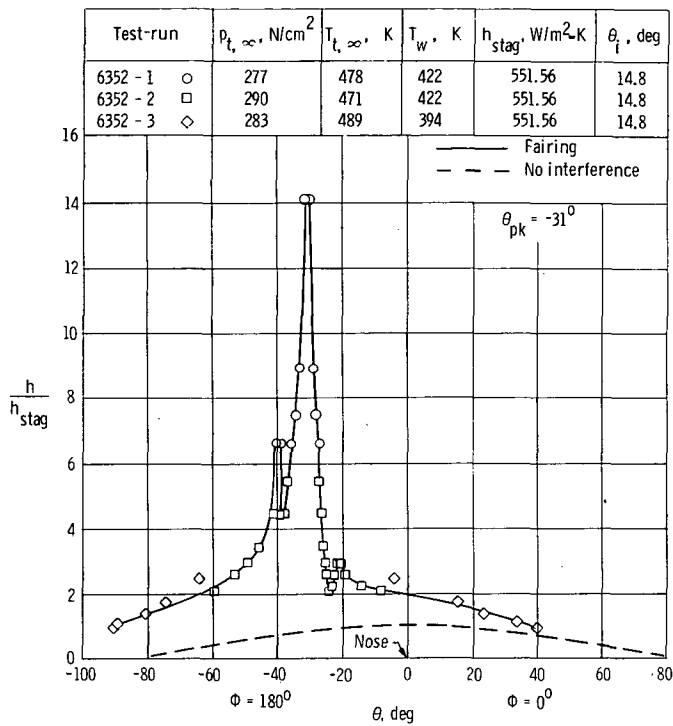
(b) Center-line heat-transfer distribution.
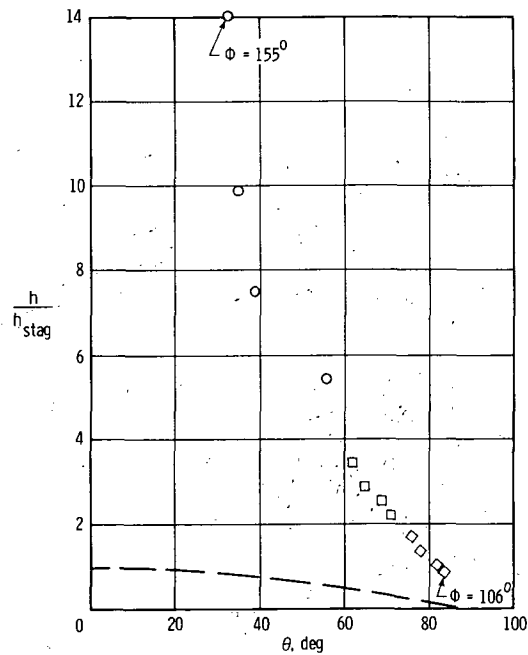
(c) Off-center-line peak heating.

Figure 28.- Concluded.

Test	Run	Model	Isotherm	h/h_{stag}	Off-center-line peak locations	
					θ, deg	ϕ, deg
6363	41	Steel	1	13.13	23	152
	42	Epoxy	2	9.68	27	140
			3	8.10	30	133
			4	6.03	48	110
			5	3.74	53	106
			6	2.59	56	105
			7	2.31	-	-
			8	2.08	63	102
			9	1.61	68	99
			10	1.32	72	97
			11	1.13	74	96
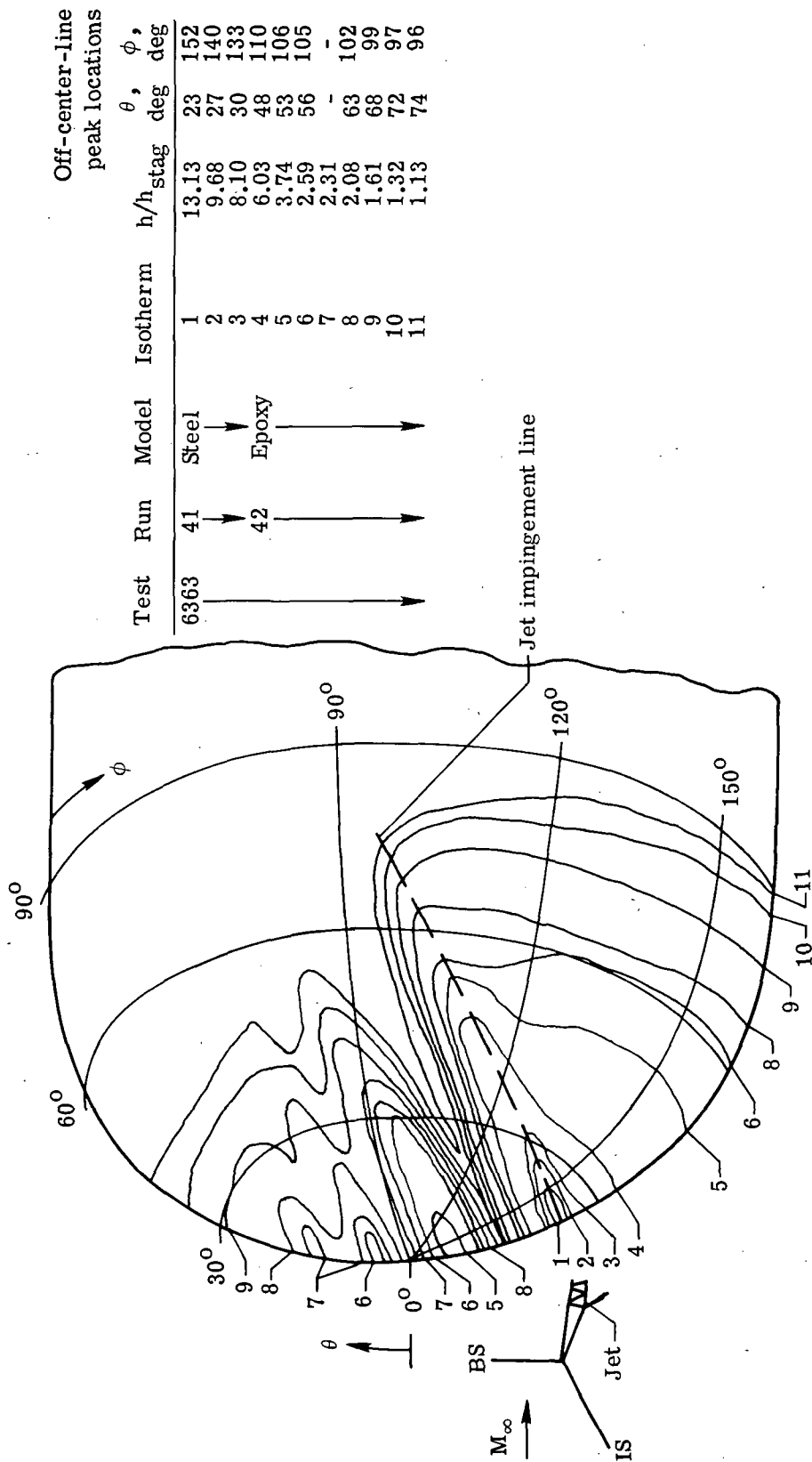
(a) Heating contours. $h_{stag} = 571.98 \ W/m^2\text{-}K$.

Figure 29.- Type IV interference on a 5.08-cm-diameter hemisphere at Mach 6 in air.

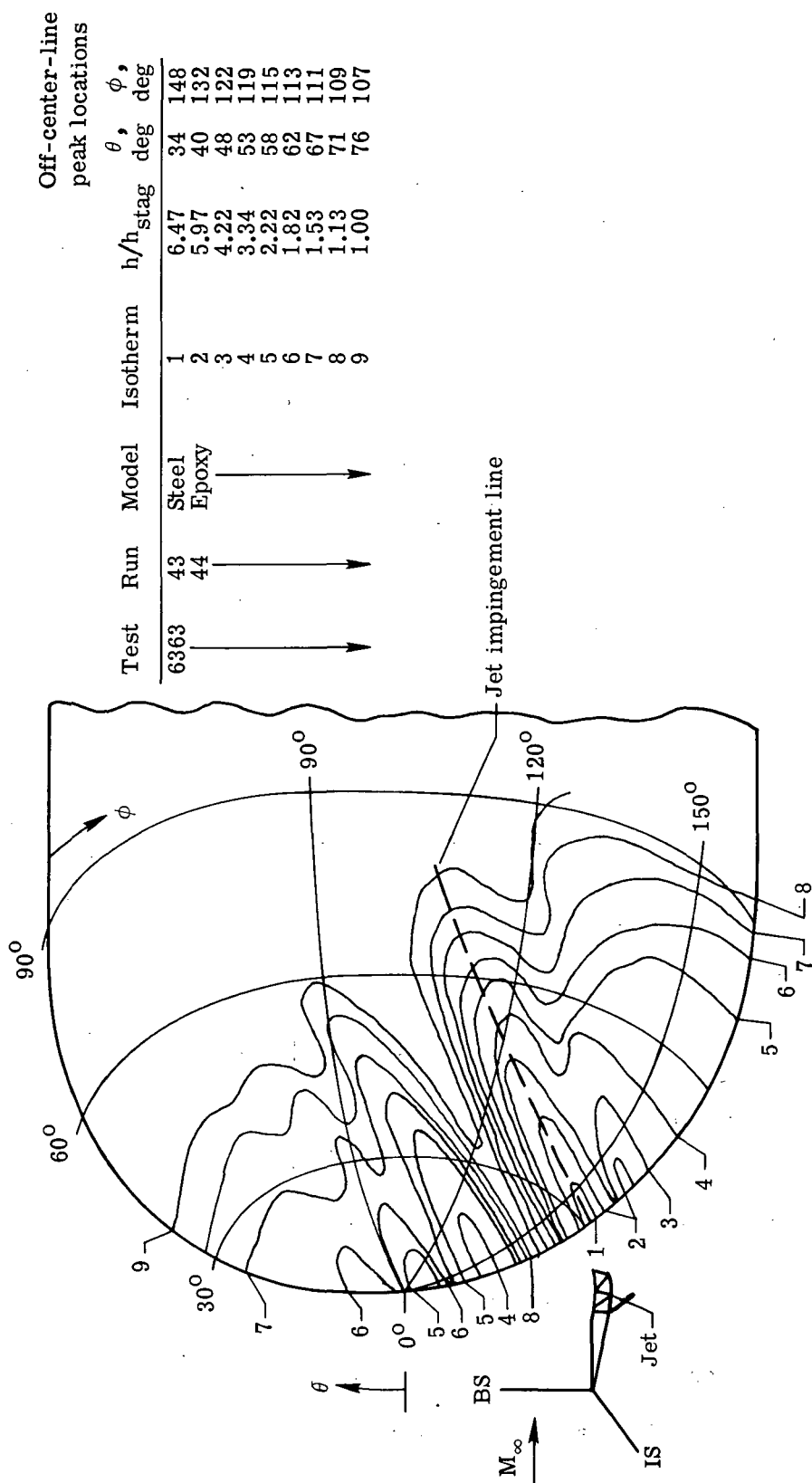$\theta_i = 19.8^\circ$; $N_{Re,\infty}/m = 25.6 \times 10^6$.
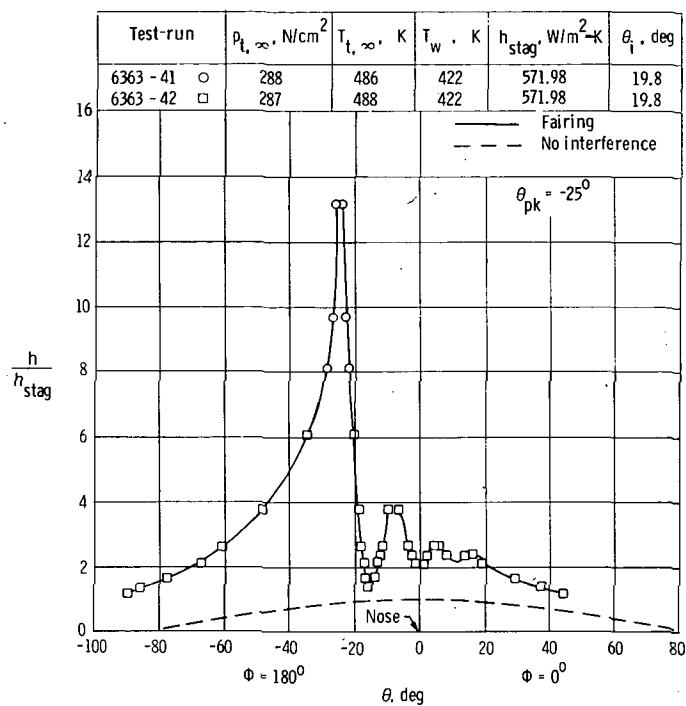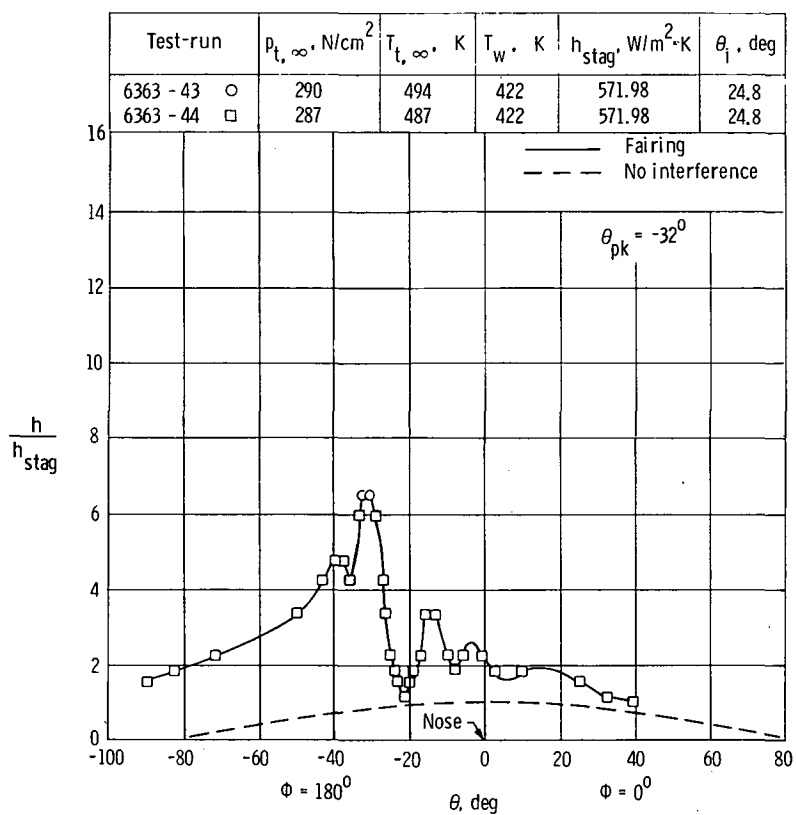
(b) Center-line heat-transfer distribution.
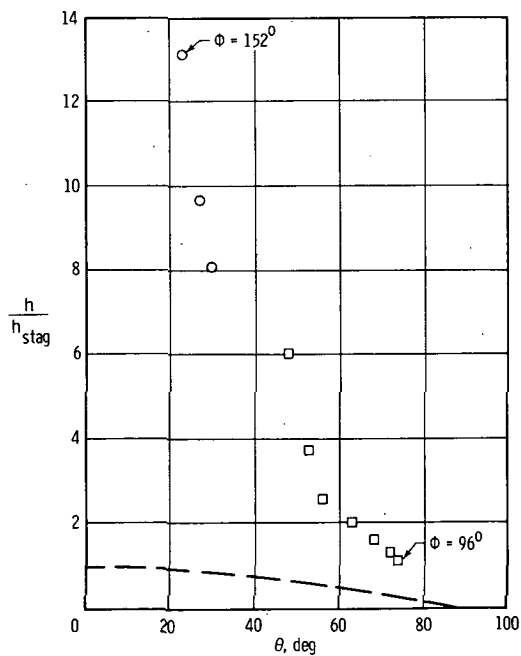
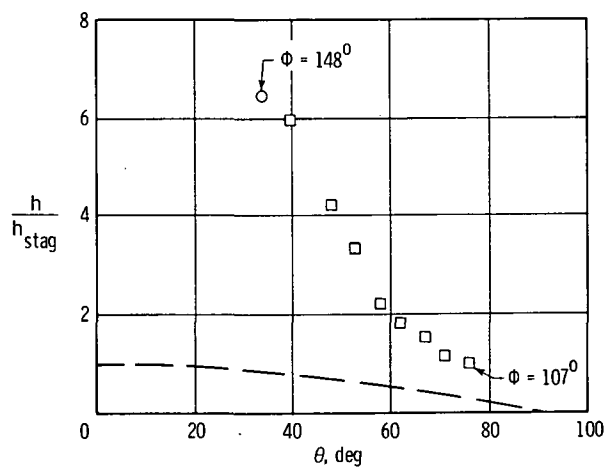

(c) Off-center-line peak heating.

Figure 29.- Concluded.

Test	Run	Model	Isotherm	h/h_{stag}	Off-center-line peak locations	
					θ, deg	ϕ, deg
6363	43	Steel	1	6.47	34	148
	44	Epoxy	2	5.97	40	132
			3	4.22	48	122
			4	3.34	53	119
			5	2.22	58	115
			6	1.82	62	113
			7	1.53	67	111
			8	1.13	71	109
			9	1.00	76	107

(a) Heating contours. h_{stag} = 571.98 W/m^2-K.

Figure 30.- Type IV interference on a 5.08-cm-diameter hemisphere at Mach 6 in air. $\theta_i = 24.8°$; $N_{Re,\infty}/m = 25.4 \times 10^6$.

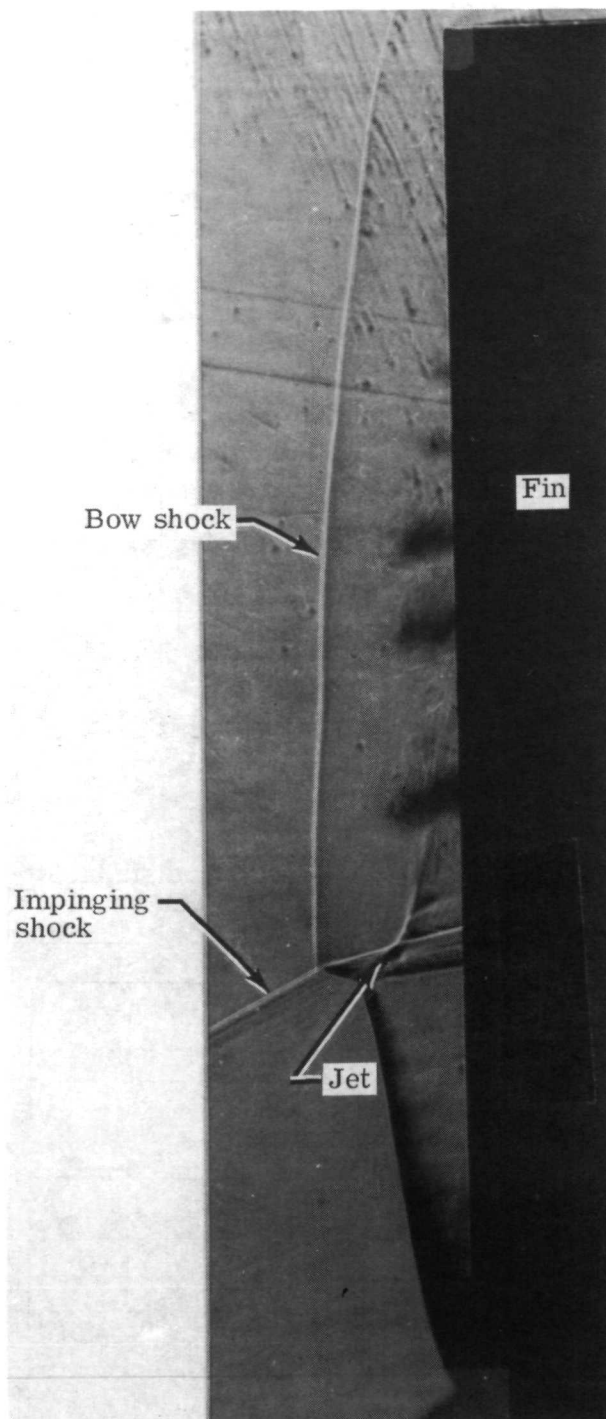| Test-run		$p_{t,\infty}$, N/cm^2	$T_{t,\infty}$, K	T_w, K	h_{stag}, W/m^2·K	θ_i, deg
6363 - 43	O	290	494	422	571.98	24.8
6363 - 44	□	287	487	422	571.98	24.8

——— Fairing
– – – No interference

$\theta_{pk} = -32^0$

(b) Center-line heat-transfer distribution.

Nose

$\Phi = 180^0$ θ, deg $\Phi = 0^0$

$\Phi = 148^0$

$\Phi = 107^0$

θ, deg

(c) Off-center-line peak heating.

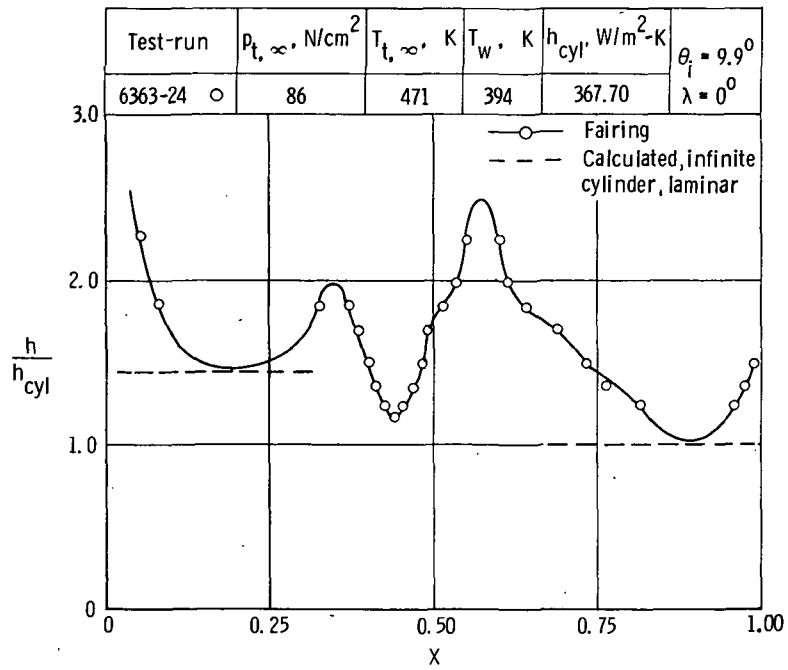Figure 30.- Concluded.

Bow shock

Fin

Impinging shock

Jet

L-73-6875

Figure 31.- Shock pattern for a type IVa interference on the cylindrical fin at
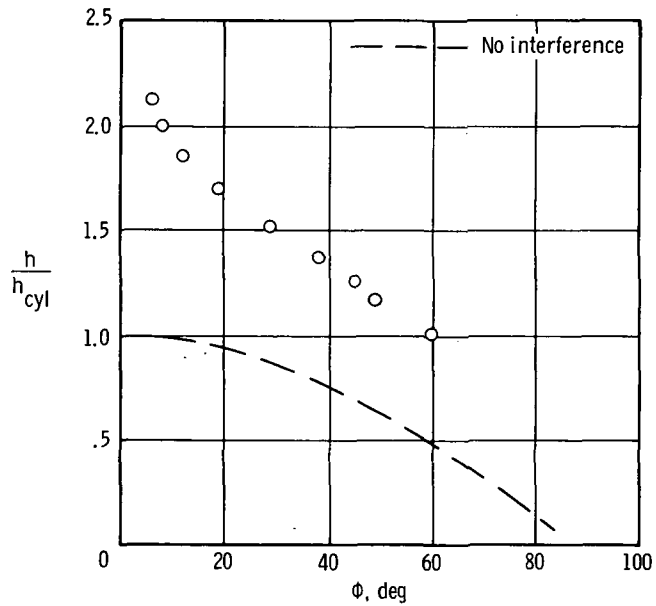Mach 6 in air. $\theta_i = 19.9^o$; $\lambda = 0^o$; $N_{Re,\infty}/m = 25.8 \times 10^6$.

Test	Run	Model	Isotherm	h/h_{cyl}
6363	24	Epoxy	1	2.13
			2	2.00
			3	1.86
			4	1.79
			5	1.71
			6	1.52
			7	1.38
			8	1.26
			9	1.21
			10	1.17
			11	1.02
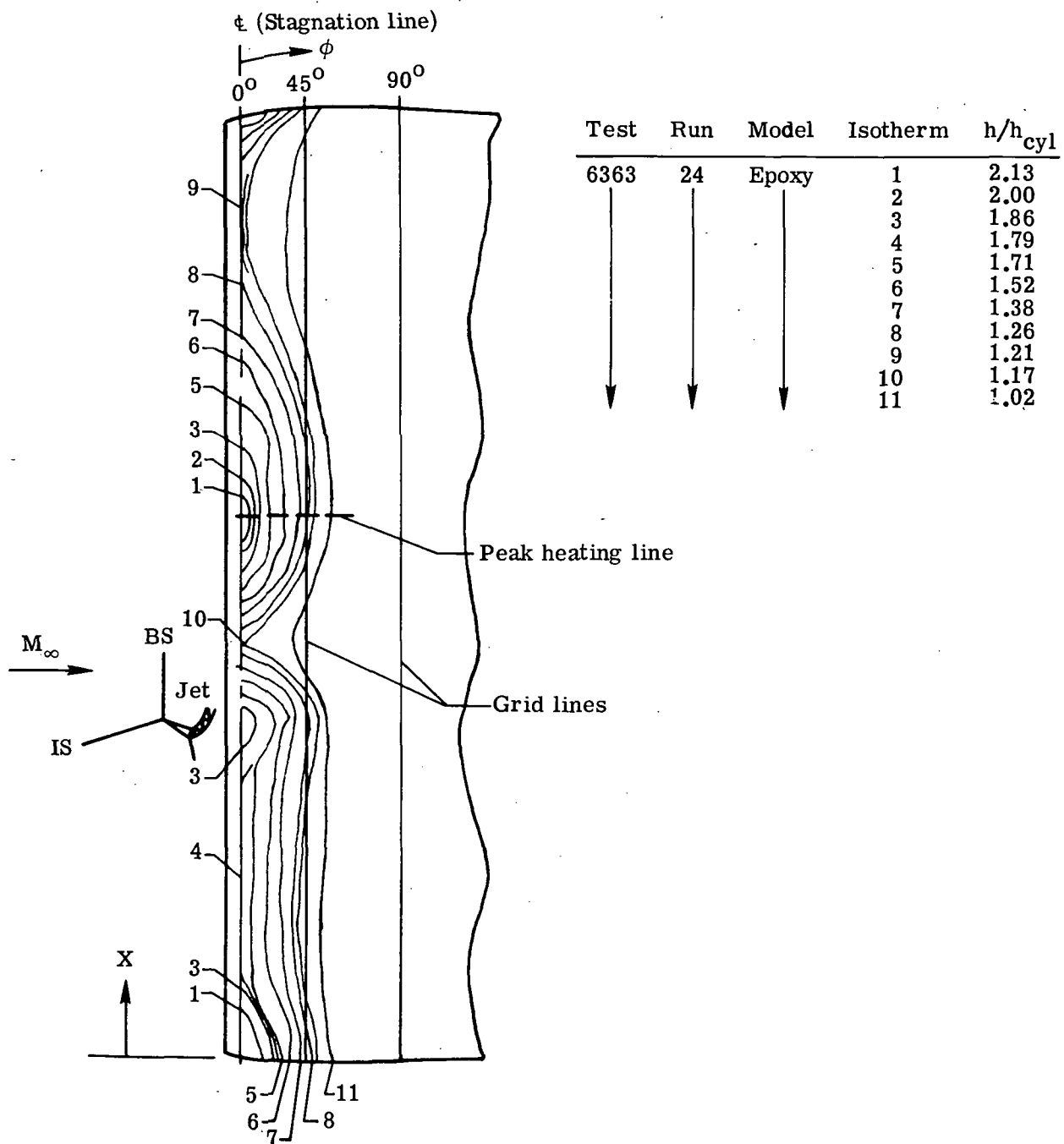
(a) Heating contours. $h_{cyl} = 367.70$ W/m^2-K.

Figure 32.- Type IVa interference on a fin at Mach 5.94 in air.
$\theta_i = 9.9^O$; $\lambda = 0^O$; $N_{Re,\infty}/m = 8.1 \times 10^6$.

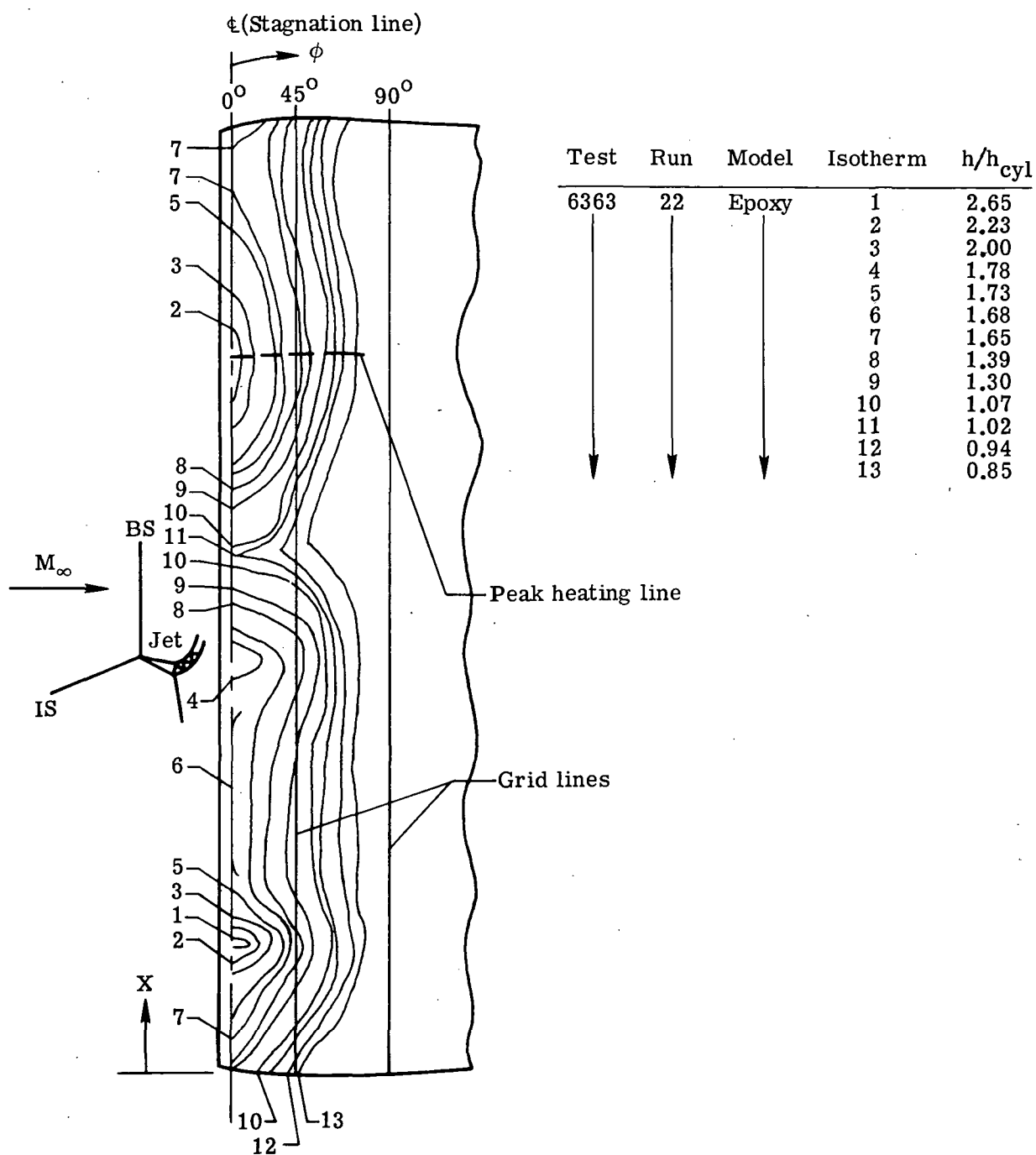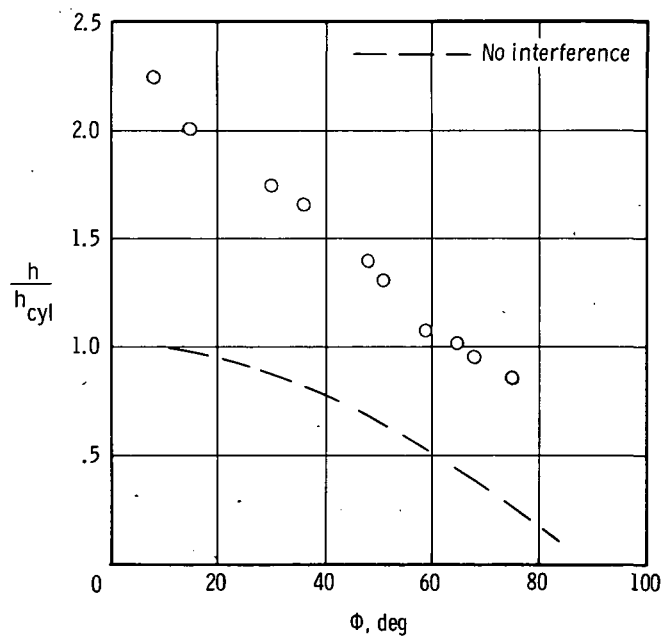| Test-run		$p_{t,\infty}$, N/cm^2	$T_{t,\infty}$, K	T_w, K	h_{cyl}, W/m^2-K	$\theta_i = 9.9^0$
6363-24	○	86	471	394	367.70	$\lambda = 0^0$

(b) Center-line heat-transfer distribution.

(c) Off-center-line heating. X = 0.57.

Figure 32.- Concluded.

Test	Run	Model	Isotherm	h/h_{cyl}
6363	22	Epoxy	1	2.65
			2	2.23
			3	2.00
			4	1.78
			5	1.73
			6	1.68
			7	1.65
			8	1.39
			9	1.30
			10	1.07
			11	1.02
			12	0.94
			13	0.85

(a) Heating contours. $h_{cyl} = 347.28$ W/m^2-K.

Figure 33.- Type IVa interference on a fin at Mach 5.94 in air.
$\theta_i = 14.9^O$; $\lambda = 0^O$; $N_{Re,\infty}/m = 7.7 \times 10^6$.

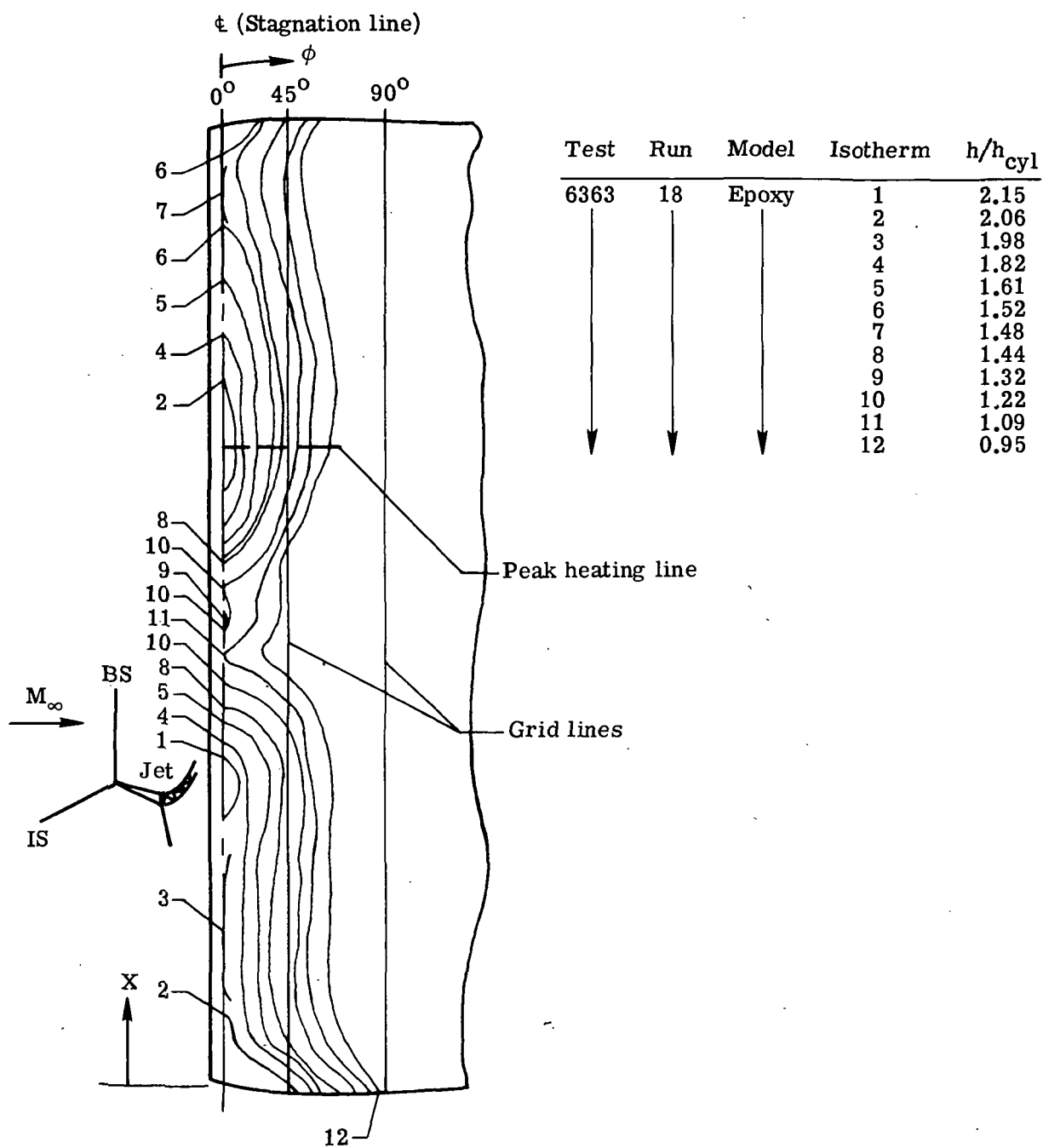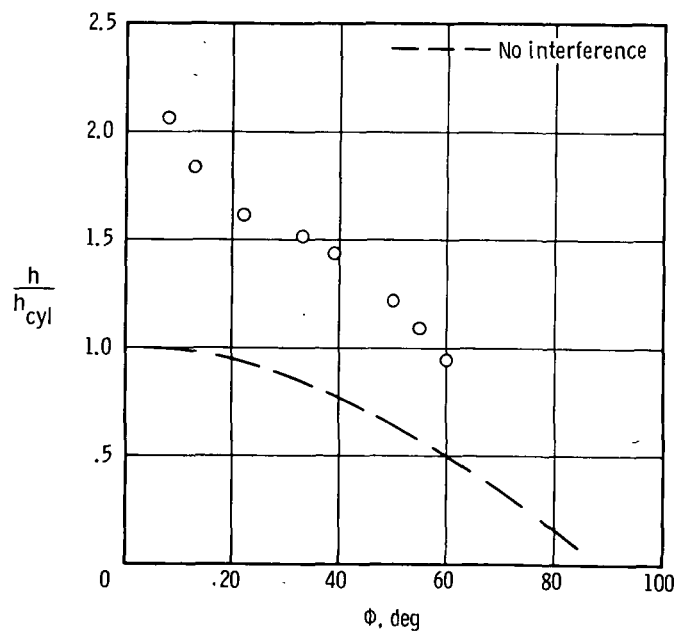| Test-run	$p_{t, \infty}$, N/cm^2	$T_{t, \infty}$, K	T_w, K	h_{cyl}, $W/m^2\text{-}K$	$\theta_i = 14.9°$
6363-22 ⭘	83	476	394	347.28	$\lambda = 0°$

⭘ Fairing
- - - Calculated, infinite cylinder, laminar
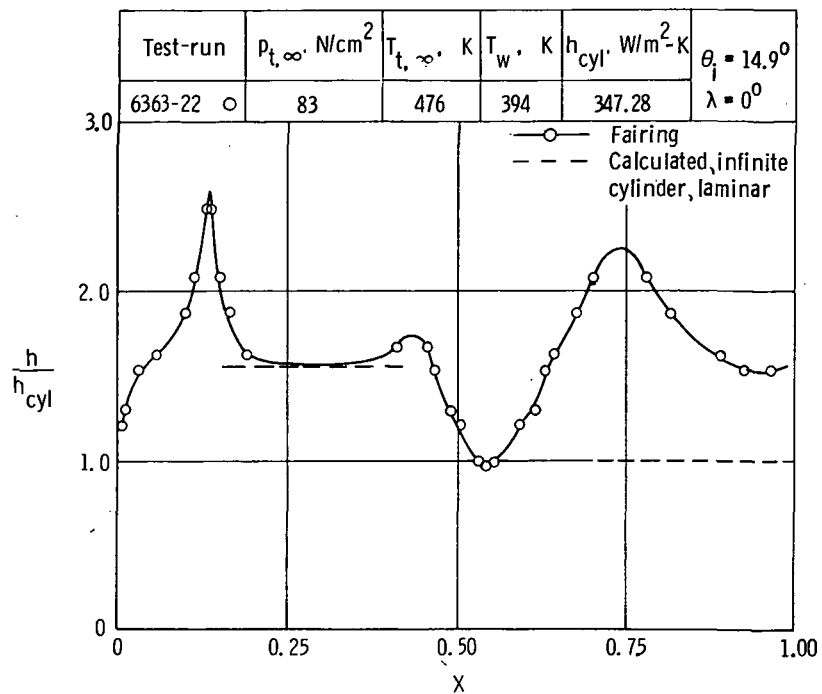
(b) Center-line heat-transfer distribution.

— No interference

(c) Off-center-line heating. X = 0.75.

Figure 33.- Concluded.

Test	Run	Model	Isotherm	h/h_{cyl}
6363	18	Epoxy	1	2.15
			2	2.06
			3	1.98
			4	1.82
			5	1.61
			6	1.52
			7	1.48
			8	1.44
			9	1.32
			10	1.22
			11	1.09
			12	0.95

(a) Heating contours. $h_{cyl} = 367.70$ W/m^2-K.

Figure 34.- Type IVa interference on a fin at Mach 5.94 in air. $\theta_i = 19.9^o$; $\lambda = 0^o$; $N_{Re,\infty}/m = 7.9 \times 10^6$.
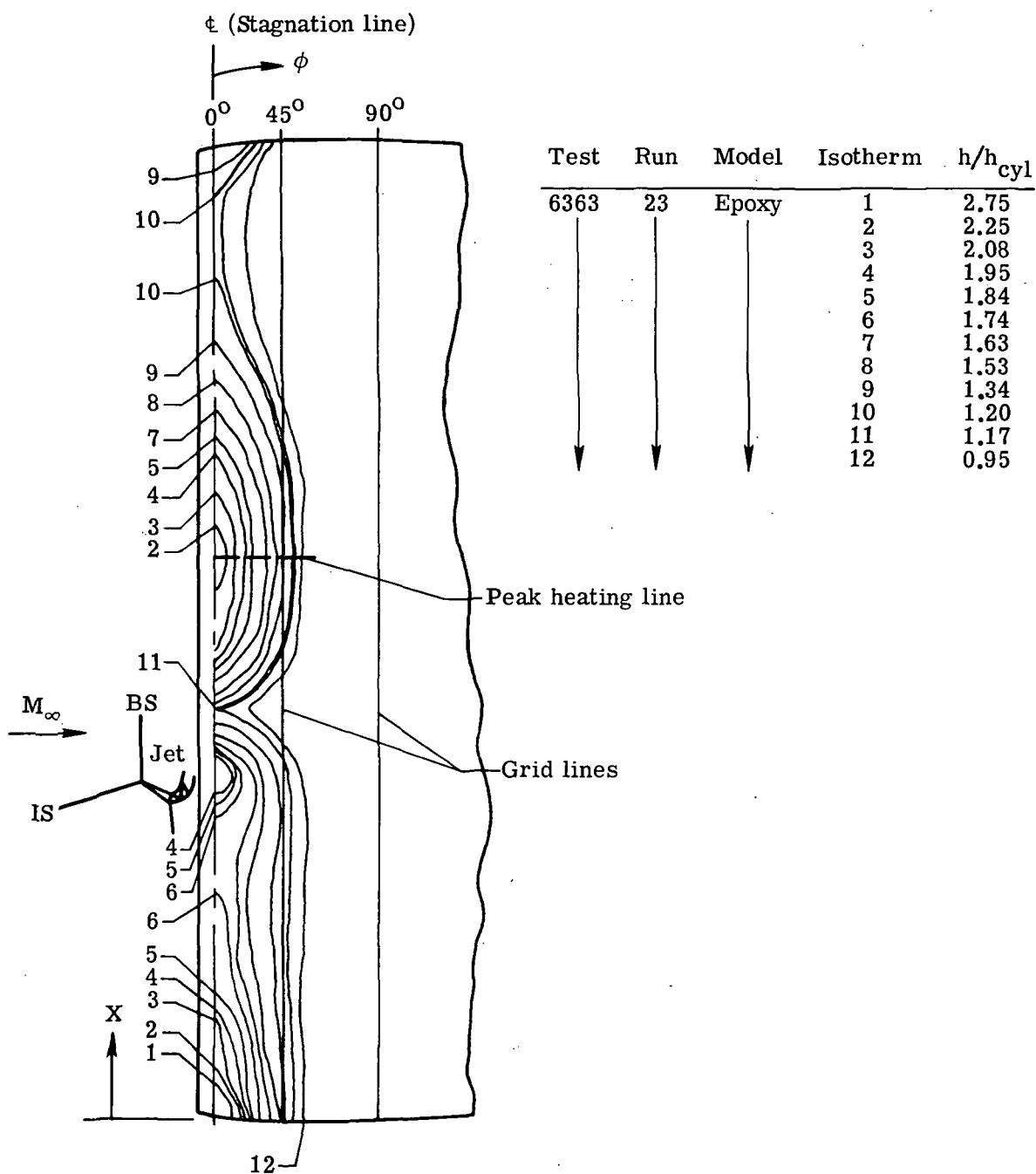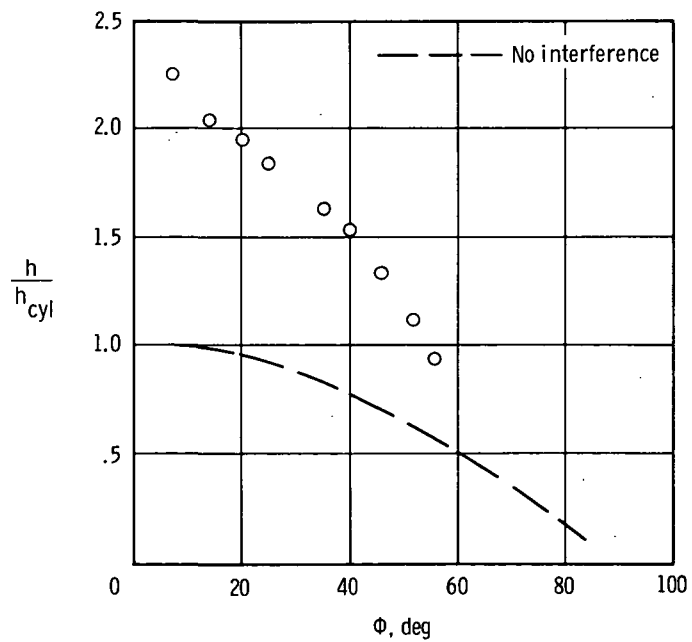
Test run	$P_{t,\infty}$, N/cm^2	$T_{t,\infty}$, K	T_w, K	h_{cyl}, W/m^2-K	$\theta_i = 19.9^0$
6363-18 ○	83	471	394	367.70	$\lambda = 0^0$

— ○ — Fairing
— — — Calculated, infinite
cylinder, laminar
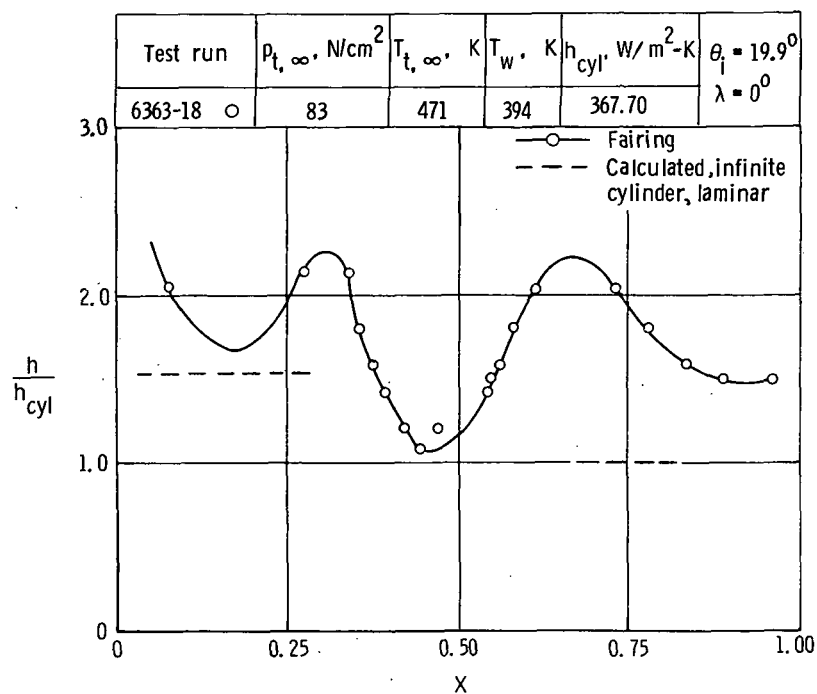
(b) Center-line heat-transfer distribution.

(c) Off-center-line heating. X = 0.66.

Figure 34.- Concluded.

₵ (Stagnation line)

φ

0° 45° 90°

Test	Run	Model	Isotherm	h/h_{cyl}
6363	23	Epoxy	1	2.75
			2	2.25
			3	2.08
			4	1.95
			5	1.84
			6	1.74
			7	1.63
			8	1.53
			9	1.34
			10	1.20
			11	1.17
			12	0.95

Peak heating line

Grid lines

M_∞

BS

Jet

IS

X

(a) Heating contours. h_{cyl} = 653.70 W/m^2-K.

Figure 35.- Type IVa interference on a fin at Mach 6 in air.
$\theta_i = 9.9°$; $\lambda = 0°$; $N_{Re,\infty}/m = 26.2 \times 10^6$.

Test run	$P_{t,\infty}$, N/cm^2	$T_{t,\infty}$, K	T_w, K	h_{cyl}, W/m^2-K	$\theta_i = 9.9^0$
6363-23 ○	293	486	422	653.70	$\lambda = 0^0$
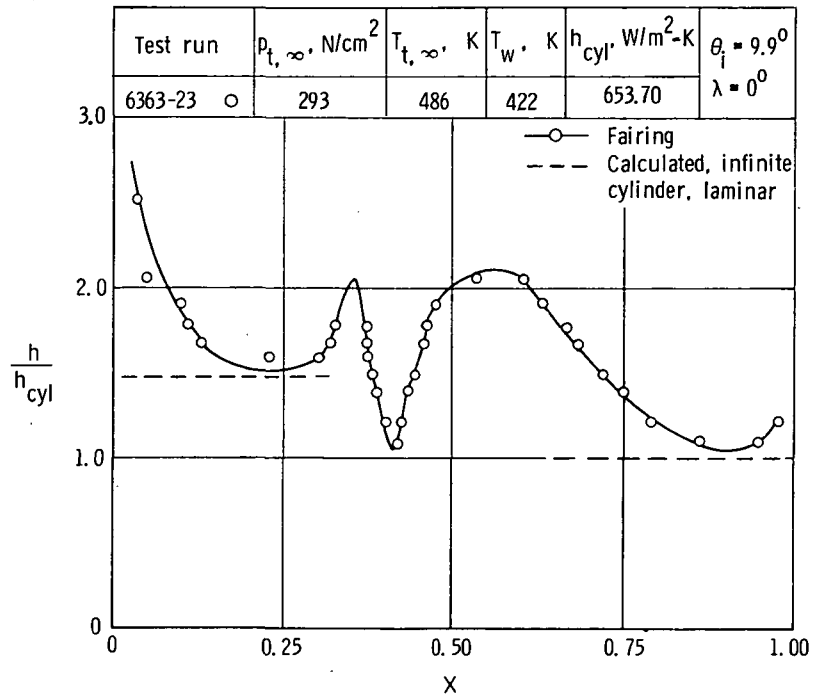
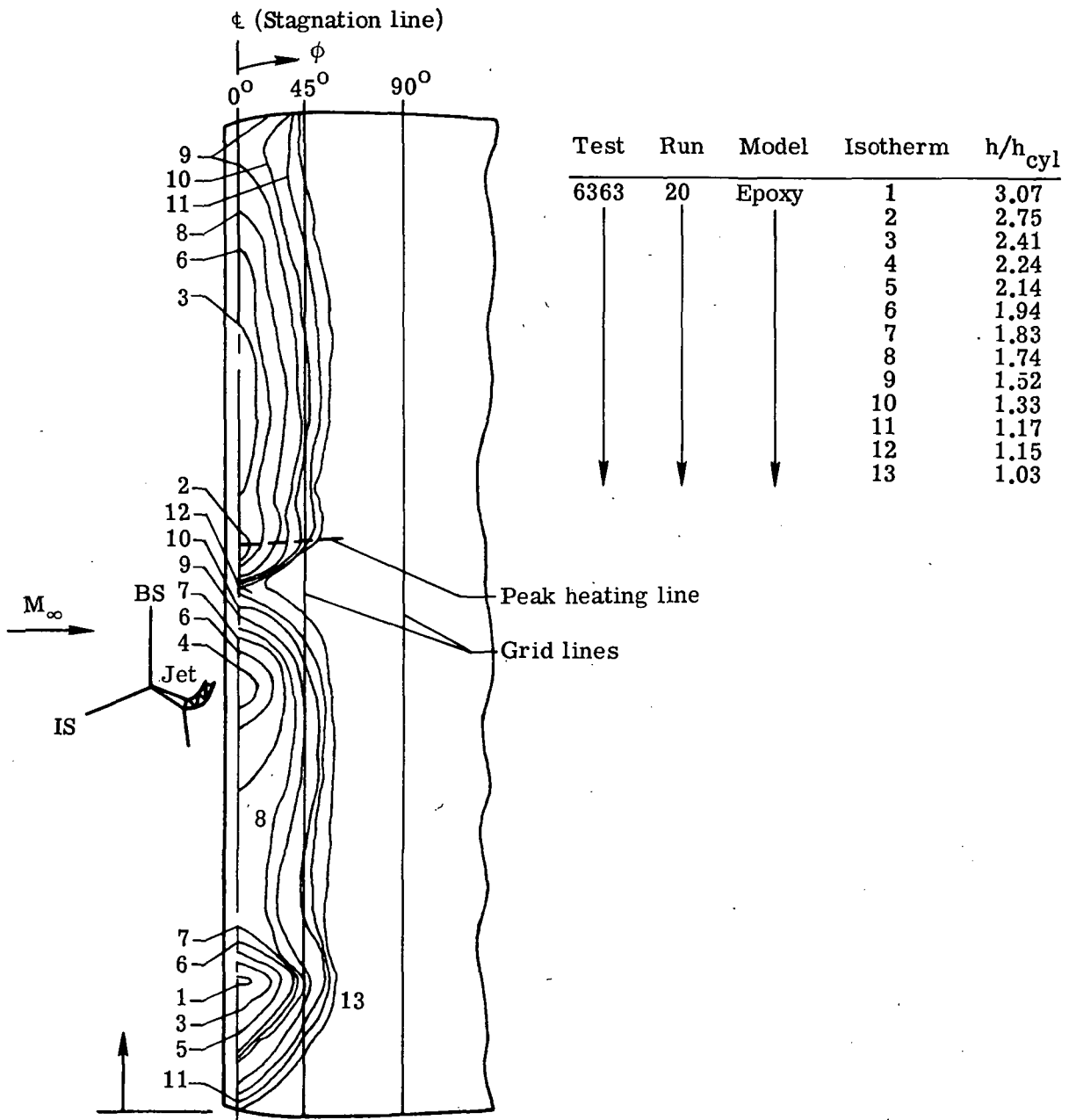
(b) Center-line heat-transfer distribution.
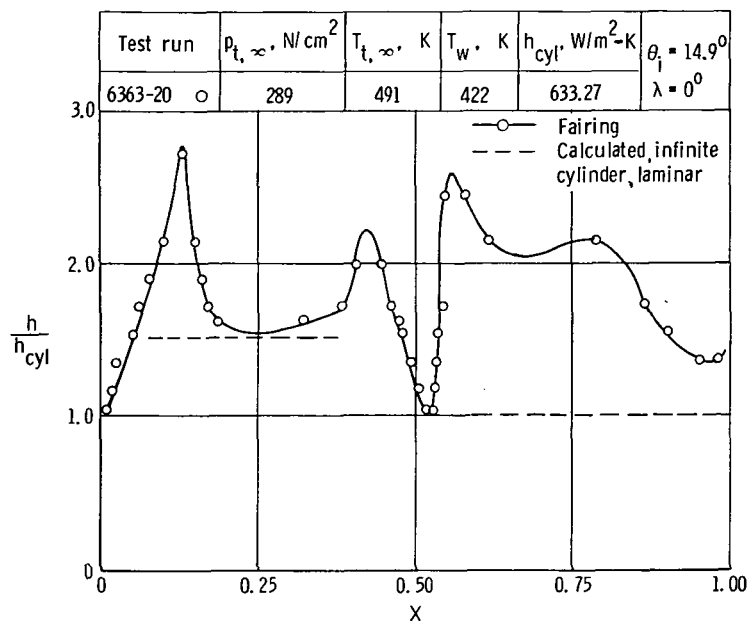

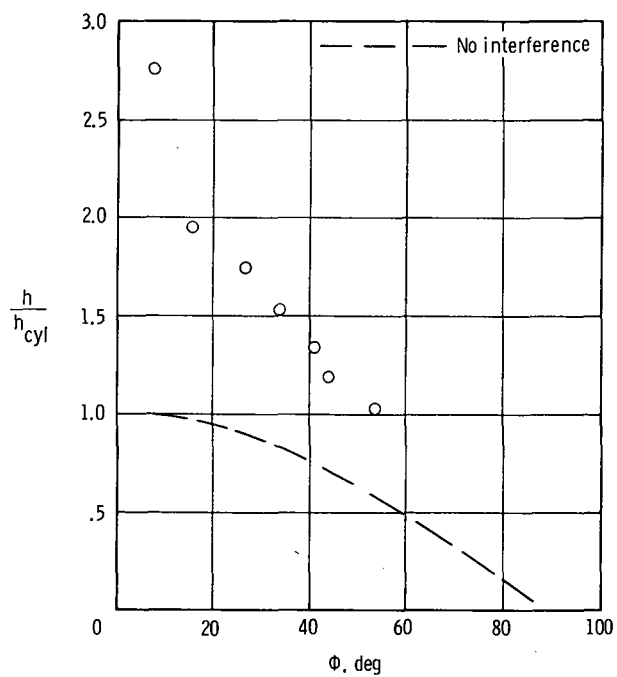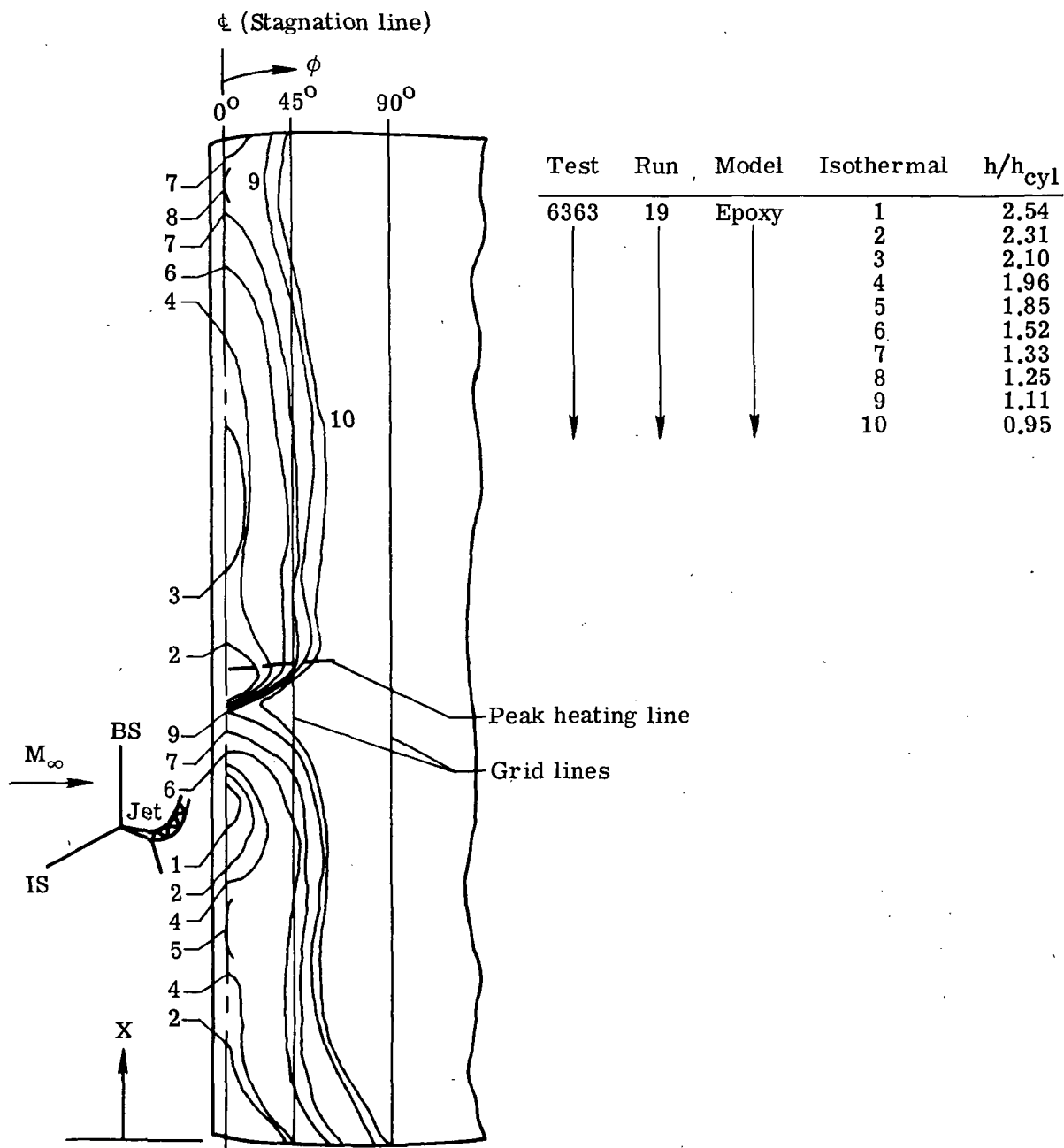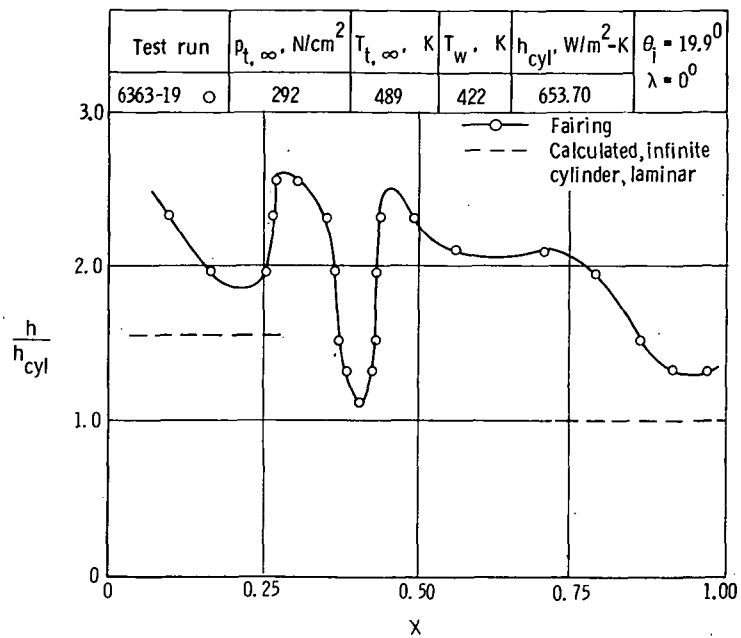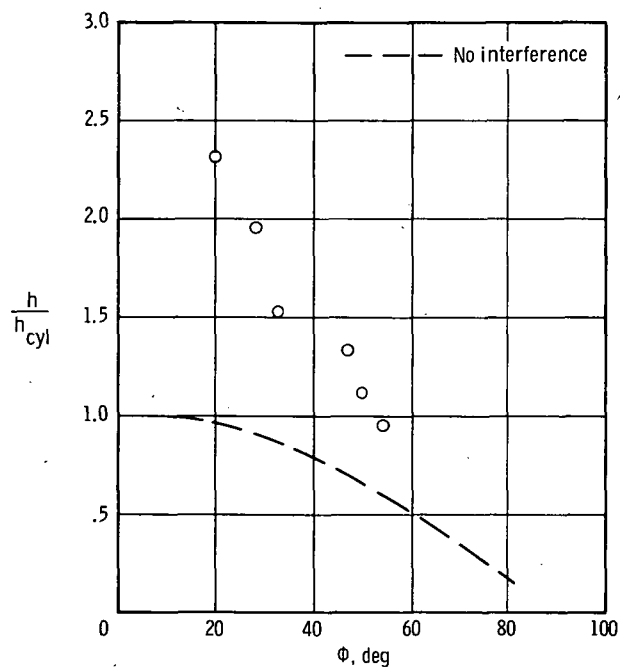(c) Off-center-line heating.   X = 0.57.

Figure 35.- Concluded.

(a) Heating contours. $h_{cyl} = 633.27 \text{ W/m}^2\text{-K}.$

Figure 36.- Type IVa interference on a fin at Mach 6 in air.

$\theta_i = 14.9^O$; $\lambda = 0^O$; $N_{Re,\infty}/m = 25.4 \times 10^6$.

The table in the figure:

Test	Run	Model	Isotherm	h/h_{cyl}
6363	20	Epoxy	1	3.07
			2	2.75
			3	2.41
			4	2.24
			5	2.14
			6	1.94
			7	1.83
			8	1.74
			9	1.52
			10	1.33
			11	1.17
			12	1.15
			13	1.03

Test run		$p_{t,\infty}$, N/cm^2	$T_{t,\infty}$, K	T_w, K	h_{cyl}, W/m^2-K	$\theta_i = 14.9^0$
6363-20	o	289	491	422	633.27	$\lambda = 0^0$

(b) Center-line heat-transfer distribution.

(c) Off-center-line heating.   X = 0.59.

Figure 36.- Concluded.

The table within the figure:

Test	Run	Model	Isothermal	h/h_{cyl}
6363	19	Epoxy	1	2.54
			2	2.31
			3	2.10
			4	1.96
			5	1.85
			6	1.52
			7	1.33
			8	1.25
			9	1.11
			10	0.95

(a) Heating contours. $h_{cyl} = 653.70 \text{ W}/\text{m}^2\text{-K.}$

Figure 37.- Type IVa interference on a fin at Mach 6 in air.
$\theta_i = 19.9^O$; $\lambda = 0^O$; $N_{Re,\infty}/m = 25.8 \times 10^6$.

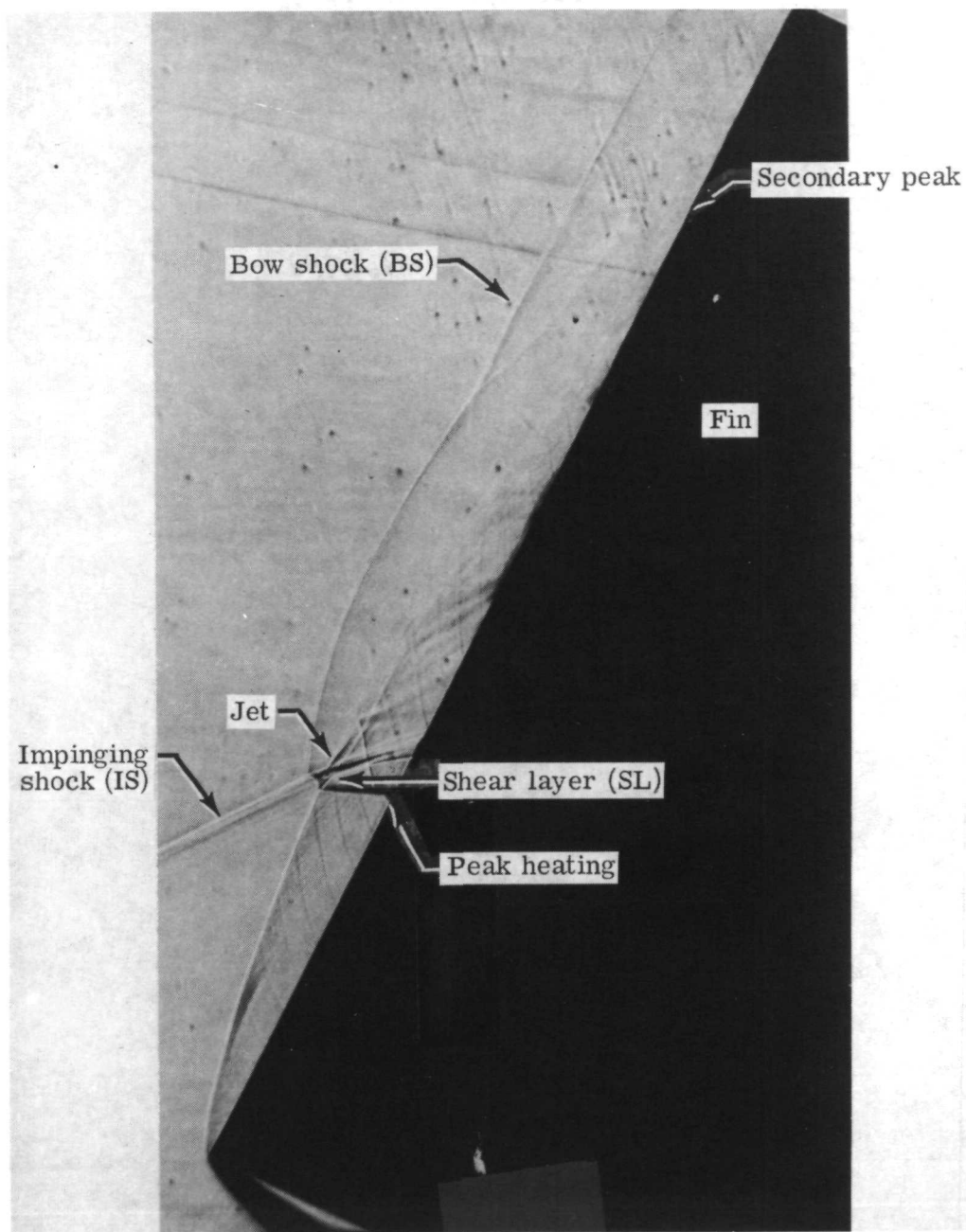| Test run		$p_{t,\infty}$, N/cm^2	$T_{t,\infty}$, K	T_w, K	h_{cyl}, W/m^2-K	$\theta_i = 19.9^0$ $\lambda = 0^0$
6363-19	○	292	489	422	653.70	

(b) Center-line heat-transfer distribution.

(c) Off-center-line heating.   X = 0.47.

Figure 37.- Concluded.

Secondary peak

Bow shock (BS)

Fin

Jet

Impinging
shock (IS)

Shear layer (SL)

Peak heating

L-73-6876

(a) Schlieren photograph.

Figure 38.- Shock and oil-flow patterns for a type V interference on a fin at
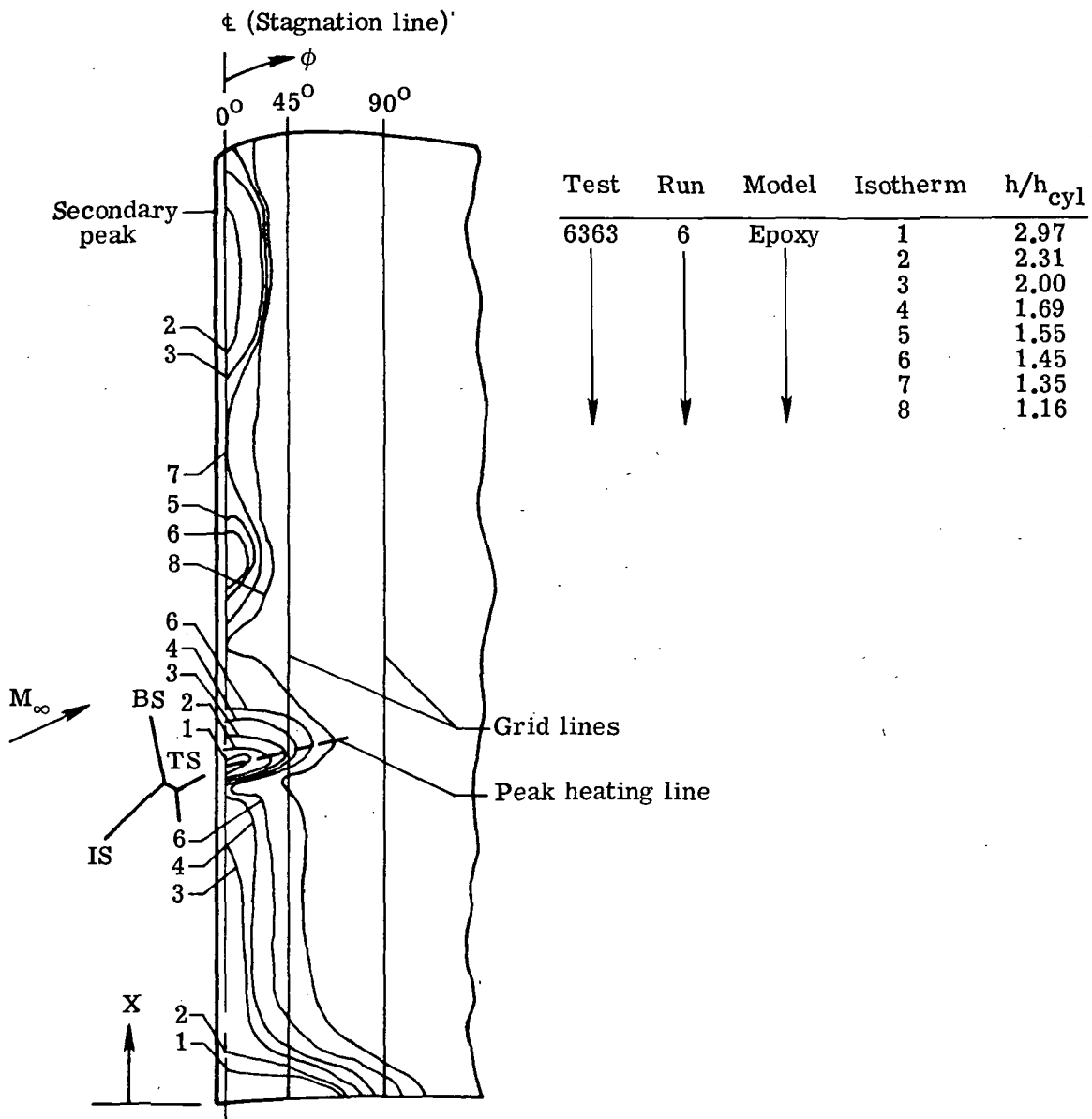Mach 6 in air. $\theta_i = 19.9^o$; $\lambda = 24.8^o$; $N_{Re,\infty}/m = 25.9 \times 10^6$.

Shock-boundary
layer interaction
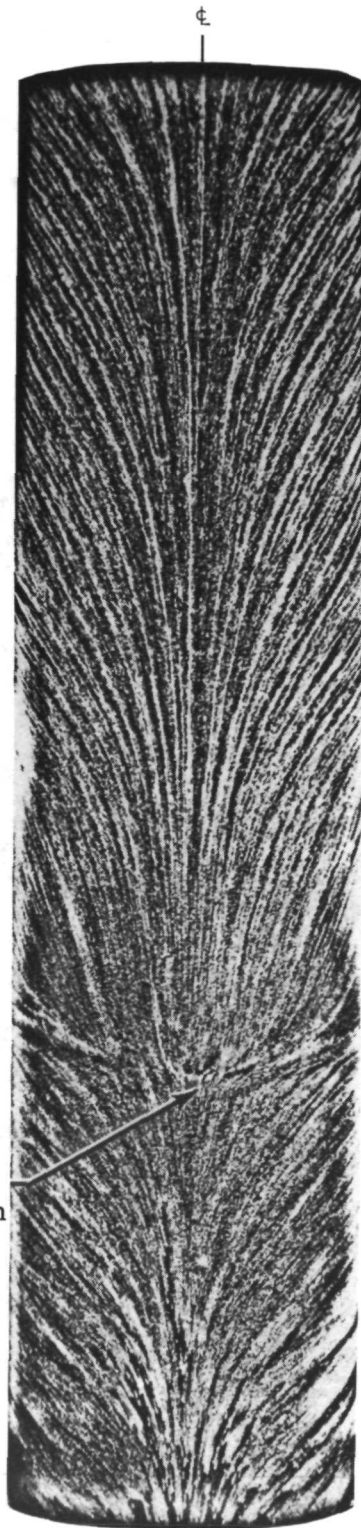
L-73-6877

(b) Oil-flow pattern.

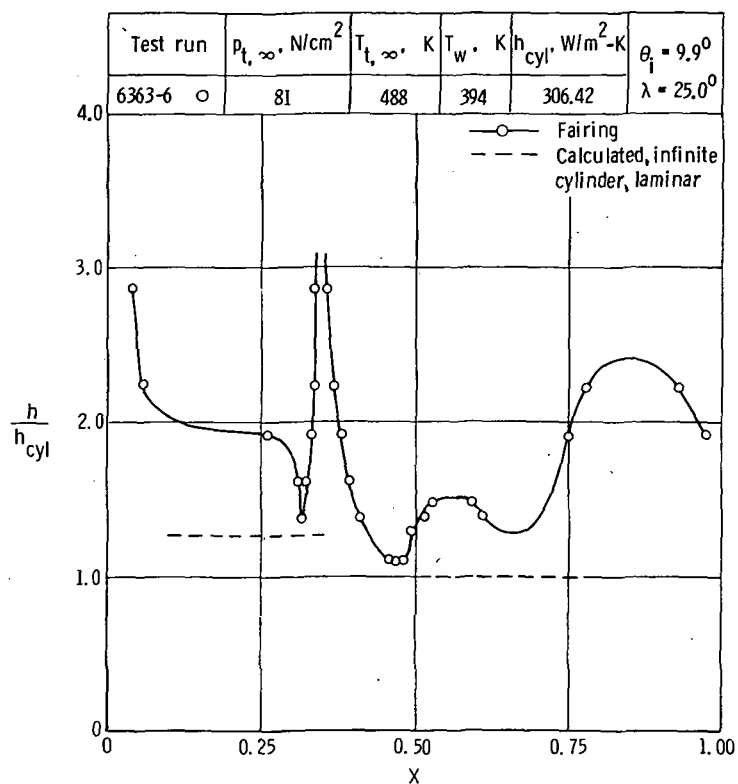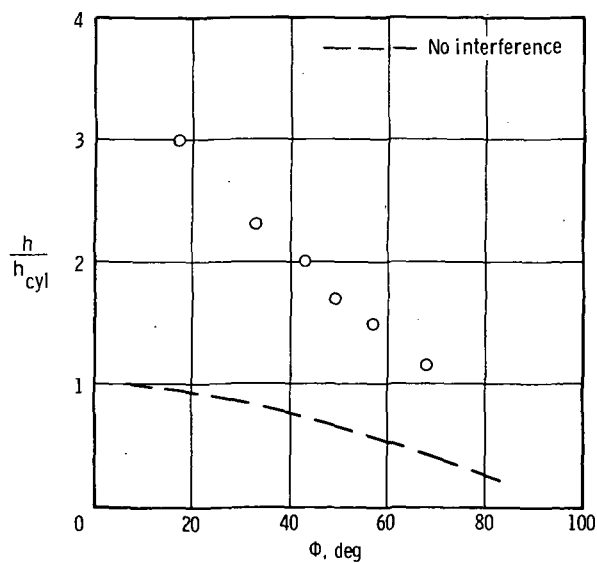Figure 38.- Concluded.

Test	Run	Model	Isotherm	h/h_{cyl}
6363	6	Epoxy	1	2.97
			2	2.31
			3	2.00
			4	1.69
			5	1.55
			6	1.45
			7	1.35
			8	1.16

(a) Heating contours. $h_{cyl} = 306.42 \ W/m^2\text{-K}$.

Figure 39.- Type V interference on a fin at Mach 5.94 in air.
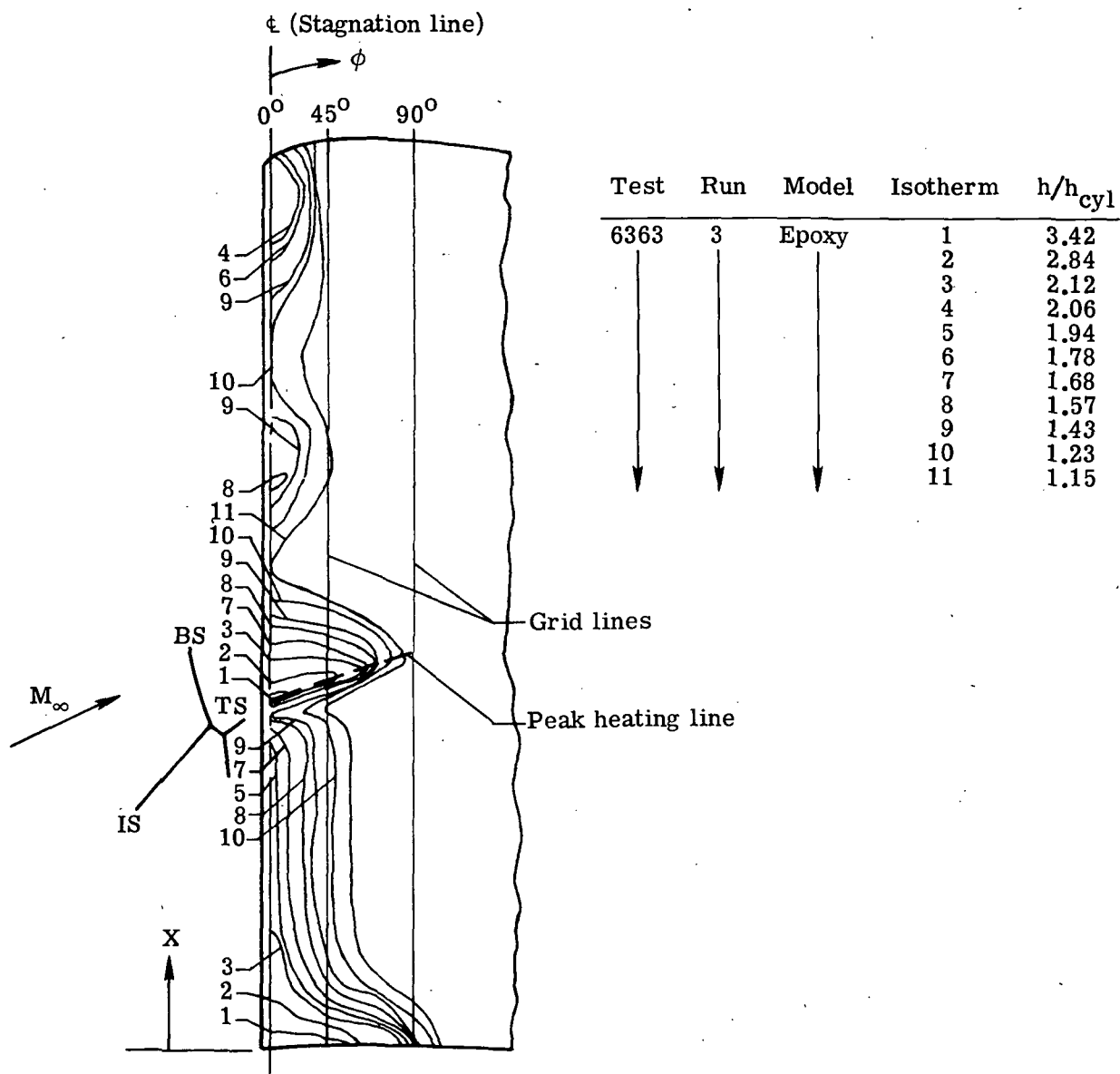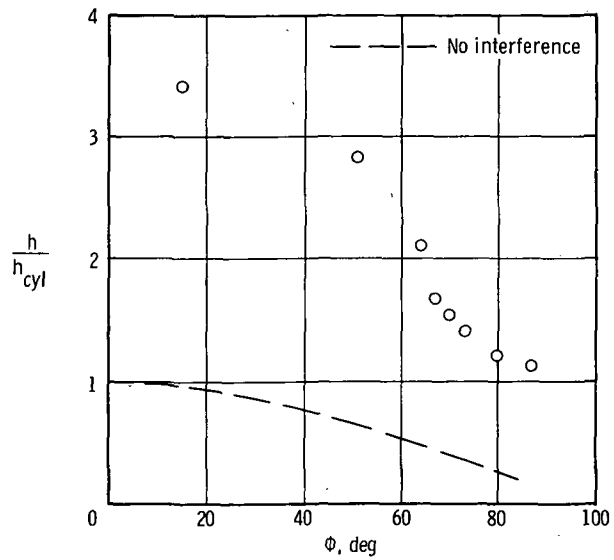$\theta_i = 9.9^\circ$; $\lambda = 25^\circ$; $N_{Re,\infty}/m = 7.2 \times 10^6$.

Test run		$p_{t, \infty}$, N/cm^2	$T_{t, \infty}$, K	T_w, K	h_{cyl}, W/m^2-K	$\theta_i = 9.9^0$
6363-6	O	81	488	394	306.42	$\lambda = 25.0^0$

————O———— Fairing
— — — Calculated, infinite
cylinder, laminar

(b) Center-line heat-transfer distribution.

— — — No interference

(c) Off-center-line heating.   X = 0.35.

Figure 39.- Concluded.

	℄ (Stagnation line)

Test	Run	Model	Isotherm	h/h_{cyl}
6363	3	Epoxy	1	3.42
			2	2.84
			3	2.12
			4	2.06
			5	1.94
			6	1.78
			7	1.68
			8	1.57
			9	1.43
			10	1.23
			11	1.15

(a) Heating contours. $h_{cyl} = 306.42$ W/m^2-K.

Figure 40.- Type V interference on a fin at Mach 5.94 in air. $\theta_i = 15^O$; $\lambda = 25^O$; $N_{Re,\infty}/m = 7.3 \times 10^6$.
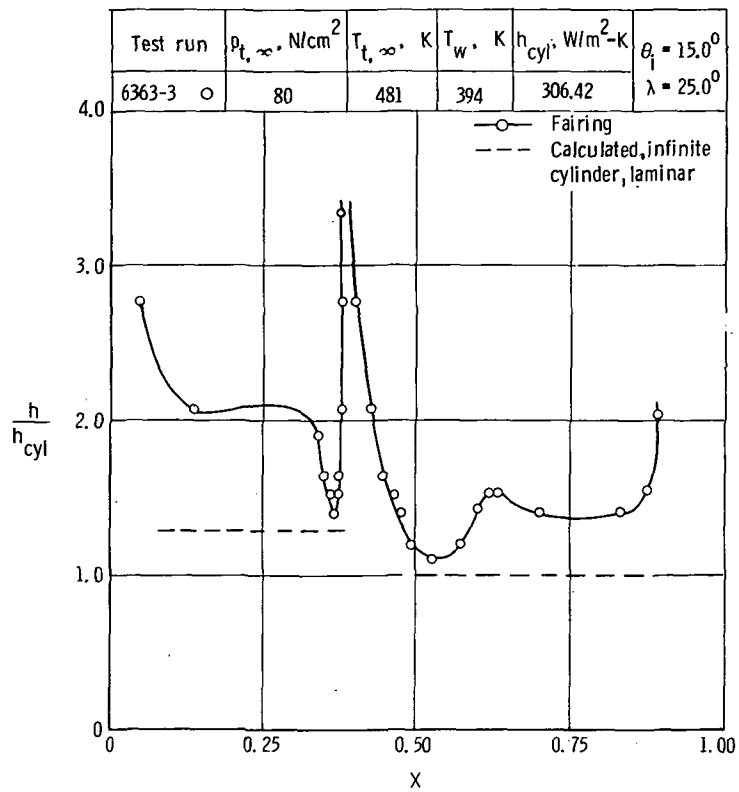
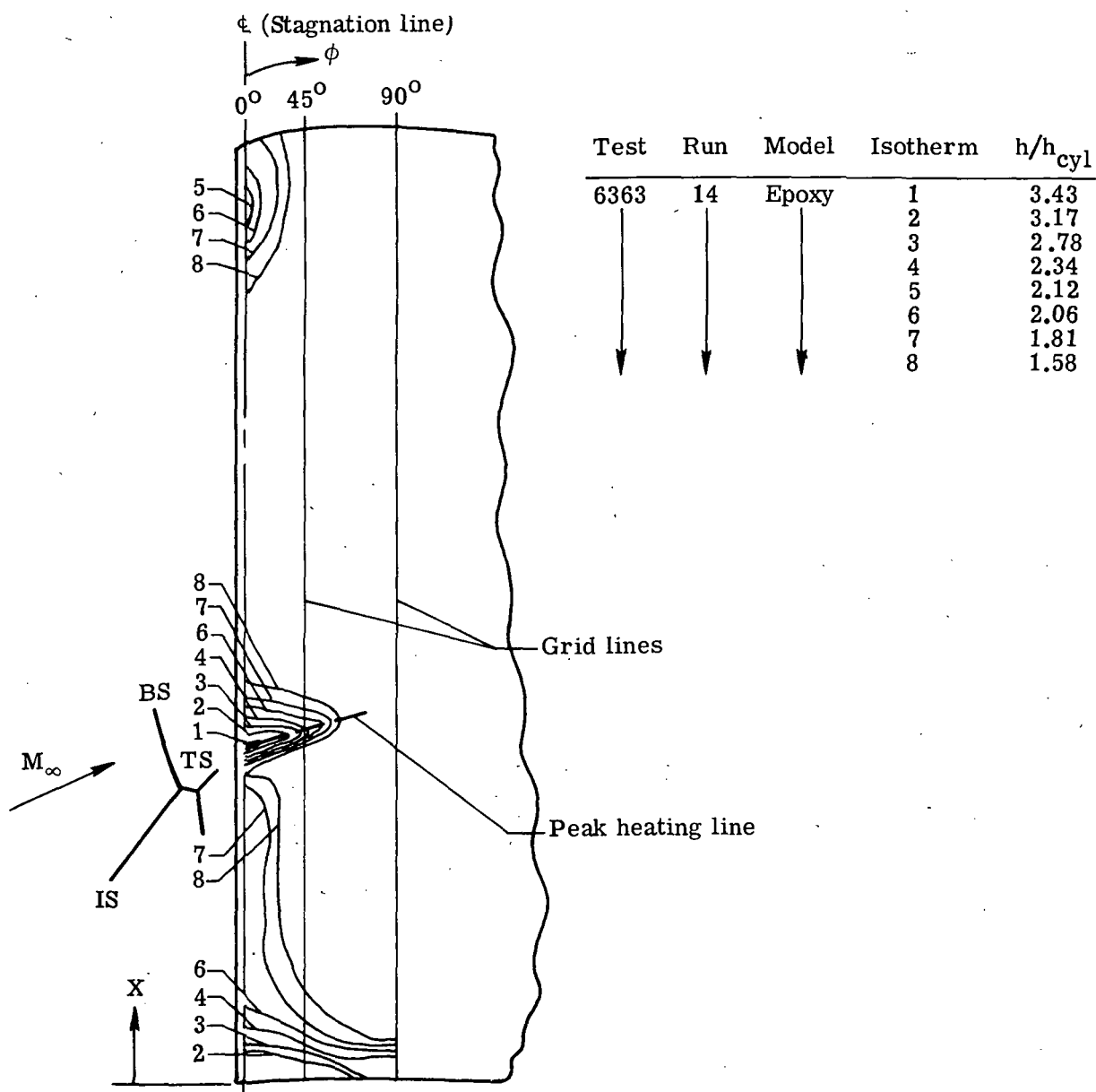(b) Center-line heat-transfer distribution.
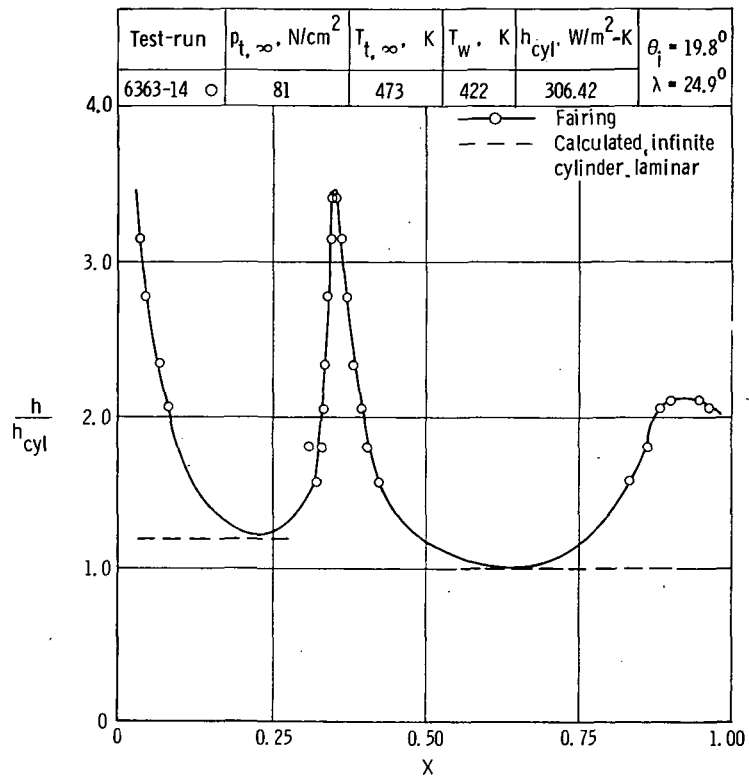

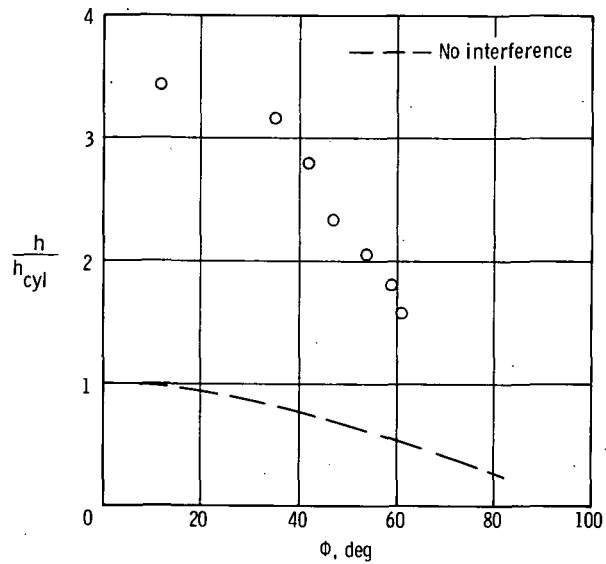(c) Off-center-line heating. X = 0.39.

Figure 40.- Concluded.

⌀ (Stagnation line)

φ

0° 45° 90°

5
6
7
8

Test	Run	Model	Isotherm	h/h_{cyl}
6363	14	Epoxy	1	3.43
			2	3.17
			3	2.78
			4	2.34
			5	2.12
			6	2.06
			7	1.81
			8	1.58

8
7
6
4
3
2
1

BS

TS

M_∞

IS

Grid lines

Peak heating line

7
8

X

6
4
3
2

(a) Heating contours. $h_{cyl} = 306.42$ W/m^2-K.

Figure 41.- Type V interference on a fin at Mach 5.94 in air.
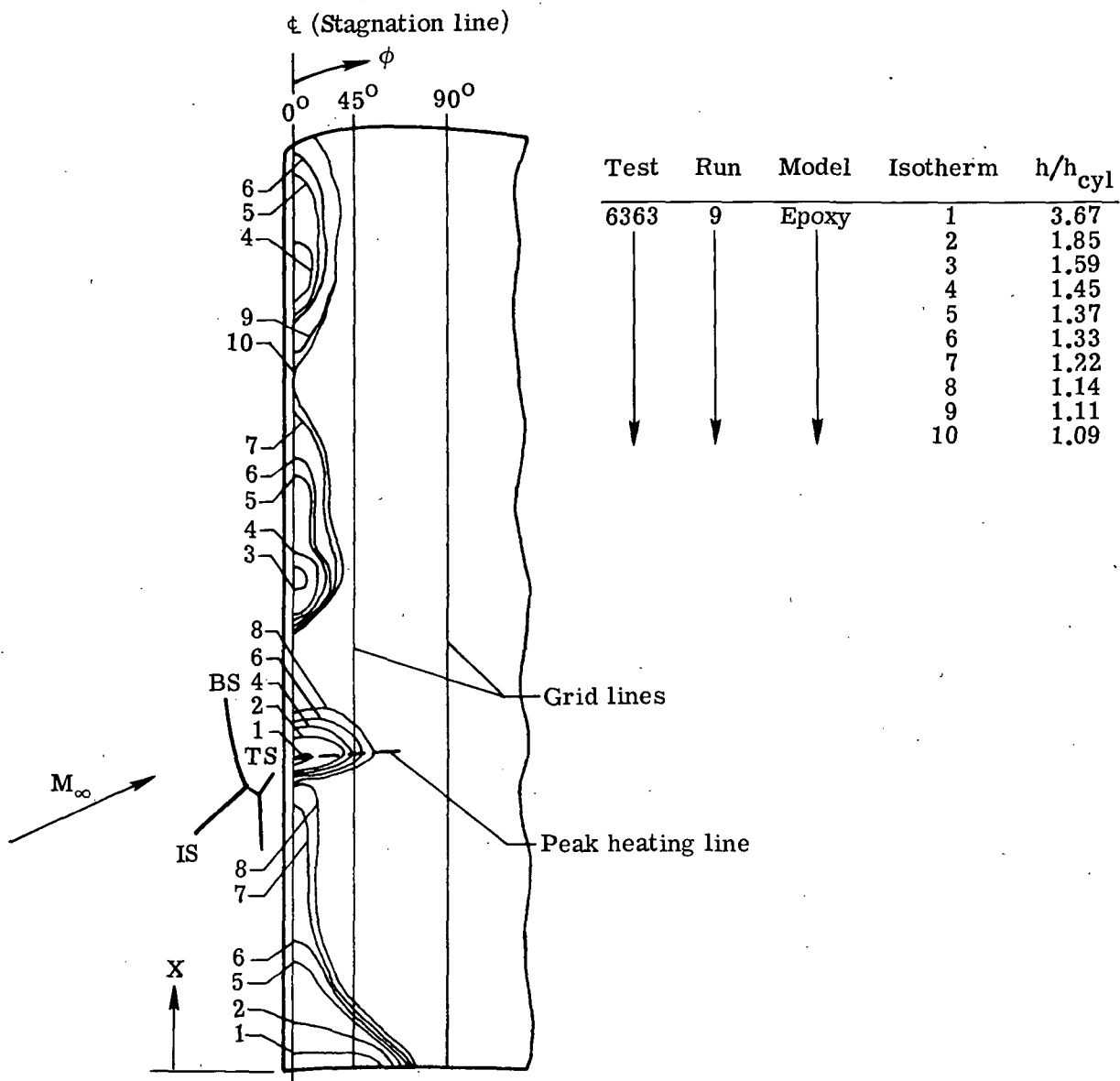$\theta_i = 19.8°$; $\lambda = 24.9°$; $N_{Re,\infty}/m = 7.6 \times 10^6$.

Test-run		$p_{t,\infty}$, N/cm^2	$T_{t,\infty}$, K	T_w, K	h_{cyl}, W/m^2-K	$\theta_i = 19.8^0$
6363-14	O	81	473	422	306.42	$\lambda = 24.9^0$

Fairing ⊶———

Calculated, infinite cylinder, laminar — — —

(b) Center-line heat-transfer distribution.

— — — No interference

(c) Off-center-line heating. X = 0.36.

Figure 41.- Concluded.

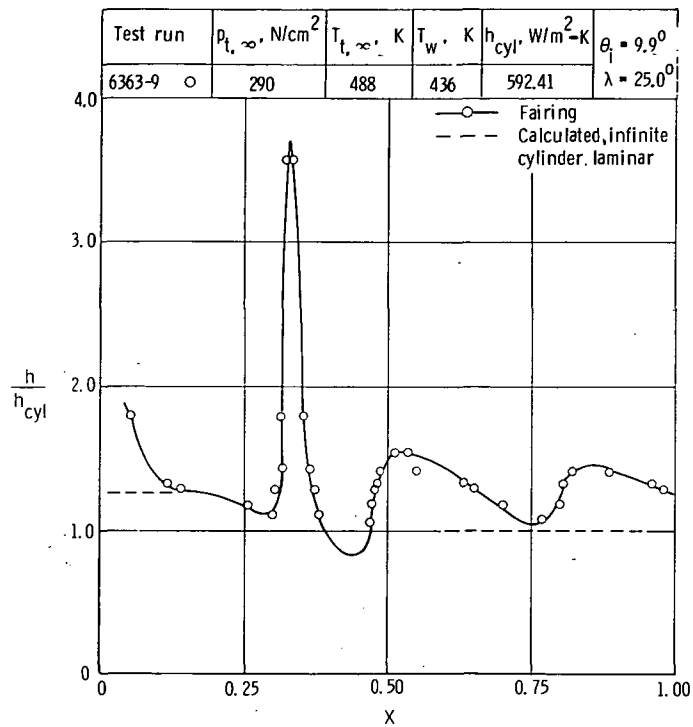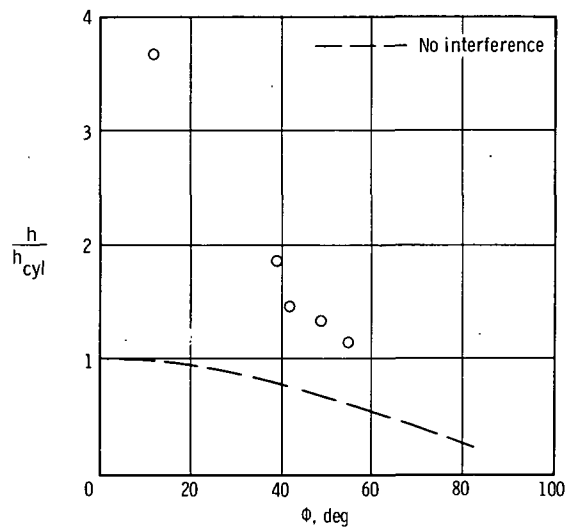| Test	Run	Model	Isotherm	h/h_{cyl}
6363	9	Epoxy	1	3.67
			2	1.85
			3	1.59
			4	1.45
			5	1.37
			6	1.33
			7	1.22
			8	1.14
			9	1.11
			10	1.09

(a) Heating contours. $h_{cyl} = 592.41 \, W/m^2\text{-}K$.

Figure 42.- Type V interference on a fin at Mach 6 in air.
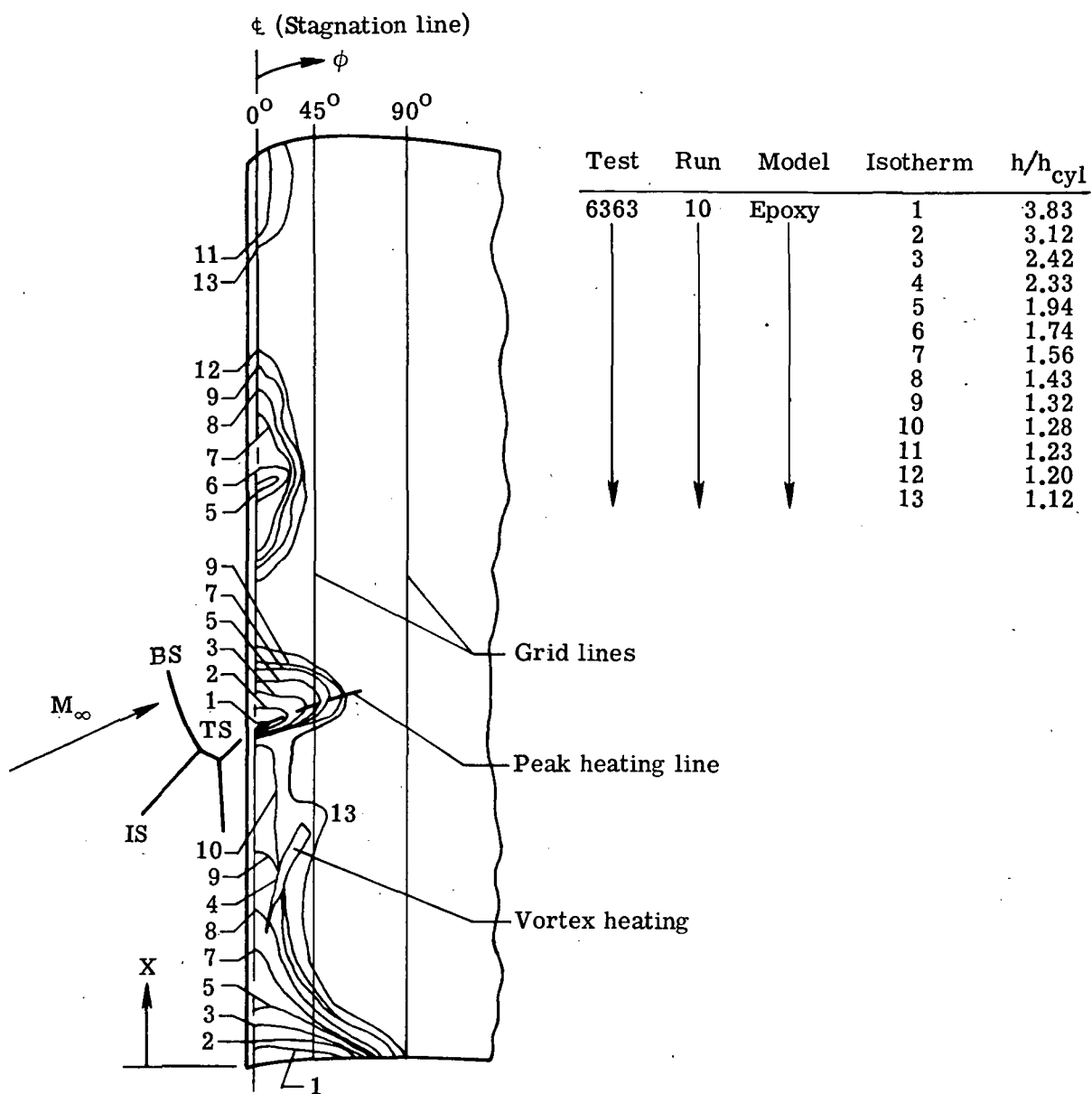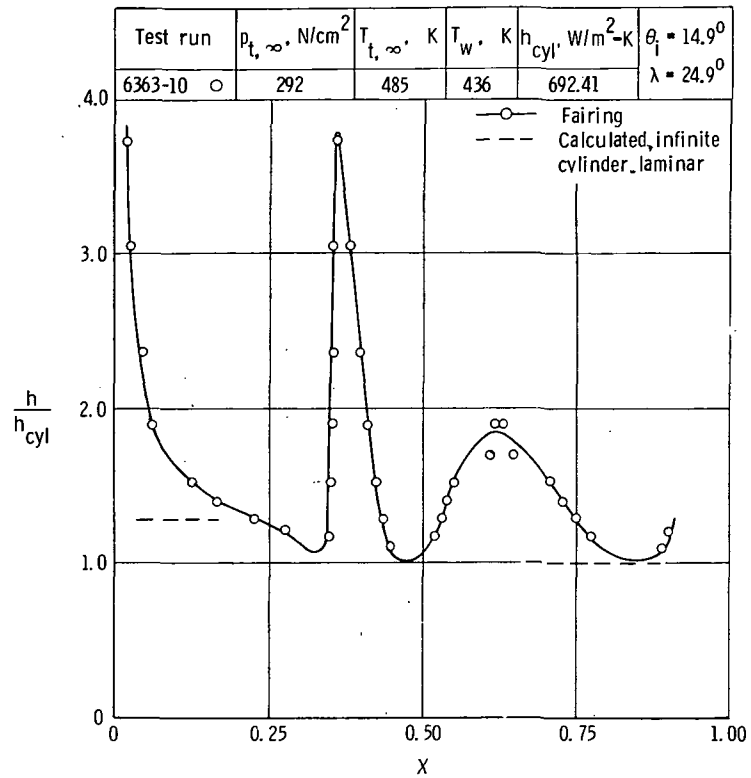$\theta_i = 9.9^O$; $\lambda = 25^O$; $N_{Re,\infty}/m = 25.7 \times 10^6$.

Test run		$p_{t, \infty}$, N/cm^2	$T_{t, \infty}$, K	T_w, K	h_{cyl}, W/m^2-K	$\theta_i = 9.9^o$
6363-9	O	290	488	436	592.41	$\lambda = 25.0^o$

(b) Center-line heat-transfer distribution.

(c) Off-center-line heating. X = 0.34.

Figure 42.- Concluded.

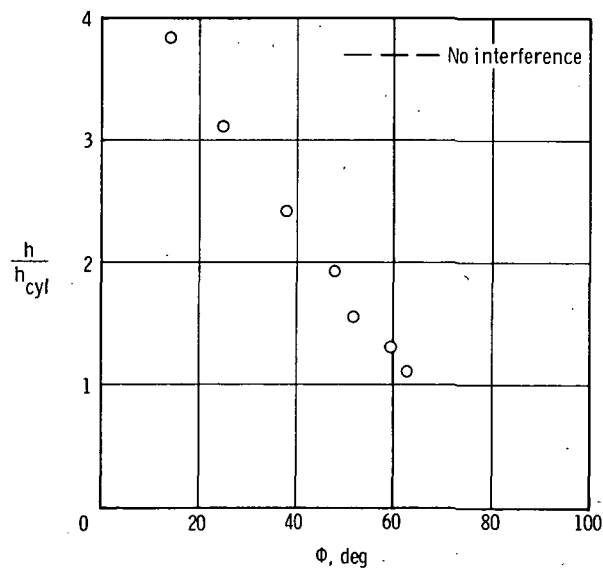| Test	Run	Model	Isotherm	h/h_{cyl}
6363	10	Epoxy	1	3.83
			2	3.12
			3	2.42
			4	2.33
			5	1.94
			6	1.74
			7	1.56
			8	1.43
			9	1.32
			10	1.28
			11	1.23
			12	1.20
			13	1.12

(a) Heating contours. $h_{cyl} = 692.41 \ W/m^2$-K.

Figure 43.- Type V interference on a fin at Mach 6 in air.
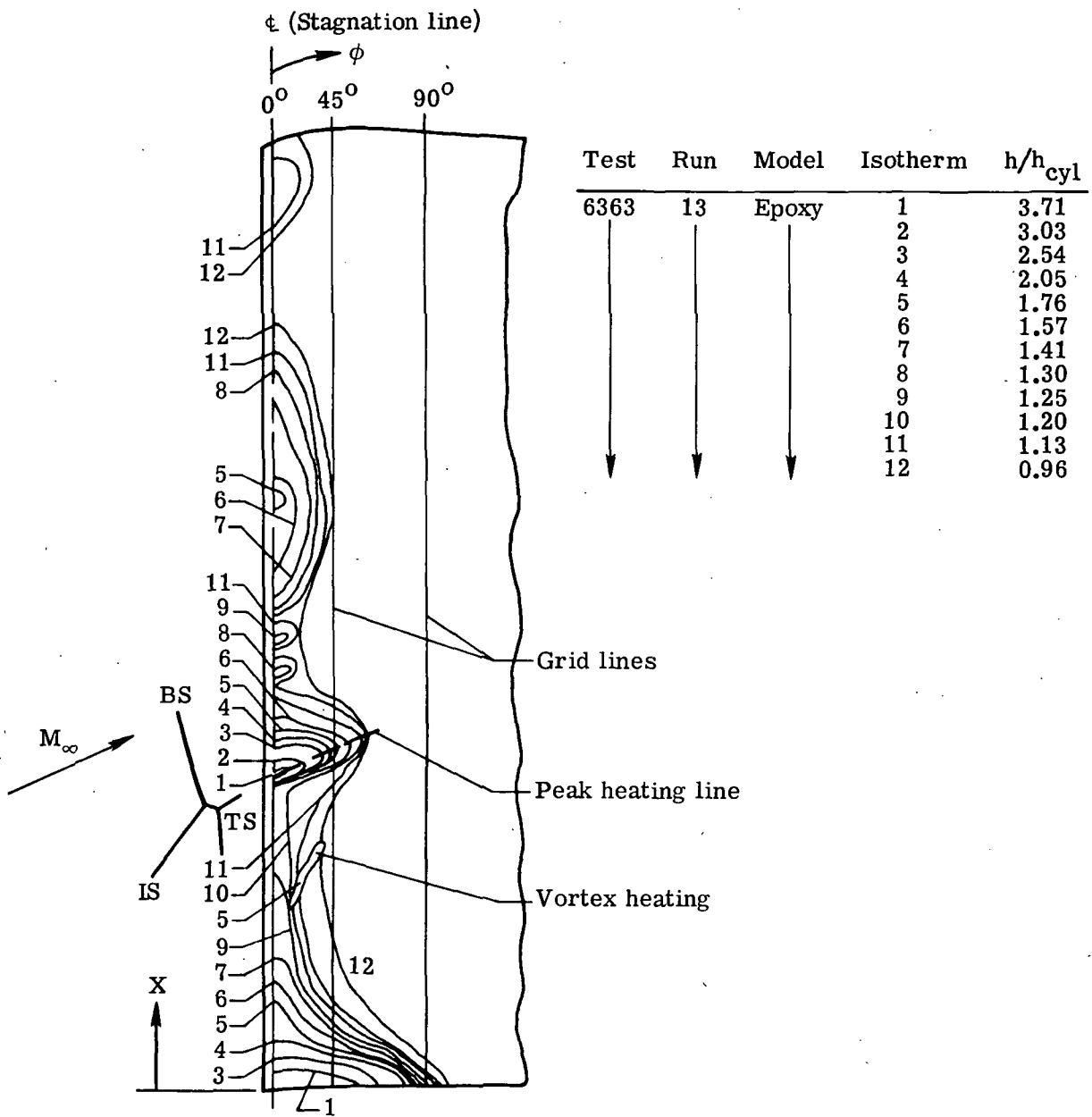$\theta_i = 14.9^O$; $\lambda = 24.9^O$; $N_{Re,\infty}/m = 26.2 \times 10^6$.

Test run		$p_{t,\infty}$, N/cm^2	$T_{t,\infty}$, K	T_w, K	h_{cyl}, W/m^2-K	$\theta_i = 14.9^0$
6363-10	○	292	485	436	692.41	$\lambda = 24.9^0$

(b) Center-line heat-transfer distribution.

(c) Off-center-line heating. X = 0.37.

Figure 43.- Concluded.

£ (Stagnation line)

ϕ

0° 45° 90°

Test	Run	Model	Isotherm	h/h_{cyl}
6363	13	Epoxy	1	3.71
			2	3.03
			3	2.54
			4	2.05
			5	1.76
			6	1.57
			7	1.41
			8	1.30
			9	1.25
			10	1.20
			11	1.13
			12	0.96

Grid lines

Peak heating line

Vortex heating

M_∞

BS
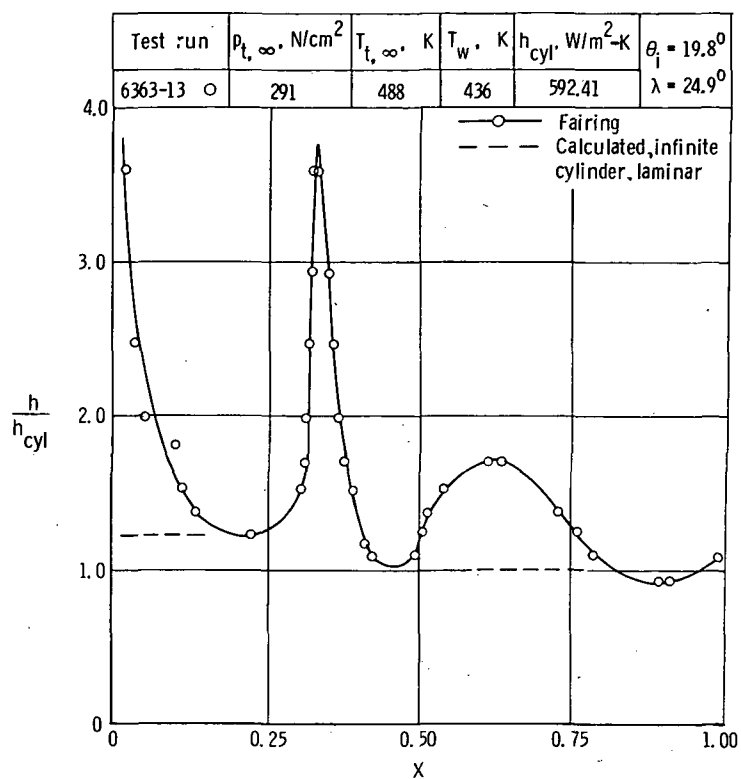
IS

TS

X
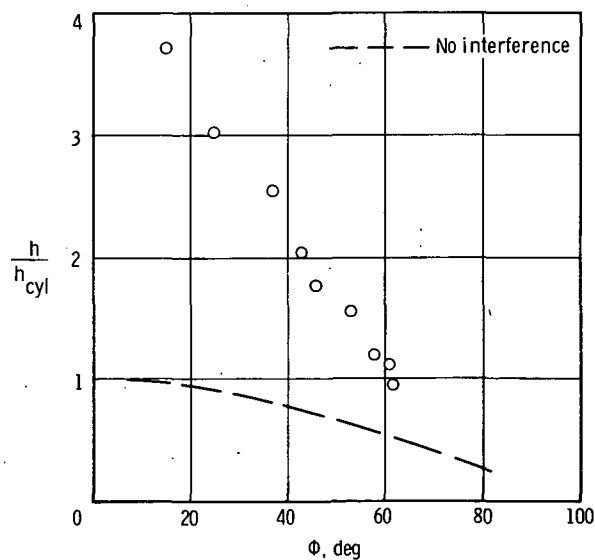
(a) Heating contours. $h_{cyl} = 592.41 \ W/m^2$-K.

Figure 44.- Type V interference on a fin at Mach 6 in air.
$\theta_i = 19.8^O$; $\lambda = 24.9^O$; $N_{Re,\infty}/m = 25.9 \times 10^6$.

Test run		$p_{t,\infty}$, N/cm^2	$T_{t,\infty}$, K	T_w, K	h_{cyl}, W/m^2-K	$\theta_i = 19.8^o$
6363-13	O	291	488	436	592.41	$\lambda = 24.9^o$

———O——— Fairing
— — — Calculated, infinite cylinder, laminar

(b) Center-line heat-transfer distribution.

— — — No interference

(c) Off-center-line heating.   X = 0.33.

Figure 44.- Concluded.

"The aeronautical and space activities of the United States shall be conducted so as to contribute . . . to the expansion of human knowledge of phenomena in the atmosphere and space. The Administration shall provide for the widest practicable and appropriate dissemination of information concerning its activities and the results thereof."
—NATIONAL AERONAUTICS AND SPACE ACT OF 1958

NASA SCIENTIFIC AND TECHNICAL PUBLICATIONS

TECHNICAL REPORTS: Scientific and technical information considered important, complete, and a lasting contribution to existing knowledge.

TECHNICAL NOTES: Information less broad in scope but nevertheless of importance as a contribution to existing knowledge.

TECHNICAL MEMORANDUMS: Information receiving limited distribution because of preliminary data, security classification, or other reasons. Also includes conference proceedings with either limited or unlimited distribution.

CONTRACTOR REPORTS: Scientific and technical information generated under a NASA contract or grant and considered an important contribution to existing knowledge.

TECHNICAL TRANSLATIONS: Information published in a foreign language considered to merit NASA distribution in English.

SPECIAL PUBLICATIONS: Information derived from or of value to NASA activities. Publications include final reports of major projects, monographs, data compilations, handbooks, sourcebooks, and special bibliographies.

TECHNOLOGY UTILIZATION PUBLICATIONS: Information on technology used by NASA that may be of particular interest in commercial and other non-aerospace applications. Publications include Tech Briefs, Technology Utilization Reports and Technology Surveys.

Details on the availability of these publications may be obtained from:

SCIENTIFIC AND TECHNICAL INFORMATION OFFICE

NATIONAL AERONAUTICS AND SPACE ADMINISTRATION
Washington, D.C. 20546